Charles University

Faculty of Science

Study program: Chemistry

Branch of study: Physical chemistry

Bc. Ondřej Veselý

Preparation of hierarchical zeolites for fine chemical synthesis

Diploma thesis

Supervisor:

Mgr. Pavla Eliášová, Ph.D.

Prague, 2019

Univerzita Karlova

Přírodovědecká fakulta

Studijní program: Chemie

Studijní obor: Fyzikální chemie

Bc. Ondřej Veselý

Syntéza hierarchických zeolitů pro přípravu chemických specialit

Diplomová práce

Školitel:

Mgr. Pavla Eliášová, Ph.D.

Praha, 2019

Prohlášení:

Prohlašuji, že jsem závěrečnou práci zpracoval samostatně a že jsem uvedl všechny použité informační zdroje. Dále prohlašuji, že tato práce ani její podstatná část nebyla předložena k získání jiného nebo stejného akademického titulu.

V Praze dne:

Podpis:

Acknowledgement:

I would like to thank my supervisor Mgr. Pavla Eliášová, Ph.D. and prof. ing. Jiří Čejka, DrSc. for their guidance and support. Furthermore I would like to express my gratitude to all my colleagues who helped me with individual measurements; namely Martin Kubů, Ph.D. (argon adsorption), Valeriya Kasneryk, Ph.D. (SEM), Michal Mazur, Ph.D. (HR-TEM), Mariya Shamzhy, Ph.D. (FTIR), Hao Pang and Maksym Opanasenko, CSc. (catalytic experiments). Moreover, I would like to thank RNDr. Lukáš Grajciar, Ph.D., Pengbo Lyu and Mingxiu Liu from the Department of Physical and Macromolecular Chemistry for providing the theoretical calculations.

List of abbreviations:

Al-MFI (Brønsted)	theoretical model of **MFI** zeolite containing only Brønsted acid sites
Al-MFI (Lewis)	theoretical model of **MFI** zeolite containing only Lewis acid sites
***BEA**	three-dimensional zeolite with 12-12-12-ring channel system
BET	the method used for the calculation of surface areas of solids (m^2/g) by physical adsorption of gas molecules; based on the Brunauer, Emmett, and Teller theory
BJH	pore size model developed by Barret, Joyner, and Halenda; based on the modified Kelvin equation corrected for multilayer adsorption
c_B	concentration of Brønsted acid sites
c_L	concentration of Lewis acid sites
C22-6-6	SDA used for the synthesis of nanosponge **MFI**
C22N6	SDA used for the synthesis of nanosponge **MTW** and ***BEA**
DHP	3,4-dihydro-2H-pyran
EDX	energy dispersive x-ray spectroscopy
FTIR	Fourier transform infrared spectroscopy
GC	gas chromatography
HRTEM	high resolution transmission electron microscopy
ICP-OES	optical emission spectroscopy with inductively coupled plasma atomizer
MFI	three-dimensional zeolite with 10-10-10-ring channel system
MTW	one-dimensional zeolite with 12-ring channel system
NMR	nuclear magnetic resonance
PDA	pore directing agent
SDA	structure directing agent
SEM	scanning electron microscopy

S_{ext}	external surface area
Si/Al	silicon to aluminium molar ratio
Si/Ga	silicon to gallium molar ratio
Si/Ti	silicon to titanium molar ratio
TEOS	tetraethyl orthosilicate
TEA-OH	tetraethyl ammonium hydroxide
TBA	tetrabutyl ammonium
TOF	turn-over frequency
TPA	tetrapropyl ammonium
TS-1	titanosilicate zeolite with the **MFI** structure
V_{mic}	micropore volume
V_{tot}	total pore volume
XRD	x-ray powder diffraction
ε (B)	extinction coefficient for Brønsted acid sites (cm/µmol)
ε (L)	extinction coefficient for Lewis acid sites (cm/µmol)
2D	two-dimensional
3D	three-dimensional

Abstrakt:

Diplomová práce je zaměřena na syntézu hierarchických (mikro-mezoporézních) zeolitů několika různými metodami a na jejich uplatnění v katalytických reakcích. Byly zkoumány texturní a kyselé vlastnosti hierarchických materiálů připravených různými postupy, stejně jako vliv topologie krystalu a typu kyselosti na výsledek reakcí. Práce byla vypracována na katedře Fyzikální a makromolekulární chemie Univerzity Karlovy pod dohledem Mgr. Pavly Eliášové, Ph.D.

Práce je rozdělena na tři části. V první části bylo zkoumáno a porovnáváno několik metod přípravy hierarchických zeolitů a jejich použití v katalytických reakcích. Desilikace, selektivní odstraňování křemíku ze struktury, je post-syntetická metoda, kterou lze použít k tvorbě mezopórů. Mezopóry vznikají jako defekty ve struktuře zeolitu. Distribuce velikostí takto vytvořených mezopórů je ovšem značně široká. Velikosti vznikajících pórů lze částečně ovlivnit použitím alkylamonných kationtů, které chrání povrch krystalu během desilikace. K desilikaci byl použit zeolit **MTW**, který obsahuje jednorozměrné, paralelně orientované mikropóry (o šířce 0,56 až 0,60 nm). Ačkoli důsledkem desilikace bylo zvětšení vnějšího povrchu krystalů, zároveň desilikace způsobila ucpání mikropórů zbytky rozpouštěné struktury v případech, kdy byly použity tetraalkylamonné ionty. Tuto překážku bylo možné odstranit následným promytím roztokem kyseliny.

Hierarchické zeolity lze také syntetizovat přímou syntézou, přidáním speciálně navržených amfifilních templátů do syntézního gelu. Hydrofobní řetězce se ve vodné syntézní směsi shlukují a brání růstu krystalů v určitém směru. Výsledný zeolit pak má formu agregátu složeného z mnoha tenkých krystalů. Zeolit **MTW** byl připraven v hierarchické formě „nanosponge“, která ve srovnání se vzorky připravenými desilikací, vykazuje nadstandardní vlastnosti, jako například velký vnější povrch a celkový objem pórů.

Katalytické vlastnosti desilikovaných vzorků a vzorku nanosponge **MTW** byly porovnány v tetrahydropyranylaci alkoholů, což je kysele katalyzovaná reakce používaná pro chránění hydroxylových skupin organických molekul při organické syntéze. Ve všech případech poskytoval vzorek nanosponge nejvyšší konverzi reaktantu. Byly pozorovány mírné rozdíly mezi jednotlivými alkoholy v závislosti na délce a struktuře jejich řetězce. Nicméně desilikované vzorky se zablokovanými mikropóry vykazovaly neočekávaně vysoké konverze a aktivitu (vyjádřenou pomocí TOF – turn-over frequency) srovnatelnou se vzorkem ve formě nanosponge. Ze získaných výsledků se došlo k závěru, že přestože desilikací vzniknou v zeolitu **MTW** mezopóry, difuzní dráha molekul reaktantů/produktů skrze přístupné mikropóry je příliš dlouhá, a zvýšení reakční rychlosti není příliš

výrazné. Naopak při znepřístupnění mikropórů probíhá reakce na aktivních centrech umístěných na vnějším povrchu katalyzátoru, kde reakční rychlost není omezena difuzí skrze mikropóry.

Úloha různých typů kyselých center (Brønstedova a Lewisova typu) v katalýze tetrahydropyranylace nebyla dosud zkoumána. Přímá příprava zeolitů obsahujících pouze Brønstedova nebo Lewisova kyselá centra je ale problematická. Proto byl použit komerční zeolit **MFI** v H^+ formě. Tyto H^+ ionty byly částečně vyměněny za ionty alkalických kovů za účelem odstranění části Brønstedových kyselých center. Tímto způsobem byla připravena sada materiálů s různou kyselostí. Vzorky **MFI** byly zkoumány v tetrahydropyranylaci 1-propanolu při různých teplotách. Z výsledků katalýzy je zřejmé, že vzorek s největší koncentrací Brønstedových kyselých center (H^+MFI) je nejaktivnějším katalyzátorem, a proto je pro katalýzu tetrahydropyranylace nejvhodnější. Zeolity obsahující převážně Lewisova kyselá centra poskytují nižší konverzi 1-propanolu, která dále výrazně závisí na teplotě reakce.

V další části práce byla studována Pechmannova kondenzace resorcinolu (1,3-dihydroxybenzenu) a etylacetátu na hymekromon (7-hydroxy-4-metylkumarin) s použitím řady zeolitů jako katalyzátorů. Zejména byl zkoumán vliv topologie, morfologie a typu kyselosti zeolitu na průběh reakce. Zeolity **MFI** (s trojrozměrným systémem 10-četných pórů), **MTW** (s jednorozměrným systémem 12-četných pórů) a ***BEA** (s trojrozměrným systémem 12-četných pórů) byly připraveny jako aluminosilikáty a gallosilikáty v mikroporézní formě a ve formě nanosponge. Konverze resorcinolu při katalýze se zvyšovala v následujícím pořadí: **MFI** < **MTW** < ***BEA**. Na druhou stranu při použití katalyzátorů se strukturou ***BEA** a v menší míře při použití zeolitu **MTW** lze pozorovat tvorbu sekundárního vedlejšího produktu. Vypočtené aktivity (vyjádřené pomocí TOF) ukazují, že hierarchický systém pórů zvyšuje rychlost reakce při katalýze pomocí zeolitů **MFI** a **MTW**, zatímco dopad na rychlost reakce katalyzované zeolitem ***BEA** je zanedbatelný. Konverze i TOF poukazují na srovnatelnou aktivitu aluminosilikátů a gallosilikátů.

Abstract:

The thesis is focused on synthesis of hierarchical (micro-mesoporous) zeolites by several different methods and their application in catalytic reactions. Performance of hierarchical materials prepared by different approaches has been investigated, as well as the effect of framework topology and type of acidity on the outcome of the reactions. The work was elaborated in the Department of Physical and Macromolecular Chemistry of Charles University under the supervision of Mgr. Pavla Eliášová, Ph. D.

The work is divided into three parts. In the first part several methods of preparation of hierarchical zeolites have been investigated and compared in catalytic reactions. Desilication, selective removal of silicon from the framework, is a post-synthetic method that can be used to introduce additional mesoporosity into a zeolite. The process leads to formation of mesopores by introducing defects into the zeolite structure. The resulting mesopore size is very broad. To partially control the pore size, alkylammonium cations may be added to the solution to protect the crystal surface. The desilication was performed on **MTW** zeolite which contains one-dimensional parallel-oriented micropores (0.56 to 0.60 nm wide). It was discovered that although the desilication leads to an increase of the external surface area, it also causes a blockage of the micropores by the framework debris when the tetraalkylammonium ions are used. This blockage was possible to remove by subsequent washing with acidic solution.

Hierarchical zeolites can also be synthesized directly by addition of specially designed amphiphilic structure directing agents into the synthesis gel. The hydrophobic chains in the water based synthesis mixture agglomerate together and prevent crystal growth in a given direction. The resulting zeolite is recovered as an aggregation of thin crystallites. The **MTW** zeolite was prepared in the nanosponge form and compared with the samples prepared by desilication. Nanosponge shows superior properties in the means of external surface area and total pore volume.

The catalytic performance of the desilicated samples and nanosponge sample of the zeolite **MTW** was compared in the tetrahydropyranylation of alcohols, an acid catalysed reaction useful for protecting hydroxyl groups of organic molecules in multistep synthesis. In each reaction the nanosponge sample gave superior conversion of reactants. Slight differences were observed between individual alcohols depending on their chain length and architecture. However, the desilicated samples with blocked micropores showed unexpectedly high conversions and activity in the means of turn over frequencies even comparable to the nanosponge. It has been concluded that despite the creation of mesopores by desilication of **MTW** zeolite, the diffusion path of the

reactant/product molecules through the accessible micropore system is too long and the increase in the reaction rate is not very pronounced. Conversely, when the micropores are inaccessible, the reaction proceeds over the active centres located on the external surface of the catalyst, where the reaction rate is not limited by diffusion through micropores.

The role of different types of the acid sites (Brønsted and Lewis) in the catalysis of tetrahydropyranylation has not been investigated so far. Direct preparation of purely Brønsted or Lewis acidic zeolites is problematic. Hence, a commercial zeolite **MFI** in the H^+ form was partially ion exchanged with alkali metal ions to poison a portion of its Brønsted acid sites and thus produce a set of materials with varying acidity. The **MFI** samples were investigated in tetrahydropyranylation of 1-propanol at different temperatures. From the catalytic tests it is clear that sample with the largest concentration of Brønsted acid sites (H^+MFI) is the most active catalyst and therefore more suitable for the catalysis. Zeolites with predominant Lewis acidity provide lower conversions of 1-propanol and their performance highly depends on the reaction temperature.

In the next part of the work the Pechmann condensation of resorcinol (1,3-dihydroxybenzene) and ethyl acetoacetate to hymecromone (7-hydroxy-4-metylcoumarine) over a set of zeolite samples was investigated to assess the effect of framework topology, morphology and acidity of zeolite on the reaction. Aluminosilicate and gallosilicate form of zeolites **MFI** (with three-dimensional system of 10-ring channels), **MTW** (with one-dimensional system of 12-ring channels) and ***BEA** (with three-dimensional system of 12-ring channels) were prepared each in bulk and nanosponge form. Conversions of resorcinol over the samples increase in the following order: **MFI** < **MTW** < ***BEA**. On the other hand, formation of secondary side-product can be observed over the ***BEA** sample and slightly less over the **MTW**. The obtained activities in the means of turn over frequencies show that the hierarchical pore system enhances the performance of the narrow-pore **MFI** and one-dimensional **MTW**, whereas the impact on ***BEA** catalyst is negligible. The conversions as well as turn over frequencies show comparable performance of the aluminosilicates and gallosilicates.

Contents:

1. Introduction

Zeolites are microporous crystalline aluminosilicates characteristic by their large surface areas and ion exchange capabilities. Thanks to these properties they became widely used as water softeners, adsorbents and heterogeneous catalysts. More than 250 structures with different topology have been prepared. [1] Size and shape of the pores differ among individual structure types as well as the connectivity of the pores and dimensionality of the channel system. This gives the zeolites unique property of admitting or rejecting molecules to enter the channel system depending on their size. The effect is referred to as shape selectivity and has a huge impact on their catalytic performance. Also the chemical composition of the framework can differ, not only silicates and aluminosilicates but also for instance germanosilicates, gallosilicates or titanosilicates are known and utilised. Each of them has distinct acidic properties characterized by different types of acid sites and suitability for catalysis of different reactions.

The presented diploma thesis has three main subjects of study:

- Synthesis of hierarchical zeolites and their application in catalysis of tetrahydropyranylation.
    - Preparation of aluminosilicate zeolite **MTW** in bulk and hierarchical forms (modified to possess additional mesoporosity which should enlarge its surface area and facilitate the molecular transport) using the top-down and bottom-up approaches.
    - Characterization of properties of both bulk and hierarchical **MTW** samples by powder x-ray diffraction, gas adsorption, infrared spectroscopy and electron microscopy.
    - Comparison of the catalytic performance of the bulk and hierarchical **MTW** samples in tetrahydropyranylation of differently sized alcohols.
- Investigation of the role of different types of acid sites in the catalysis of tetrahydropyranylation.
    - Preparation of a group of samples with **MFI** topology with different nature and concentration of acid sites.
    - Characterization of acidic properties of the **MFI** samples by infrared spectroscopy.
    - Determination of the role of different types of acid sites in the mechanism of the tetrahydropyranylation of alcohols.
    - Assessment of the effect of diffusional limitations of the materials on the overall reaction rate.

- Synthesis of zeolites of different structure, morphology and composition and their application in Pechmann condensation catalysis.
    - Preparation of a set of zeolites with **MTW**, ***BEA**, and **MFI** topology with both bulk and hierarchical morphology, in aluminosilicate and gallosilicate form.
    - Characterization of properties of the gallosilicate and aluminosilicate samples by powder x-ray diffraction, gas adsorption and infrared spectroscopy.
    - Comparison of the performance of the gallosilicate and aluminosilicate samples in the catalysis of the Pechmann condensation of phenols. The study is predominantly focused on examining the effect of the pore size, pore connectivity, nature of the active sites and their accessibility on the overall conversion of reactants and product selectivity.

2. Theoretical part

2.1. Zeolites: structure, history and use

A group of materials referred to as molecular sieves has attracted much attention, especially in the field of heterogeneous catalysis. Generally, molecular sieve is any solid material, which possesses a system of pores of a diameter comparable to kinetic radii of molecules. Certain materials, such as zeolites, possess periodically ordered pores, whereas in others (e.g. carbon materials, polymers) the pores are randomly oriented. Beyond that, composition of individual members of this group can differ (e.g. carbon materials, aluminophosphates, aluminosilicates or metal-organic frameworks), as well as their structure, morphology and crystallinity (e.g. microporous crystalline aluminosilicates – zeolites or mesoporous amorphous silica such as MCM-41). [2] The pore size can vary vastly, so the pores are classified depending on their size: macropores of a diameter larger than 50 nm, mesopores with a diameter between 50 and 2 nm and micropores with diameter smaller than 2 nm, including ultra-micropores with diameter smaller than 0.7 nm. [3]

Zeolites are one of the important subgroups of molecular sieves. They are a group of silicates, aluminosilicates and their derivatives which contain periodically ordered micropores within their crystalline structures. The size of the pores usually lies between 0.4 up to 1 nm depending on the exact topology of the crystalline structure. [1]

The zeolites have been known to humanity ever since the ancient Rome, where the zeolite-rich volcanic tuff was often used for building due to its relative softness and good heat insulation properties. [4] First scientific description of these materials comes from Swedish mineralogist Axel Cronstedt who also gave them the name “zeolites” (from Greek words *zeo* - to boil and *lithos* – stone, referring to their hydratation-dehydratation properties). However, the research had not proceeded until more advanced techniques of characterization such as x-ray powder diffraction and porosimetry were developed. The true interest in zeolites came in 1930s, particularly thanks to Richard M. Barrer et al. who set the groundwork for their synthesis method. Twenty years later faujasite-type zeolites found their first application in oil refining. In 1960s Mobil company introduced the concept of using organic cations for directing the zeolite synthesis towards specific crystalline phases. This led to discovery of new frameworks. Following milestones in zeolite science include the discovery of **MFI** zeolite in 1970s, aluminophosphate frameworks, titanosilicates, extra-large pore zeolites etc. Nowadays the research is mainly focused on hierarchical and layered zeolite materials. [5-7]

About 80 % of the commercially produced zeolites are used as ion exchangers. Zeolites with high aluminium content (ideally Si/Al = 1) are preferred for this application because such materials have higher ion exchange capacity than high silica zeolites. They are predominantly used as water softening additives in laundry detergents, adsorbing the "hard" Ca^{2+} ions and thus preventing precipitation of its insoluble salts. Another large scale use of zeolites is radioactive waste treatment, more specifically adsorption of the radioactive isotopes of caesium ions. High silica zeolites are on the other hand preferred in catalysis of fluid catalytic cracking (FCC) in oil refineries, biomass conversion and in recent years also in fine chemicals production. Natural zeolites cannot be used in chemical industry due to the presence of impurities and defects which could compromise the reaction pathway and product purity. Yet they find a wide field of use as nutrient release agents in agriculture or cement strength enhancers. [8]

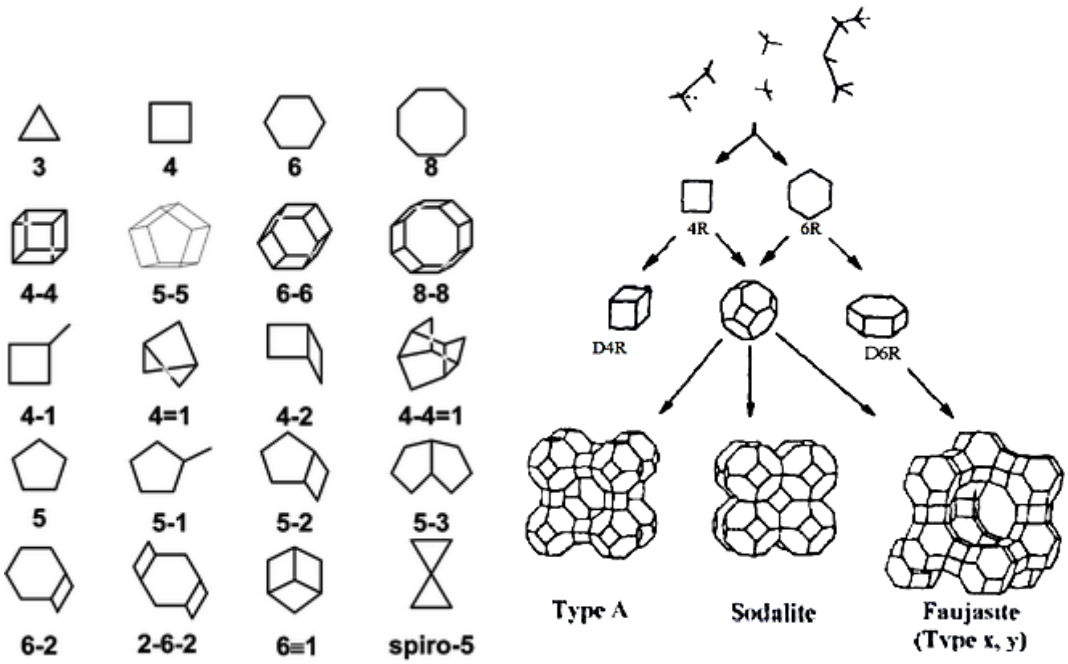

Figure 1: Examples of secondary building units (left) [9] and their location in the zeolite structure (right). [10]

The silicate tetrahedra are primary building units of the zeolite framework. Multiple tetrahedra are connected into larger objects, such as rings, prisms or more complex shapes, via oxygen atoms located in the corners. These are referred to the secondary building units (SBU), see Figure 1. The final zeolite framework is then formed by connecting multiple secondary building units of one or several types in an ordered manner. It is important to mention that the secondary building units are not necessarily real entities that can exist separately (like for example in the synthesis mixture). It is only a theoretical model used for describing the framework and to identify relationships between

different structures. To this day more than 250 framework types have been approved by the International Zeolite Association (IZA). [11] Although the exact topology of individual structures may vary, often similar behaviour has been observed for zeolites with comparable pore size. Therefore it is convenient to sort the structures on their pore systems. Most often the number of silicate tetrahedra which form the pore opening is used to describe the pore size. Zeolites with 8-ring pores with a diameter between 0.3 and 0.45 nm are referred to as "small pore zeolites", ones with 10-ring pores of a diameter 0.45 – 0.60 nm as "medium pore zeolites", frameworks with 12-ring pores of a diameter 0.60 – 0.8 nm as "large pore zeolites" and structures with 14-ring and larger pores as "extra-large pore zeolites". [12] The structures can also be divided depending on the number of dimensions their channels are oriented in. We distinguish one-dimensional zeolites (e.g. **MTW**, ***MRE**), two-dimensional (e.g. **UTL**) and three-dimensional (e.g. ***BEA**, **MFI**). The channels may intersect in multiple directions and sometimes form cavities at the intersections (e.g. in **FAU**, **LTA**) or pass each other independently (e.g. **YFI**). [1]

Framework density, which is defined as the number of tetrahedrally coordinated atoms (silicon, aluminium, titanium etc.) per 1 nm^3, is one of the main parameters for recognizing the material as a zeolite. For zeolite frameworks the value usually lies between 12.1 and 20.6 T/nm^3. Nonetheless, there are few exceptions such as the **RWY** structure with framework density 7.6 T/nm^3 or **IRR** with 11.8 T/nm^3. On the other hand frameworks like sodalite (**SOD**), with framework density 16.7 T/nm^3, are considered to be a zeolite despite having no micropores. [1, 13]

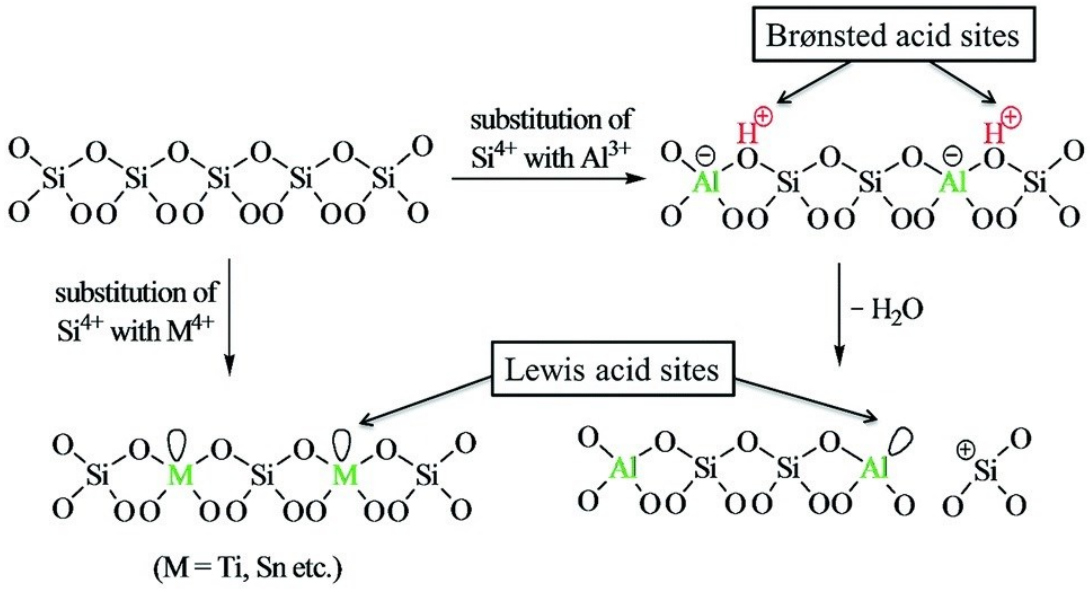

Figure 2: Types of acid sites within zeolite framework. [14]

Silicon atoms in the zeolite framework can be substituted with other elements, most usually by aluminium. Due to its lower oxidation number, compared to silicon, ($Si^{IV} \leftrightarrow Al^{III}$) aluminium introduces a negative charge to the framework. The charge needs to be compensated by an extra-framework cation such as alkali or alkaline earth ion, organic quaternary ammonium ion or proton. The protons form so called bridging hydroxyl groups (≡Si-(OH)-Al≡) that are Brønsted acid sites (Figure 2). They behave like catalytically active centres for acid catalysed reactions. Moreover, aluminium often causes a defect in the structure being bound only to three neighbouring silicon tetrahedra, keeping an exposed free orbital and thereby providing Lewis acidity (Figure 2). The presence of the charge in the framework is not only advantage for an application in catalysis, but also for ion exchange capability and tuneable hydrophilicity of the material. Depending on the aluminium content we distinguish between "low silica zeolites" with the molar ratio Si/Al lower than 2, "intermediate silica zeolites" with the Si/Al range in between 2 and 10 and "high silica zeolites" with Si/Al higher than 10. [13] The thermal stability of the structure increases (from about 700°C up to 1300°C) with increasing silicon content and at the same time the structure becomes more hydrophobic due to the lower charge. Also the number of acid sites and the extra-framework cations decreases with higher silicon content, however, the strength of individual acid sites increases. [12] Up to now two directly connected aluminate tetrahedra within the framework have not been observed. Therefore, the Si/Al ratio cannot drop below 1. This phenomenon is referred to as the Loewenstein´s rule [15] Additionally, other *p*-elements, such as phosphorus, germanium, gallium or tin, can be introduced into the structure instead of the silicon. Each of these elements offers new properties, including tuneable acid site strength and different framework stability.

Some *d*-elements can also take the place of silicon in the framework. Titanium is the one that probably attracts the most attention. Titanosilicates have been recognized as very good catalysts for oxidation reactions in the presence of hydrogen peroxide. Such reactions include hydroxylation of aromatic molecules, epoxidation of alkenes. [16, 17] Although, the structures of titanosilicates correspond to their aluminosilicate counterparts their chemistry is immensely different. Unlike silicon or aluminium the titanium usually prefers octahedral coordination, which unfortunately is not very catalytically active in the structure, because the octahedrally coordinated titanium is almost completely shielded by the silicate tetrahedra. Furthermore, the preparation of titanosilicates is way more difficult compared to silicates or aluminosilicates, especially due to the fondness of titanium to polymerize and to form titanium oxide phase. [18] The synthesis conditions need to be more specific if the element is to be successfully incorporated into the framework. Nevertheless, properly synthetized titanosilicates exhibit purely Lewis acidity due to the free orbital located on titanium atom. [19]

2.1.1.MTW

The framework of **MTW** zeolite contains one-dimensional 12-ring channels (Figure 3). [1] Usually, this zeolite can be prepared in high silica composition with the lowest Si/Al ratio of 31. [20] The **MTW** zeolite was first synthetized in the Mobil Oil laboratories in 1974 using synthesis mixture containing tetraethylammonium cations. [21] Later it was discovered that use of other tetraalkylammonium ions (e.g. methyltriethylammonium) can lead to formation of the structure as well. [22]

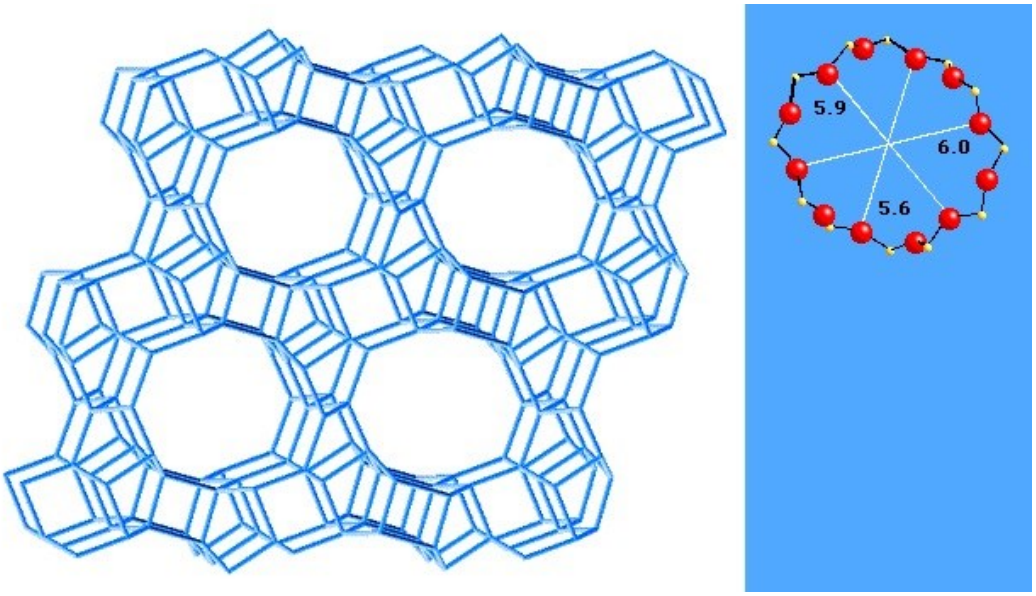

Figure 3: The **MTW** structure (left) and the diameters (in angstroms) of the 12-ring channel (right). [1]

The discovery of a synthetic route of **MTW** without the need of organic additives was a great success. The omission of organics by using only **MTW** seed crystals made the preparation significantly cheaper, enough to be industrially applicable. Hence, the zeolite was employed in few industrial processes as catalyst for hydrocracking, aromatic alkylation or isomerization. [23-25]

2.1.2.*BEA

The framework of zeolite ***BEA** is made of so called [5^4] units (two pentagons sharing one edge and connected by oxygen bridge in corners opposite to the shared edge). These units are connected via 4-rings forming layers with 12-ring holes (Figure 4). Assembly of these layers forms the three-dimensional structure with the neighbouring layers related by 90° rotation. However, the direction of the rotation (clockwise/counter-clockwise) is usually random throughout the framework, thereby making the structure distorted. This feature is marked by the asterisk (*) before the three-letter

code. [8] The phenomenon can be observed by a broad peak in the powder x-ray diffraction patterns in the low angle region. Surprisingly, the impacts on the catalytic behaviour are insignificant. [26] The distorted ***BEA** structure can be described as a combination of two borderline structures, polymorphs. In the structure of the polymorph A all the layers are related by 90° clockwise rotation whereas in the polymorph B by counter-clockwise rotation. As a result these two structures are chiral and could introduce a new type of shape selectivity. Nevertheless, neither of these two polymorphs has been prepared in their pure form yet. [27] Another structure called polymorph C, where the relation between adjacent layers alternates regularly between clockwise and counter-clockwise rotation, has been successfully prepared in a form of germinate. As this structure is not distorted anymore it is recognized as an independent framework type marked **BEC**. [28] Zeolite ***BEA** is widely used in the chemical industry, most notably in alkylation and trans-alkylation processes. [29]

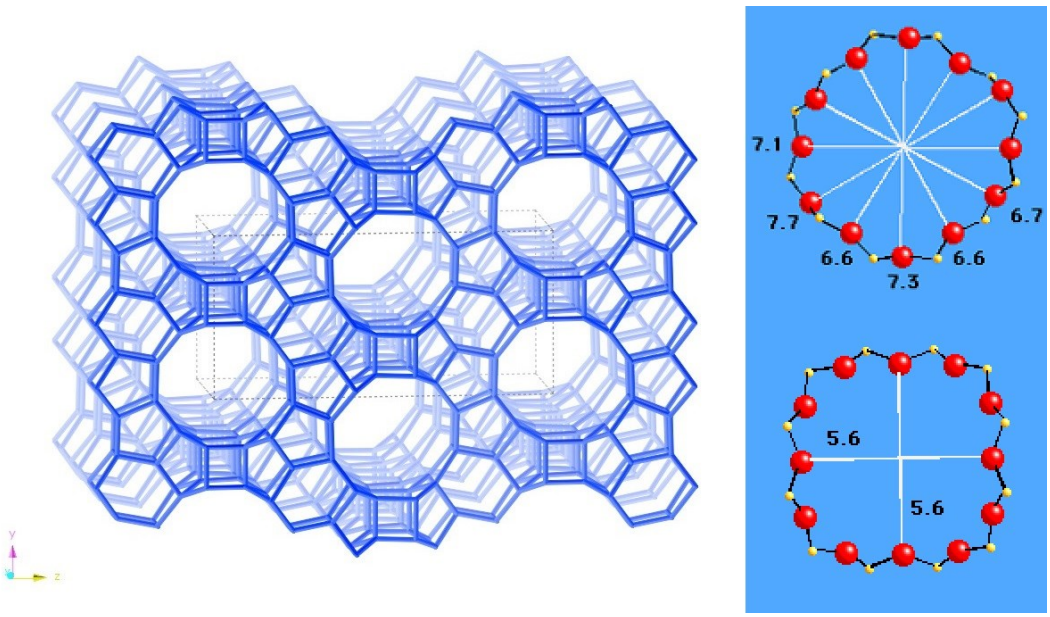

Figure 4: The ***BEA** structure (left) and the diameters (in angstroms) of the 12-ring channels (right). [1]

2.1.3.MFI

The **MFI** structure is one of the most important zeolites from the industrial point of view. Its framework is composed of pentasil units linked to chains. These pentasil chains are connected via oxygen bridges to form sheets with 10-ring holes. Such layers, related by inversion, are linked by oxygen bridges to form a three-dimensional structure with interconnected 10-ring pores (Figure 5). The same layers can also be related by mirroring, thus forming the **MEL** structure. Due to their similarities, sometimes an unwanted intergrowth of these two structure types can be observed. [8]

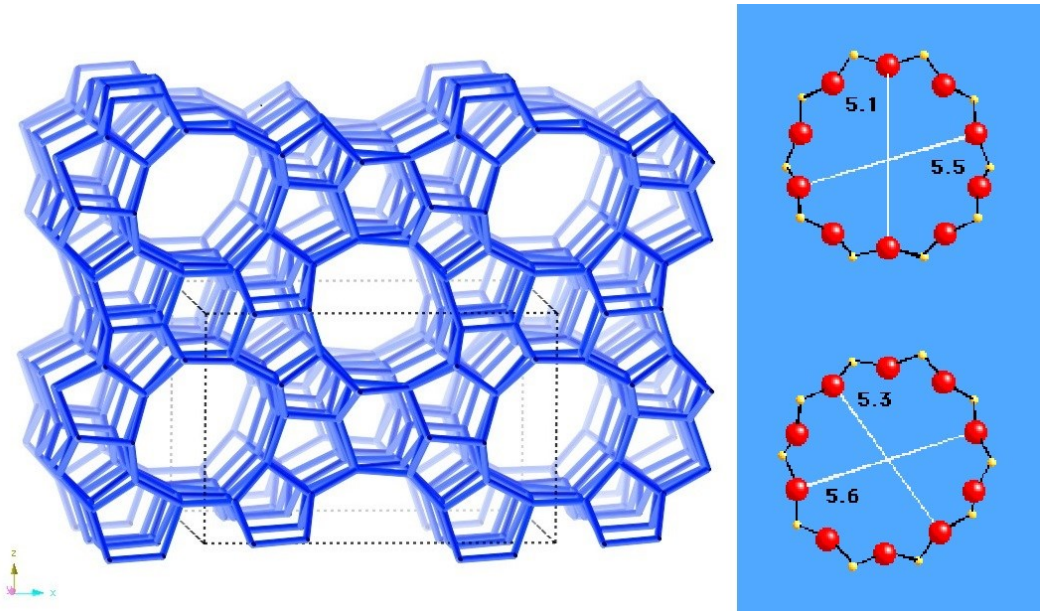

Figure 5: The **MFI** structure (left) and the diameters (in angstroms) of the 10-ring channels (right). [1]

The discovery of **MFI** zeolite has become a milestone in the synthesis of zeolites. It has been used mainly in the petrochemical industry due to its good sorption and catalytic properties. It became popular especially due to its 10-ring channels which offer different shape selectivity than, up to that time, widely applied faujasite (**FAU**, 12-rings). It was also the first high-silica zeolite synthesized without the use of organic templates. [30]

Zeolites with the **MFI** structure have been studied and successfully prepared in variety of composition. Except the pure silicate and aluminosilicate form its titanosilicate analogue, TS-1, has attracted its fair share of attention. TS-1 was first prepared in 1983 by M. Taramasso. [31] It turned out to be a very good catalyst for oxidative reactions, igniting an interest in titanosilicates and their catalytic properties. Today the TS-1 is produced commercially. [19]

2.2. Principles of synthesis

Hydrothermal synthesis is the most common approach for the preparation of zeolites. Most of the known zeolites can be obtained by this process. The principle of this method is the crystallization of the zeolite from an aqueous solution of silicon and aluminium sources at high temperature (between 100 and 200°C) and pressure. [12] These conditions alter some physico-chemical properties of the components in the mixture. At higher temperatures, the reactivity of the compounds increases, the solubility of the individual substances changes and also the viscosity of the water decreases, thereby increasing the mobility of the ions. [32] The required pressure is achieved by heating the closed reaction vessel properly filled with the synthesis mixture (filling

usually up to 50 to 80% of its volume). The vessel has to be able to withstand a high autogenous pressure. Therefore, steel autoclaves with a Teflon lining are usually used. The Teflon liner prevents corrosion of the autoclave, sticking of a product on the walls while being resistant to high temperatures and it does not interfere with the reaction mixture.

The process of formation of a zeolite structure is a complicated combination of continuous dissolution, precipitation, polymerization, de-polymerization, nucleation and crystallization. It is still not fully described due to its complexity and difficulty of characterizing the synthesis mixture *in-situ*. [33] Nevertheless, several factors are well-known and described to have an essential impact on the outcome and they are discussed below.

Different sources of silicon, aluminium and other elements may affect the final product morphology or synthesis time due to differences in their solubility and reactivity, caused for example by the surface area. More easily soluble chemicals saturate the solution faster, which results in faster nucleation and generally smaller crystal size. [34]

The molar ratio of silicon and aluminium (or other element), Si/T, plays an important role in the structure and crystallinity of the product and is crucial for its stability. Only few zeolite structures exist in a very wide range of Si/T (e.g. **MFI** 15 - ∞) and none has been prepared in the whole range so far. Most zeolites crystalize only within a specific window of Si/T ratios. It is also important to mention that the Si/T molar ratio in the synthesis mixture is not always the same as the Si/T molar ratio of the product. These values may vary significantly depending on the structure, compound and a chemical source. [35]

Solvent content, usually water, directly affects the concentration of other compounds. Higher water content in the mixture decreases the concentrations of reactants, resulting in a lower number of nucleation centres. The final product is consequently mostly formed by larger crystals. On top of that water interacts with other inorganic and organic compounds in the mixture, which together help to stabilize the resulting structure and direct the reaction towards the desired product. [33]

Alkali hydroxides are used as **mineralizing agents** in the synthesis mixture in most cases. The hydroxyl anions hydrolyse the silanol groups and separate the siloxane bonds, thereby increasing the solubility of the silicone source and enabling the crystallization. The solubility of the silica increases with increasing hydroxyl ion content, while the solubility of the aluminium sources remains approximately constant. [33] Thus, with the increasing pH value, the aluminium content of the final product increases. As some types of structures prefer smaller amounts of aluminium in the crystal framework, it is not suitable for them to be prepared at high pH. In such cases, fluoride ions can be

used as the mineralizing agent. Also organic molecules present in the mixture are more stable at lower pH. On the other hand, a strongly alkaline environment and high synthesis temperatures may lead to decomposition of organic structure-directing-agents by Hoffman degradation.

Most zeolite syntheses are carried out in basic environment, which is achieved by addition of an alkali metal hydroxide to the reaction mixture. The **charge balancing cations** also have their purpose in forming structural units. It is believed that a solvation shell of water molecules is formed around the cations. The water molecules are then replaced with silicate or aluminate tetrahedra, which connect together into larger building units. [36] The choice of the cation is also important. Some structures are formed exclusively in the presence of sodium cations (e.g. **FAU**, **LTA**, **MTW**), some prefer potassium ions (e.g. **TON** or **KFI**) and some occur in environments containing both cation types (e.g. ***BEA**, **FER** or **OFF**).

Successful synthesis of most known zeolite structures is achieved by addition of so called **"structure-directing agent"** (SDA). This term is used for organic cations like tetraalkylammonium halides or hydroxides. They facilitate the crystallization process of a particular structure. The SDA molecules organize silicate tetrahedra by weak inter-molecular interactions and give rise to certain building blocks. [37] The process is not equivalent to the templating effect though. There is a correlation between the SDA size and the diameter of the pores; nevertheless, the shape of the SDA molecule does not exactly match the shape and orientation of the pores and cavities. Typically, under different conditions, one SDA can be used to synthesize several structures, for instance zeolites ***BEA**, **MTW**, **FAU** and **EMT** can be prepared using tetraethylammonium cations. [38] On the contrary, the same structure can be prepared using various organic molecules, e.g. zeolite **UTL** can be prepared with more than 10 different SDAs. [39] SDA molecules remain entrapped within the structure after the synthesis and need to be removed by high temperature treatment. The calcination is usually performed in a temperature range between 450 and 600 °C and in air, nitrogen or oxygen atmosphere.

Temperature Is the last major factor that impacts the synthesis of a zeolite. It is important to highlight that zeolites are not thermodynamically stable phases, only metastable. Hence, a particular structure can only be observed within a certain temperature range and time interval before more stable and usually denser phases (e.g. cristobalite, quartz) are formed. [33] It is essential to cool the autoclave down rapidly after the required synthesis time to avoid recrystallization of the product to more stable structures.

2.2.1. Synthesis of hierarchical zeolites

As mentioned in Section 2.1 the molecular sieves can be generally divided into macroporous, mesoporous and microporous materials. The pore size determines the maximum size of molecules which can enter the channel system as well as the rate of diffusion. Zeolites fall within the microporous category. The narrow size of the pores provides zeolites with their product and reactant shape selectivity in catalysis, because only molecules of certain size can enter or exit the channel system. At the same time small channel diameters limit the diffusion rate of both reactants and products and thereby leaving a portion of the active sites located deeper inside the crystal unused. In order to overcome this drawback the research has been focused on synthesis of hierarchical zeolites. Materials defined by at least two different pore sizes can be viewed as hierarchical. [40] In the case of zeolites we usually use that term for micro-mesoporous structures. Although it is not always the case by the definition, interconnectivity of the two pore types is crucial for any potential application. The advantages of the hierarchical materials include catalysis of reactions with bulky molecules and shorter diffusion path length which closely correlates with the reaction rate. [40]

There are several general methods that can be used to introduce mesopores into a zeolite structure. Most of them can be sorted into one of two groups: “bottom-up” where the hierarchical material is prepared directly or “top-down” where the additional mesoporosity is introduced into a bulk sample post-synthetically. Other options include partial crystallization of amorphous silica-alumina material (e.g. MCM-41 or SBA-15) or seeding the surface of the mesoporous matrix with zeolite crystals. [41]

2.2.1.1. „Bottom-up“

All of the above mentioned methods require multiple synthesis steps to prepare the hierarchical material (including at least the synthesis of the parent bulk zeolite and its subsequent treatment and calcination). But there are also other approaches where the micro-mesoporous structure can be formed directly. **Hard templating** is probably the simplest method. The method uses solid particles for displacement of the growing crystals to form mesopores. It is required of the particle material to be stable during the whole synthesis and do not interfere with the reaction mixture. In most cases carbon nanoparticles or nanorods are added to the synthesis gel and the crystallization is carried out as usual. [40] The carbon particles become trapped by the growing zeolite crystals and act as mechanical obstacles for the crystal growth. When the synthesis is completed the carbon remains in the zeolite until it is removed by calcination along with the SDA and then leaves empty space in the

crystals. The size of the mesopores is directly controlled by the size of the particles. Except carbon other materials like for example polystyrene beads may be used as well. [40, 42]

Soft templating method uses specially designed structure directing agents to introduce the mesoporosity into the final product. The SDA molecule always consists of two parts: hydrophilic part and hydrophobic chain. The hydrophilic part is usually made of multiple quaternary nitrogen atoms connected via short chain (about 6 carbon atoms long) and plays the role of typical structure directing agent. The hydrocarbon chains (12 to 22 carbon atoms long) tend to accumulate and form micelles due to their hydrophobic nature. This way the crystal growth is inhibited in the direction of the chains and it leads to a structure composed of nano-sized aggregates and possibly intergrown thin nanocrystals with large external surface. [43, 44] The high external surface area not only makes the catalytically active sites more accessible but also limits the deactivation of the catalyst caused by coke deposition. [45, 46] Much effort has been put into studying these special structure directing agents in order to prepare materials of different morphologies and properties. Some of the examples include molecules with multiple hydrocarbon chains [47], other type possesses additional organosilane group at the hydrophilic end, which becomes directly attached to the zeolite during the synthesis. [48] Some SDAs even take the advantage of π-π interactions between aromatic rings to position the SDA molecules in a particular order to prepare well organized self-pillared mesostructures. [49]

2.2.1.2. „Top-down“

“Demetallation” is a very promising method for introduction of mesoporosity into zeolite crystals. Its concept is based on selective removal of particular element from the framework, which leads to creation of defects and thus additional porosity. The demetallation is very popular due to its relative simplicity and ability to control, to a certain extent, its rate by various factors such as temperature or concentration of the treatment solution. [50, 51]

Dealumination is the first example. Low-silica zeolites are unstable under acidic conditions. However, zeolites with higher silica content can sustain their structure during the treatment. [52] The removal of aluminium leads to formation of mesopores and improved thermal stability of the low-silica frameworks. At the same time, with the decrease of the aluminium content the concentration of acid sites decreases as well. The main reason why the dealumination is not suitable for introduction of mesoporosity in high silica zeolites is the low aluminium content which leads to poor interconnectivity of the pores. Instead, closed cavities inside of the crystal are often created. Needless to say such cavities cannot contribute to accessibility of the active sites at all. [40]

Dealumination can be performed both in solution, using various types of inorganic and organic acids, or in gas phase by steaming, which is used mainly in industrial processes. The method can be altered to create high silica zeolites which would be difficult to obtain by conventional synthesis. In such cases the dealumination is carried out in the presence of silicon tetrachloride and the aluminium is immediately replaced by the silicon atoms. [53]

Similar post-synthetic modification is **desilication**, the treatment of a zeolite with base solution. The method is more appropriate for creating mesopores since silicon is the prevalent type of T-atom in the zeolite framework. Depending on the Si/Al ratio the desilication proceeds with different rate. Structures with Si/Al higher than 50 dissolve nearly uncontrollably, whereas, desilication of zeolites with Si/Al between 50 and 25 leads to formation of mesopores in their structure. When the aluminium content is even higher, the desilication almost does not progress, as the silicon tetrahedra in direct connection to aluminium are not affected by the base. [5, 54] Only when the degree of the desilication exceeds certain level, the aluminium is extracted from the framework and tends to deposit on the crystal surface species along with fragments of the dissolved framework. This extra-framework species can be removed by subsequent washing with acid solution. [40] Either way, the procedure often leads to a wide distribution of mesopores. In order to better control the pore size distribution a method which utilizes so called pore directing agents (PDAs) was developed. [55]

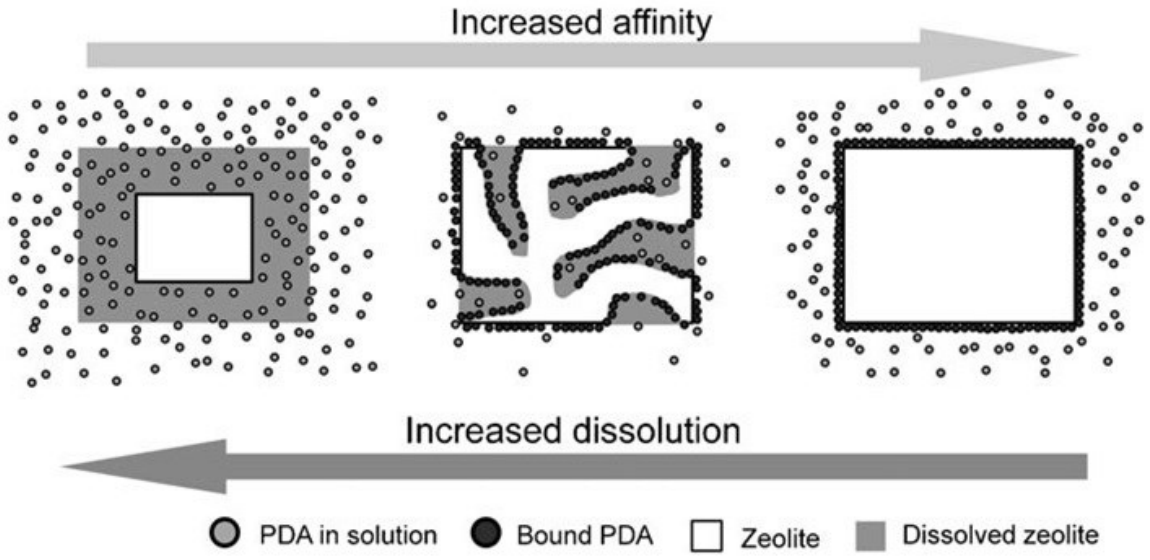

Figure 6: Adsorption of the pore directing agent on the zeolite crystal during desilication and the impact of dissolution of the crystal. [55]

These molecules, usually tetraalkylammonium hydroxides, are added to the basic solution and during the treatment, adsorb on the surface of the crystal and protect it from dissolution. This results in narrower pore size distribution in the final sample. Depending on the PDA concentration the effect may prevent the desilication completely (in Figure 6, the right picture). Also it allows the desilication of high-silica zeolites to proceed in a controlled rate when only portion of the crystal surface is being protected by the adsorbed PDA molecules (Figure 6, the middle picture). [5]

2.2.2. Acidity modification

As stated earlier, the silicon in the framework can be replaced by another element (e.g. aluminium, germanium, gallium) without altering the crystalline structure. This process is called isomorphous substitution. By replacing the silicon atom we can tune the physico-chemical properties of the material. For instance, many zeolites exhibit different stability depending on the substituted atom. Typical example are the extra-large pore zeolites (larger than 14-ring pores), which are usually more stable in the form of germanosilicates or gallosilicates rather than aluminosilicates. Another important aspect of the substitution is the possibility of introducing negative charge into the framework by replacing the silicon with an atom in lower oxidation state (B^{3+}, Al^{3+}, Ga^{3+}, Fe^{3+} etc.). As a result, the negative charge of the framework needs to be compensated by an extra-framework cation. This gives the zeolite its ion-exchanging and catalytic abilities. Moreover, the silicon can be replaced by an element with free orbitals (Ti^{4+}, Zr^{4+}, Sn^{4+}). These substituted atoms provide the framework with Lewis acidity. [56, 57]

Isomorphous substitution can be performed directly by changing the synthesis mixture and adding or replacing sources of required elements. However, this method may not be suitable for all cases. As mentioned above, certain structures prefer specific elemental composition of the synthesis mixture in order to successfully crystalize. In such cases the substitution can be carried out post-synthetically by extracting one element from the framework and replacing it with another one. Good example may be the extraction and replacement of boron by aluminium, gallium or titanium [58] or replacement of germanium by aluminium in zeolites **UTL**, **IWW** or **UOV** and their further use in catalysis. [59-61]

There are several factors influencing the success of the isomorphous substitution. The ionic radii ratio of the silicon and the substituent is possibly the most important factor. It is required to be lower than the maximal acceptable value (see formula (1) [62])

$$\Delta r / r_{Si} < 0.15 \qquad (1)$$

With increasing difference of ionic radii (Table 1) the substitution becomes energetically less favourable. Similarly the electronegativity ratio of given elements influences the substitution. Several more rules can be observed, such as the ion being more easily incorporated into the framework if it leads to a decrease of its coordination number. [62]

Table 1: Electronegativity and ionic radius of the most common substituent ions in zeolite frameworks.

	Si^{4+}	Ge^{4+}	B^{3+}	Al^{3+}	Ga^{3+}	Ti^{4+}
Electronegativity	1.90	2.01	2.04	1.61	1.81	1.54
Ionic radius (Å)	0.26	0.39	0.11	0.39	0.47	0.42

MFI zeolite is a good example to show the effect of the substitution on the stability of the structure as well as the requirements for its synthesis. Although the aluminosilicate **MFI** can be easily prepared under relatively broad range of conditions, its titanosilicate analogue, TS-1, requires a very specific synthesis gel composition. Usually titanium(IV)ethoxide is used as the titanium source. Crucial point of the synthesis is the requirement for the mixture being free of any alkali metal cations. Therefore, alkali hydroxides cannot be used for introducing the hydroxyl ions to the mixture. Instead they need to be added in the form of counter-ions of the SDA, such as tetraethylammonium hydroxide. [18] Using fluoride media for the synthesis is also not recommended. It was observed to lead to a formation of extra-framework octahedral titanium species. It causes reduced yields in epoxidation catalysis as octahedral titanium centers decompose the hydrogen peroxide during the catalysis.

Ions in lower oxidation state introduce negative charge into the framework, which is balanced out by cations located in the extra-framework positions, held by ionic interactions. The nature of the cations can vary from alkali or alkaline earth metal ions, tetraalkylammonium ions to rare earth metal ions and their complexes. The nature of the ion can significantly impact the properties of the material. Most notably in catalysis where mainly zeolites in protonated form are used as acid catalysts with Brønsted acidity. Ion exchange has another practical application in liquid and gas separation. By exchanging the molecular sieve into different ionic form we can tune the pore size to separate given molecules more efficiently. Good examples are the 5A, 4A and 3A molecular sieves, used in gas chromatography or as drying agents, which all have the structure of A-type zeolite (LTA) but exchanged to Ca^{2+}, Na^{+} and K^{+} forms, respectively. This is very important from the industrial perspective because it enables preparation of materials with different properties from one zeolite

structure by relatively simple procedure. [56] Furthermore, due to its flexibility the zeolite framework itself can be affected by exchanging it into another ionic form. Gismondine, one of the most flexible structures, is known to shift between three types of deformed structure with different symmetry depending on the water content and type of extra-framework cation. [63] Not every cation can be exchanged into the extra-framework positions though. Depending on its size and the size of the micropores some cations either cannot be introduced into the pores at all or the ion exchange is only partial due to high diffusion limitations. This is referred to as the "ion sieving" effect. [64]

2.3. Zeolites in catalysis

The application in acid catalysis is the most studied side of zeolite science. Their main use resides in the oil refining where they replaced the previously used silica-alumina based catalysts in the fluid catalytic cracking (FCC) process. Namely the Y type zeolite (**FAU**) is used along with **MFI** additive which improves the resulting hydrocarbon chain-length distribution. Besides the FCC process zeolites are also used for the isomerization of light gasoline, hydrocracking of heavier fractions, dewaxing and isomerization of xylenes. [65, 66]

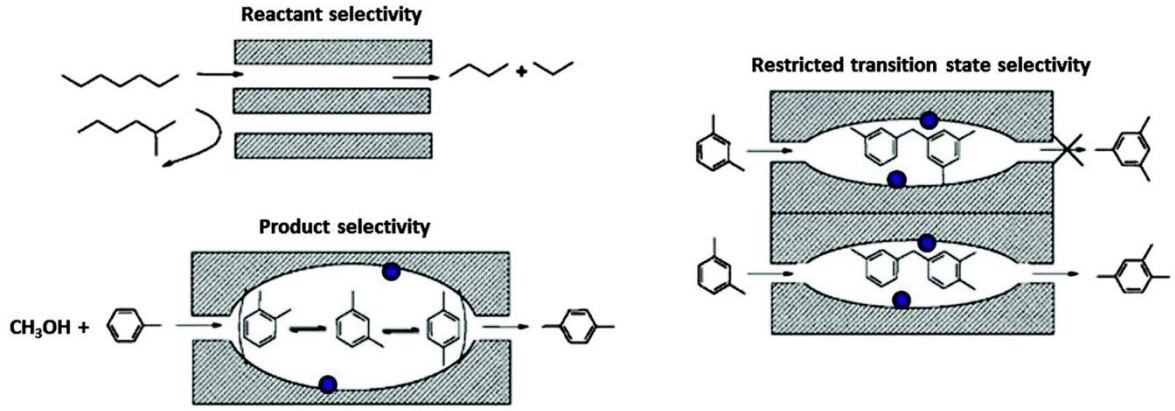

Figure 7: Types of shape selectivity. [67] (blue dots represent the active sites within the framework)

The popularity of zeolites in catalysis lies in combination of their two important properties: a tuneable strength of the acid sites and shape selectivity of the porous framework. Due to the pore diameters being close to kinetic radii of certain molecules, diffusion of larger molecules (with respect to the pore size) in or out of the channel system is limited or completely prohibited, which is referred to as mass transfer shape selectivity (or product/reactant selectivity). The framework also imposes steric constraints onto the transition state, making some of the intermediates energetically more favourable and thus promotes formation of specifically shaped products and suppresses

formation of bulkier side-products. Proper choice of the size and shape of the pores can be used to direct the reaction towards the desired direction or distribution of product molecule sizes (e.g. chain-length distribution in FCC). [68-70] On top of that there are considerable advantages of using zeolite based catalysts in comparison with commonly used homogenous catalysts such as mineral acids. Zeolites are solid, crystalline, and therefore easier to handle, store and separate from the reaction mixture. They can also be regenerated and used repeatedly. Unlike the inorganic acids the zeolites are not corrosive and thus cheaper, easier to use and present lower threat to the environment.

In recent years zeolites have also found applications in catalysis of organic synthesis and preparation of fine chemicals. [71] Background and importance of several such reactions that have been investigated in this study are discussed in the following chapters.

2.3.1.Tetrahydropyranylation of alcohols

Essential part of organic synthesis is protection of certain functional groups between individual steps to prevent generation of unwanted side-products and preserve particular functional groups in harsh environment in which they would otherwise not be stable.

Tetrahydropyranylation is used for protecting hydroxyl groups by acid catalysed reaction of given alcohol with 3,4-dihydro-2H-pyran forming an ether (Figure 8). Use of tetrahydropyranylation has many advantages, namely high stability of the product in basic environment, resistance to reducing and alkylating agents as well as organometallic compounds like Grignard reagents. On top of that the reaction is relatively simple. The reaction of alcohol with dihydropyran can be performed between room temperature and 60°C using dichloromethane, dioxane, hexane or even dihydropyran itself as a solvent. [72] After finishing the reaction, the tetrahydropyranyl groups can be deprotected again by acid catalysed hydrolysis or alcoholysis, depending on the chosen product. One possible drawback of the reaction is formation of diastereoisomers when protecting alcohols which already contain chiral centres. Tetrahydropyranylation is often used for example in chemistry of biomolecules such as carbohydrates, steroids or nucleotides, which are generally quite bulky molecules. [73]

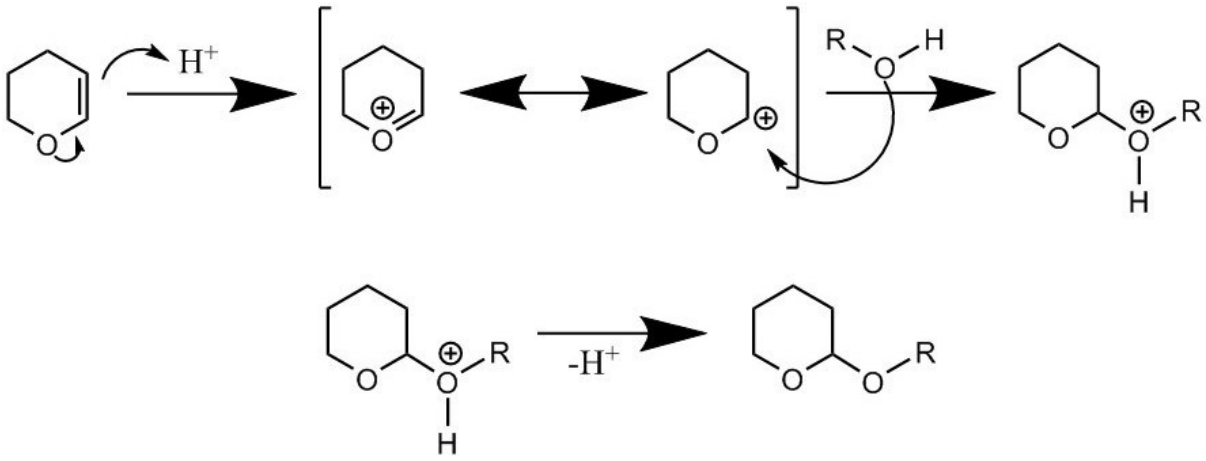

Figure 8: Mechanism of tetrahydropyranylation of alcohol (re-drawn from [73]).

As described in the literature tetrahydropyranylation can be catalysed both by Brønsted and Lewis acids. The Lewis acid based catalysts generally provide milder reaction conditions, however, the large quantities of the catalyst are usually required in order to achieve reasonable conversions. [72] The tetrahydropyranylation has been often successfully carried out using various inorganic acids, heteropolyacids or complex organic catalysts. [74-76] Still, usage of mentioned materials comes with several disadvantages. The reaction conditions may be too harsh for more sensitive substrates or functional groups, the catalysts are often toxic, corrosive, costly to prepare and generally have negative impact on the environment. Zeolites, on the other hand, are nature-friendly, allow protection of more sensitive molecules due to milder reaction conditions and above that they exhibit the shape selectivity for products and reactants. [77, 78]

2.3.2.Pechmann condensation of phenols

Coumarin and its derivatives are a group of lactones with an aromatic ring directly connected to the main lactone cycle. Many of them occur in nature but also are prepared synthetically as intermediates in pharmaceutical, agrochemical and fragrance industries. Some of their applications include enzyme inhibition, reducing inflammation, use as insecticides and antioxidants. There are several methods for coumarin preparation, such as Perkin [79], Reformantsky [80] or Wittig [81] reactions. Pechmann condensation is a reaction that attracted probably the most attention. Here the coumarin is prepared in relatively simple manner by acid catalyzed reaction of some type of activated phenols, depending on the desired product, with β-ketoester. Despite the reactions popularity its mechanism is not fully understood as no intermediates were successfully observed so far. [82] Most research papers agree on the mechanism consisting of three steps: transesterification, electrophilic aromatic substitution and dehydration. Different sources suggest different order of the

three steps but the sequence of electrophilic aromatic substitution followed by transesterification and finally dehydration (illustrated in Figure 9) is presumed to be the most probable one. [82, 83]

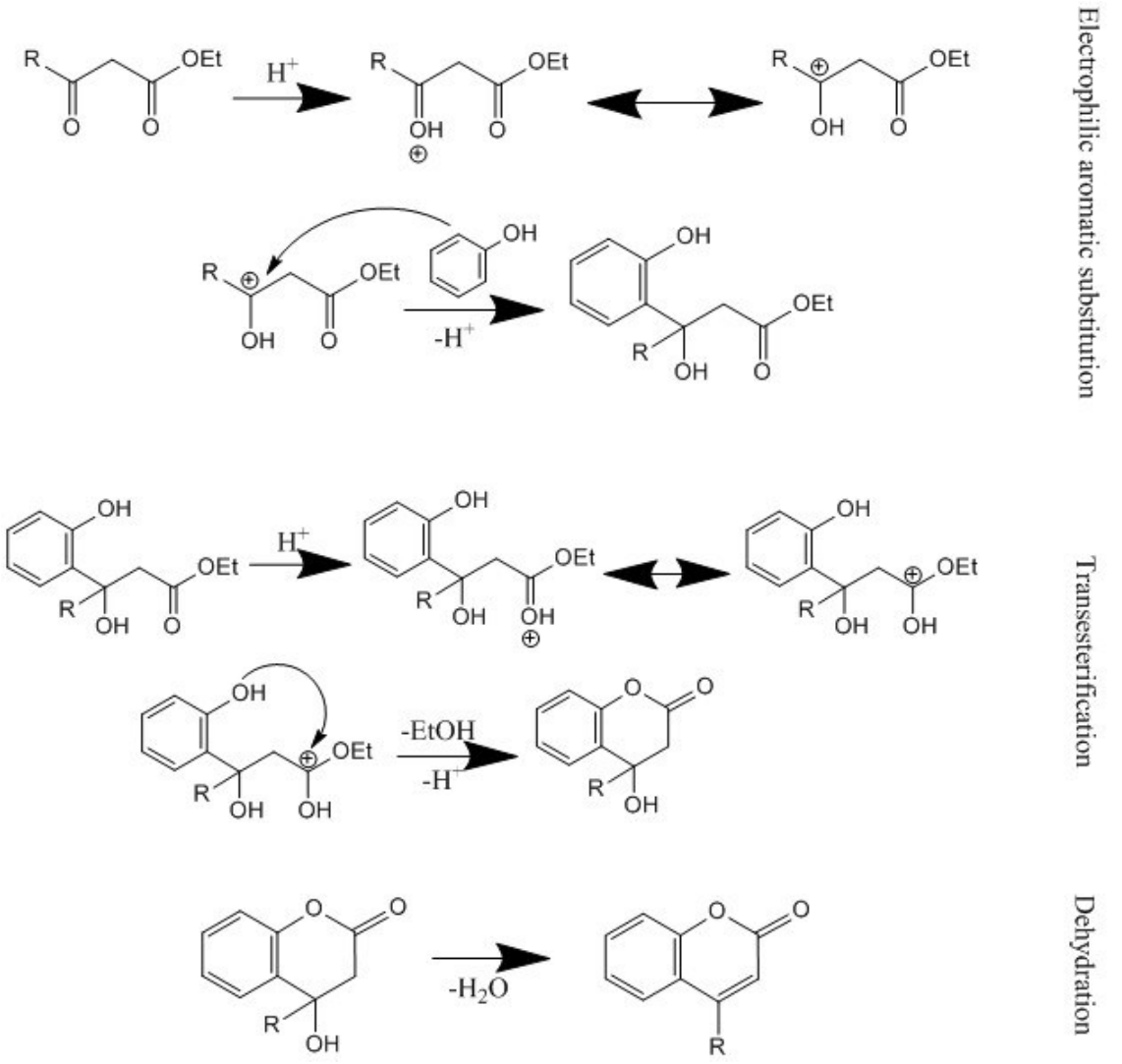

Figure 9: Possible mechanism of Pechmann condensation (re-drawn in accordance with [82, 83]).

In the past strong inorganic and organic acids were used as homogenous catalysts for the reaction. [84, 85] However, their application is far from optimal due to their corrosive properties, large quantity requirements and their difficult separation. On the contrary, heterogeneous solid catalysts, such as zeolites, possess many advantages compared to the mineral acids (as widely discussed in 2.3). Except for their easier and safer usage zeolites were reported to give reasonable conversions in lower quantities and work under milder conditions which limit unwanted consecutive reactions of the product. [86, 87]

2.3.3.Madon-Boudart test

The catalytic tests give us important parameters like conversions of reactants, yields of products, selectivity and reaction rate. In order to compare results of multiple experiments the parameters need to be normalised either by the mass of the catalyst, its surface area or amount of the active sites. Moreover, the conditions such as temperature or concentration of the reactants have strong influence on the rate of the reaction or selectivity.

The rate of a reaction can be influenced not only by the concentration and strength of active sites of the catalyst but also by the rate of diffusion of reactants and products. While external diffusion can be eliminated by proper stirring of the reaction mixture, internal diffusion, diffusion into the catalyst's pores, is linked to textural properties of the material itself.

The purpose of the Madon-Boudart test is to determine whether the internal diffusion affects the overall reaction rate. The test is carried out by performing a set of catalytic experiments on multiple catalysts with the same crystal morphology, structure and porosity, but different concentration of active sites. Ideally, when the reaction rate is not affected by the diffusion, the reaction rates should be linearly dependent on the concentration of active sites. [88]

2.4. Methods of characterization

In order to properly characterize prepared materials (in a powder form) a combination of several methods is required. These methods can provide an insight on the morphology, crystallinity, porosity, acidity and chemical composition of the samples.

2.4.1.X-ray diffraction (XRD)

Many properties of zeolites are highly dependent on their structural topology. Determining the structure is therefore a key step of the characterization. The likely fastest and certainly most common method is the x-ray powder diffraction as most of synthetic zeolites are prepared in a powder form.

X-Rays, Röntgen radiation, are electromagnetic waves with the wavelength in between 0.01 and 10 nm. Unlike visible light or electron beams the x-ray radiation cannot be focused by any optics due to its refractive index being close to one. However, the radiation can interact with matter, more specifically with the electrons. Upon the contact with the material, absorption or scattering of the radiation occurs. Atoms in different position within the sample cause scattering with a different phase shift, which results in an interference of the radiation (Figure 10). This phenomenon is called

diffraction and can be used to acquire the information about electron density and from that the actual structure of the material. [89]

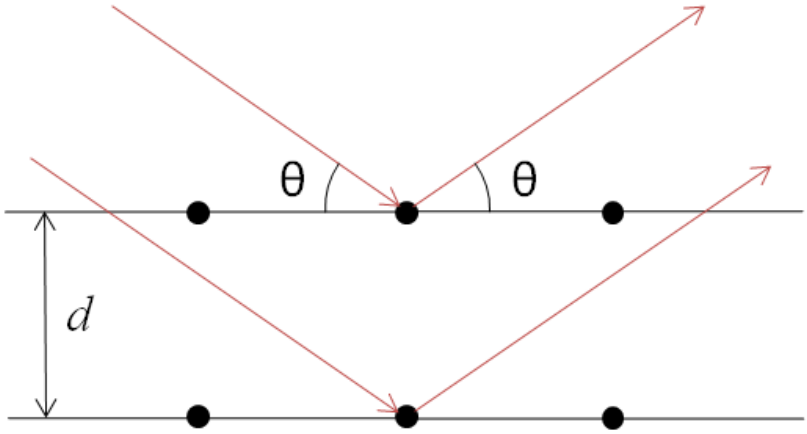

Figure 10: Diffraction x-ray radiation on crystal planes.

Crystalline materials, including zeolites, diffract incoming radiation. The radiation of the wavelength λ is scattered by a row of atoms equally displaced with the distance *d*. If the path difference is an integer number of the wavelength the constructive interference occurs. This is summed up by the Bragg equation (2), where θ is the impact angle of the radiation, λ is wavelength of the radiation, *d* is the distance between two planes and *n* is the order of the diffraction.

$$2dsin\theta = n\lambda \qquad (2)$$

Single crystal diffraction is one of the techniques. The crystal is placed into a holder and rotated in the x-ray beam giving a pattern of diffraction spots. Although the obtained pattern contains all the information needed to solve the structure, the method is not widely used in the zeolite science. The main problem is the crystal size. Zeolites rarely grow as crystals larger than few micrometers, which is not suitable for the single crystal measurement. On top of that one crystal is not necessarily a good representation of the whole sample. Due to these reasons the powder x-ray diffraction is used more often. Here, the sample powder is composed of large number of small crystals with random orientation in relation to the x-ray source. Thus, the diffraction spots overlay into a set of concentric circles, from which the diffraction pattern can be extracted as a dependency of intensity of the diffraction on the θ angle (usually depicted as 2θ angle). The overlap of the diffraction spots may complicate the assignment of diffraction intensities to the specific structural planes and thus make the structure solving difficult. The diffraction pattern, however, can be viewed as a "fingerprint" of the structure and used to identify multiple phases in the sample. [89]

2.4.2. Fourier transform infrared spectroscopy (FTIR)

Energy corresponding to the changes of molecular vibrations (fluctuations of molecular bond lengths and angles) falls into the infrared region of electromagnetic radiation. Vibrations accompanied by a change of dipole moment of the molecule can be observed by the infrared spectroscopy. Frequency of any vibration differs with the mass of the vibrating atom or group and is also affected by its weak interaction with the surroundings (solvent, other atoms in its proximity etc.). Due to this phenomenon infrared spectroscopy can be used to identify functional groups in a sample and to get information about its structure.

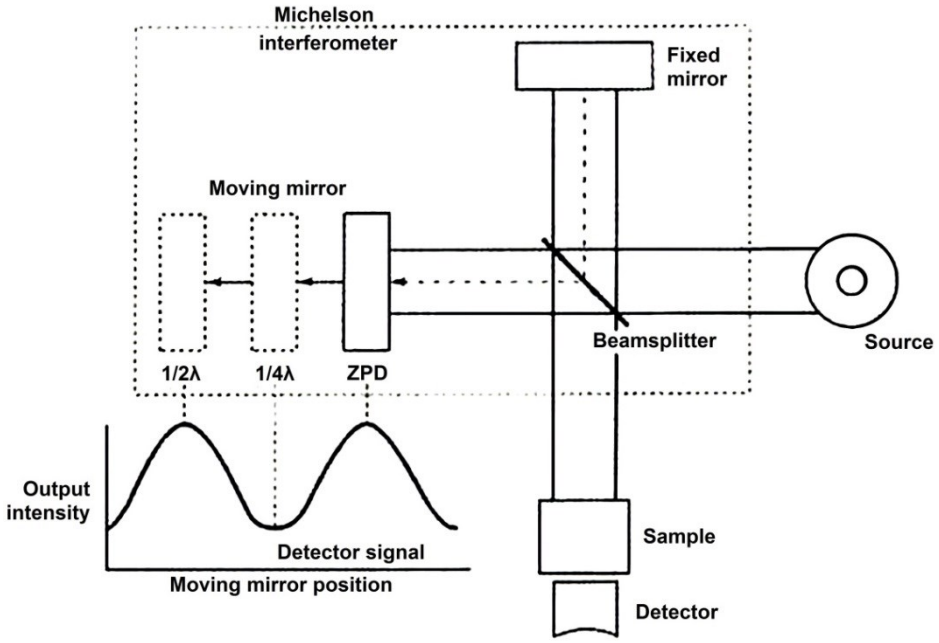

Figure 11: Schematics of Michelson's interferometer (re-drawn in accordance with [90]).

Glass absorbs most of the range of the infrared wavelengths and therefore some other IR-transparent material needs to be used for the optic parts (e.g. KBr, CsI, ZnSe).

Today's most widespread setup is the Fourier transform infrared spectroscopy (FTIR), based on the Michelson's interferometer (Figure 11). The sample is irradiated with wide range of wavelengths at the same time, the IR beam is split into two beams of the same intensity and their interference is controlled by a movable mirror. The interferogram, dependency of the intensity of the detected light on the mirror position, is recalculated into the final spectra using the Fourier transformation (see equation (3); *I(v)* - intensity dependent on the wavelength, δ – mirror position, *I(δ)* - intensity dependent on the mirror position).

$$I(v) = \int I(\delta) 2\pi v \delta d\delta \qquad (3)$$

The infrared spectroscopy can provide us both qualitative and quantitative information about the studied materials. It provides the information about the nature of bonds between atoms. This includes both the zeolite framework and also molecules adsorbed on its surface. As zeolites can easily adsorb various molecules and water moisture from the air the FTIR experiments have to be performed under vacuum conditions. Therefore degas at higher temperatures is required, especially prior to the adsorption of probe molecules, in order to obtain a spectra sufficient for quantitative analysis.

The vibrations of the framework itself, the stretching and bending of T-O units, can be observed within the frequency range between 1500 and 200 cm^{-1}. Overtones of these vibrations are visible in the 2100 to 1500 cm^{-1} region, usually in the form of three broad bands. [91-93] Another set of bands present in the spectra are the vibrations of hydroxyl groups on the external surface of the zeolite or as defects in the crystal lattice. This includes vibrations of the terminal silanol groups around 3745 – 3740 cm^{-1}, broad band of silanol groups perturbed by hydrogen bonding with their surroundings around 3500 cm^{-1} and vibrations of bridging hydroxyl groups (the Brønsted acid sites) between 3650 and 3550 cm^{-1} (Figure 12). [94]

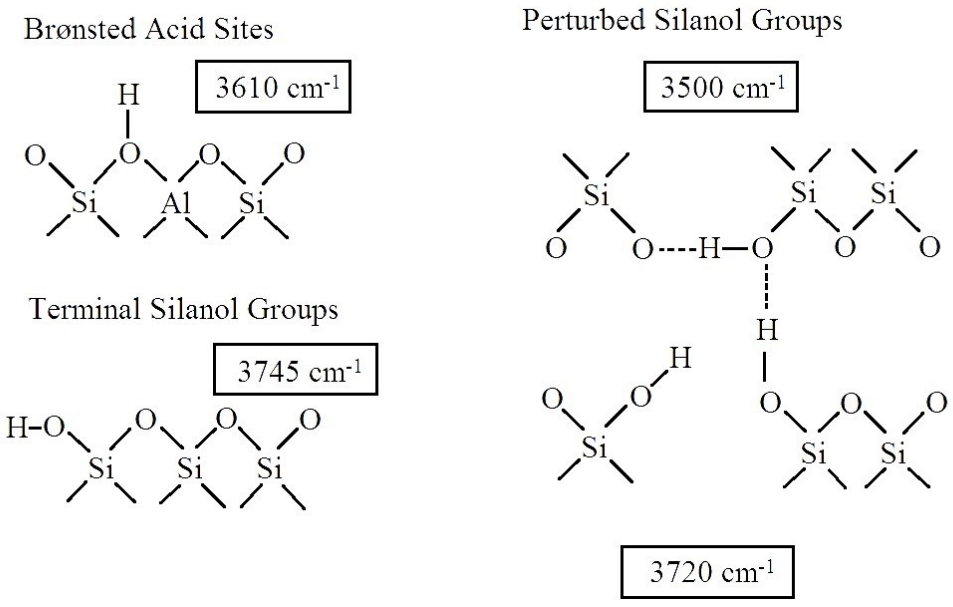

Figure 12: Types of hydroxyl groups in zeolite framework and their respective wavenumbers. [91]

For quantitative analysis the acid sites in the zeolite framework are studied by adsorption of probe molecules onto the surface of the sample; generally, strong Lewis bases such as ammonia, pyridine or 2,6-di-tert-butylpyridine. Size of the molecule should be comparable to the size of intended reactant to determine which acid sites are accessible to it. Either the free electron pair of

the probe can interact with the Lewis acid site's free orbital or the probe molecule can accept a proton and form an electrostatic interaction (Figure 13Figure 13). The proton transfer may affect the vibration frequencies of the probe molecule adsorbed on the Brønsted site. Therefore its vibration frequency is different than for the pyridine adsorbed on Lewis site and thus we can discern the two types of acid sites. The concentration of acid sites in the zeolite sample is directly proportional to the intensity of given vibration mode of the probe molecules. [91, 92] Except the concentration, the intensity depends also on the extinction coefficient of the probe, which can vary depending on the type of acid site. For instance, for zeolites the extinction coefficient for pyridine interacting with zeolite framework were determined to be $\varepsilon_{Brønsted}$ = 1.67 cm/µmol for Brønsted sites with band at 1545 cm^{-1} and ε_{Lewis} = 2.22 cm/µmol for Lewis sites with band at 1455 cm^{-1}. [95, 96] The coefficient is proportional to the square of the dipole moment change and can be experimentally determined from the linear correlation between the intensity of particular band and the gravimetric uptake of the adsorbate. [97]

The strength of the acid sites can differ depending on the composition as well as their location within the framework. For determining the relative strength of acid sites the temperature programmed desorption technique is used. The changes in surface coverage of the probe are monitored depending on the temperature (usually performed in several steps of desorption and subsequent measurement). The stronger is the probe-site interaction the higher is the temperature when desorption occurs. Since the peak intensity is proportional to the number of adsorbed molecules, the temperature profile reflects the distribution of acid sites depending on their relative strength. [91]

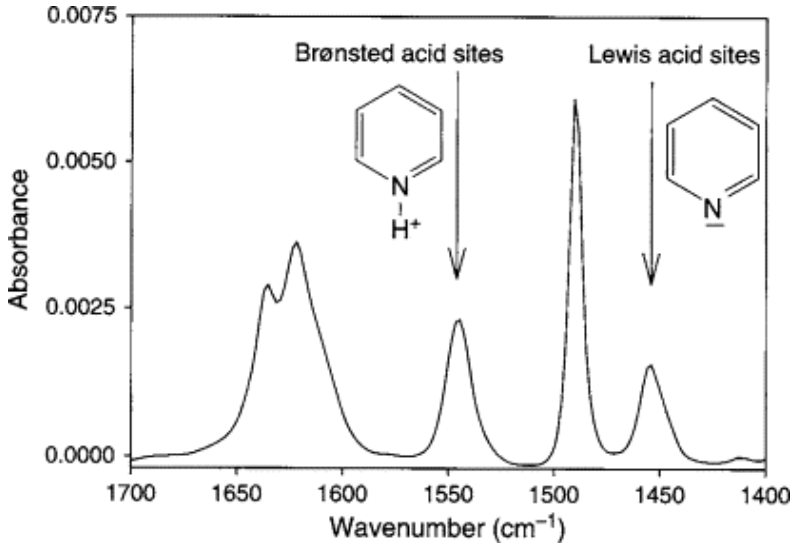

Figure 13: Difference in wavenumbers of pyridine adsorbed on Brønsted (typically at 1545 cm^{-1}) and Lewis acid sites (typically at 1455 cm^{-1}). [91]

2.4.3.Gas adsorption

Surface area and pore volume are one of the outstanding features of zeolites, generally referred to as textural properties. They are commonly measured by weak reversible adsorption (physisorption) of gases, adsorptive, onto the surface of the sample. The amount of adsorbed gas, normalized on weight of the sample, depends on the pressure, temperature and character of the adsorbent. If the adsorption takes place at a constant temperature lower than the critical temperature of the adsorptive, the dependency of the amount of adsorbed gas on the pressure gives an isotherm containing information about the surface area and porosity of the sample.

Prior to the measurement any adsorbed moisture or contaminants have to be removed from the sample under vacuum and at elevated temperature. Argon or nitrogen at their subcritical temperature are most commonly used for the measurement. The behaviour of the adsorbed molecules varies according to the size of the pores in which they are adsorbed. Macropores larger than 50 nm can be viewed approximately as a flat surface. On the contrary, in micropores, that are less than 2 nm wide, interactions between the adsorbed molecules and the pore walls are more significant. Ergo the micropores are filled by the adsorptive molecules at low pressure and as the pressure increases pores of larger diameter are being filled too. The width of mesopores enables adsorption of the gas molecules in multiple layers. The intermolecular interactions, along with their interaction with the surface, result in a capillary condensation, a condensation of gas below its saturation pressure. Difference in mechanism of filling and emptying the mesopores can be observed as a hysteresis loop between the adsorption and desorption branch of the isotherm. [40]

There are various methods for calculating the textural properties from the adsorption isotherm. The Brunauer-Emmett-Teller (BET) method is likely the most common one. It is based on the Langmuir theory enhanced with multilayer adsorption. In principle it describes an equilibrium state of continuous adsorption-desorption and evaporation of the gas. The amount of adsorbed gas *n* can be derived from the formula (4), where p_0 is the saturation pressure of the adsorptive, n_m is monolayer capacity and *C* is constant proportional to the heat of adsorption. [89]

$$\frac{1}{n(^{p}/_{p_0}-1)} = \frac{1}{n_m C} + \frac{C-1}{n_m C}(^{p}/_{p_0}) \qquad (4)$$

The distribution of pore diameters can be calculated by several methods such as the Barret-Joyner-Halenda (BJH), which calculates the pore radius r_0 based on the modified Kelvin equation (5), where γ is the surface tension of the fluid, ϑ is the contact angle and t_c is the thickness of the adsorbed layer.

$$ln {}^{p}/_{p_0} = \frac{-2\gamma cos\theta}{RT\Delta\rho(r_0 - t_c)} \quad (5)$$

The most commonly used adsorptives are nitrogen and argon. The nitrogen has boiling point of 77.3 K and is cheaper. Nevertheless, its diatomic molecules are not spherical, which reduces accuracy of the measurement, especially when micropore sizes are the concern. On top of that its quadrupole moment may cause unequal adsorption affinity towards different materials. Argon has a boiling point at 87.0 K, has similar kinetic diameter as nitrogen, spherical particles and is inert towards specific interaction with functional groups of the material. For these reasons it is the recommended adsorptive for measuring textural properties of porous materials, such as zeolites. [98]

2.4.4.Electron microscopy

Electron microscopy is a powerful tool for investigating structural properties of zeolites. Due to the shorter wavelength of electrons in comparison with the visible light the electron microscopy enables observation of samples up to nanometer or even sub-nanometer scale. This can be useful for phase identification, studying morphology of the sample and for structure determination. Unlike the x-ray diffraction techniques it does not suffer the problem of diffraction lines overlap in powder diffraction and requires smaller amount of sample for successful analysis thanks to stronger interaction between electrons and the sample atoms. [99, 100]

Source of the electrons can be either heated filament or so called field emission gun, where the electrons are ejected from the electrode by strong electric field. The electrons are further accelerated by an anode plate and focused into a narrow beam. The wavelength of the electrons, which is indirectly proportional to their energy, is a crucial factor that affects the resolution of the obtained image. Higher energy means higher resolution, however, also increases the risk of causing a partial or complete damage to the studied material. [101]

There are several techniques that differ in the instrumentation and information they can provide, first being the scanning electron microscopy (SEM). Here the electrons (with energy between 0.4 and 40 keV) are focused to a narrow beam which is scanned across the sample surface in lines to give the whole image. Depending on the interaction we can detect multiple types of electrons. Some of the primary electrons pass their energy to the electrons in the sample which are being emitted as secondary electrons. The detected intensity depends on the intensity of the incident radiation and also the geometrical relation between the source and the sample surface, which is useful for determining the sample morphology. Elastic scattering of the primary electrons

can occur as well. Those are being referred to as back-scattered electrons. The probability of back-scattering grows with the size of the irradiated atom. Therefore the observation of back-scattered electrons gives us the information about mean atomic number in the local spot, which can be used for estimating the local composition and distinguishing separate phases. One problem of zeolites and similar materials is their poor conductivity. After some time too much of the charge remains on the sample surface which compromises the resulting image. To overcome this problem the sample is coated with a thin conductive metal layer (Au or Pt) prior the measurement. [99, 102]

The principle of transmission electron microscopy (TEM) is more similar to the original optical microscope than the SEM. In this case the electron beam is transmitted through an ultra-thin specimen. The transmitted electrons give us the negative image of the sample structure. The TEM generally uses stronger electron sources (between 40 and 400 keV), thus providing better resolution than SEM. Unlike SEM it characterizes the whole volume of the sample particles instead of only the surface. Therefore it is useful for studying fine microstructures such as defects in crystal framework, local intergrowths of different phases, porosity and interlayer spacing in layered materials. [100] The high electron energy naturally increases the damage caused to the sample. Zeolites and zeolite-related materials are highly susceptible to the damage due to intense heating, ionization and defect formation caused by the incident radiation. [99]

If the primary electron has high enough energy it can cause a sample electron in a lower orbital to be ejected. The empty space is filled by electrons from higher orbitals, emitting a quantum of x-ray radiation. The energy of the radiation corresponds to the energy differences between two energetic levels in the atom and gives a set of characteristic energies for every element. This phenomenon is the base principle of the energy dispersive x-ray (EDX) analysis which is being used for studying the local chemical composition of the sample. The method presents a route for elemental mapping of the sample. However, its accuracy is not absolute as the emitted radiation can be absorbed by other atoms in the framework. For example oxygen content in zeolites cannot be accurately determined successfully by this method. The method is suitable for estimating the amount of more scarce atoms (e.g. Al, Ga, Ti) in the framework. [99, 102]

2.4.5.Optical emission spectroscopy (ICP-OES)

The Si/T molar ratio is a good indicator for assessment of the acidity, stability and other properties of the sample. In order to determine the actual content of the heteroatom in the structure and thereby confirm its incorporation to the framework, elemental analysis is required. The applied method is the optical emission spectrometry with inductively coupled plasma (ICP-OES).

To carry out this method, it is necessary to first mineralize the samples of the zeolite before the analysis itself. Since zeolites are non-soluble in common solvents, the mineralization is performed at elevated temperature in concentrated hydrochloric acid, nitric acid and hydrofluoric acid mixtures. Excess of the hydrofluoric acid is then bound to the complex formed by the addition of borate. The solution is, in the form of an aerosol, delivered to a plasma torch where the atomization of the sample takes place. The presence and concentration of individual elements in the sample can be determined from the radiated spectrum according to the intensity and position of the spectral lines. The method is not absolute and requires additional calibration. [103]

2.4.6.Nuclear magnetic resonance (NMR)

Nuclear magnetic resonance is one of the most widely used analytical methods for studying the structure of organic molecules. Some structure directing agents required for preparing certain zeolite samples are not commercially available therefore they need to be prepared prior to the synthesis from other, more common chemicals. The purity of these organic substances has to be verified in order to assure crystallization of the desired structure proceeds without formation of any undesired phases.

The studied sample is required to contain atoms with non-zero nuclear spin, for example ^{1}H or ^{13}C. The analysis takes place in a strong magnetic field which causes the magnetic moments of these nuclei to turn parallel to the direction of magnetic induction. An electromagnetic radiofrequency pulse diverts the vectors of magnetic moments from their equilibrium position. During relaxation, return to equilibrium position, the magnetic moments perform a precession motion around the axis, which can be recorded as the current induced in the measuring coil. The frequency of this precession depends on both the gyromagnetic ratio, which is the characteristic property of the observed nucleus, as well as the electron density around it, which shields the outer magnetic field to a certain extent. Multiple bonds or presence of electronegative elements in the vicinity of the atom thereby change its resonant frequency. The differences in the resonance frequencies of the examined nuclei are expressed by the chemical shift δ (6), where ν is the resonant frequency of the core and the ν_0 resonant frequency of the standard.

$$\delta = \frac{\nu - \nu_0}{\nu_0} . 10^6 \qquad (6)$$

Since the sample is studied in a solution it is necessary to assure the solvent does not affect the measured spectrum by overlapping with the sample signals. For this purpose, deuterated organic solvents such as methanol d4 or deuterated chloroform are used. [104]

2.4.7.Gas chromatography (GC)

Progress of the catalysed reaction is monitored by analysis of periodically taken samples of the reaction mixture. One of the most common methods for separating and analysing mixtures of organic compounds is the gas chromatography. The principle of chromatographic methods is separation of individual compounds of the sample depending on retardation by their interactions with stationary phase while being carried through a column by the moving phase. For gas chromatography it is the adsorption-desorption equilibria of the compound between solid stationary phase and moving gas phase referred to as carrier gas.

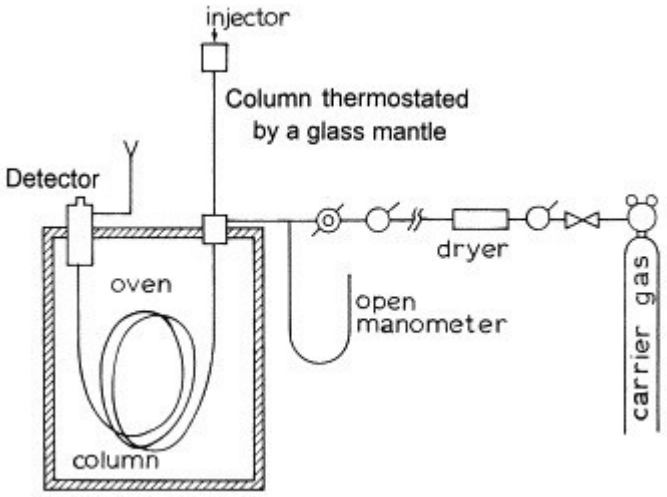

Figure 14: Schematics of the gas chromatograph. [105]

First, the sample is vaporized and injected into a flow of a carrier gas which works as the moving phase. For analysis of organic compounds helium and nitrogen are the most usual carrier gases. Prior mixing with the sample the gas usually passes through a cleaning system which is intended to remove any moisture or impurities (such as traces of other gases) from the carrier gas. After injection the gas leads the sample through a column whose walls work as the stationary phase. Quartz capillaries of inner diameter between 0.1 and 0.6 mm and length around 15 to 60 m are commonly used. The walls of the column can also be modified with additional functional groups or coated with a layer of liquid stationary phase. This way, polar or special columns with specific interactions to certain molecules may be manufactured. The brittle column is covered by a protective layer of polymeric material which makes it more flexible and resistant to mechanical damage. The column is being heated to specific temperature during the measurement in order to affect the adsorption-desorption equilibria of the sample components and thereby ease their separation. Detector placed at the end of the column reacts to presence of the separated compounds by monitoring a property of the output gas which depends on the concentration of the

sample molecules in the gas. Flame ionization detector (FID) is suitable for detecting most organic compounds. The output gas is being burned in a hydrogen-oxygen flame. The organic molecules split to radicals and by following oxidation turn to CHO^+ ions, increasing the ionization of the gas and thus increasing the current between electrodes placed beyond the flame. For linear hydrocarbons the response of the detector linearly increases with the number of carbon atoms in the chain of the analysed molecule. For molecules containing unsaturated bonds and heteroatoms this dependence becomes more complicated. In such cases the response is often approximated by so called "effective carbon number" of the molecule. [105, 106]

3. Experimental part

3.1. List of used chemicals

Commercially available chemicals used for preparing the SDAs and zeolite samples are listed in Table 2: List of used chemicalsTable 2. Commercially available zeolite samples used in the experiments are listed in Table 3.

Table 2: List of used chemicals.

Chemical	**Purity**	**Manufacturer**
1,4-bis(chloromethyl)benzene	98%	Sigma Aldrich
1-bromhexane	98%	Sigma Aldrich
1-bromodocosane	98%	TCI
1-decanol	98%	Sigma Aldrich
1-hexadecanol	99%	Sigma Aldrich
1-hexanol	98%	Sigma Aldrich
1-propanol	99.90%	Riedel-de Haën
2-cyclohexylethanol	99%	Sigma Aldrich
3,4-dihydro-2H-pyran	99%	Alfa Aesar
3,5,5-trimethylhexan-1-ol	85%	TCI
Acetone	99.97%	Lachner
Acetonitrile	99.96%	Lachner
Aluminium nitrate nonahydrate	99.40%	Lachner
Aluminium sulphate	95%	Fluka Analytical
Ammonium nitrate	99.30%	Lachner
Diethylether	99.95%	Lachner
Ethyl acetoacetate	99%	Sigma Aldrich

Gallium nitrate hydrate	99.90%	Alfa Aesar
Hydrochloric acid	37%	VWR
Chloroform	99.92%	Lachner
Lithium chloride	99%	Sigma Aldrich
Ludox HS-40	40% in H_2O	Sigma Aldrich
Mesitylene	98%	Alfa Aesar
N,N,N',N'-tetramethyl-1,6-diaminohexane	98%	TCI
n-dodecane	99%	Acros organics
n-hexane	99.60%	VWR
Nitrobenzene	99%	Alfa Aesar
Potassium hydroxide	89.60%	Lachner
Resorcinol	99%	Sigma Aldrich
Sodium aluminate	80 - 90%	Riedel-de Haën
Sodium hydroxide	99.20%	Lachner
Sodium chloride	100%	Lachner
Sodium nitrate	100%	Lachner
Sodium silicate solution	55% w. in H_2O	Sigma-Aldrich
Sulphuric acid	98%	Lachema
t-butanol	99%	Sigma Aldrich
Tetrabutylammonium hydroxide	40% in H_2O	Fluka Analytical
Tetraethylammonium hydroxide	40% in H_2O	Sigma Aldrich
Tetraethylortosilicate	98%	Sigma Aldrich
Tetrapropylammonium bromide	98%	Acros organics
Tetrapropylammonium hydroxide	25% in H_2O	Acros organics
Toluene	99.80%	Lachner

Table 3: List of used commercial zeolite samples.

Zeolite (structure)	**Si/T molar ratio**	**Abbreviation**	**Code**	**Manufacturer**
MFI	140	MFI-140	CBV2802	Zeolyst
MFI	75	MFI-75, H^+MFI	CBV1502	Zeolyst
MFI	15	MFI-15	CBV3020	Zeolyst
TS-1 (MFI)	28	TS-1	Lot. 2493-88	Zeolyst

***BEA**	19	cBEA	CP814C	Zeolyst

3.2. Synthesis of the organic SDA

To synthesize the nanosponge zeolite samples SDAs $[C_{22}H_{45}\text{-}N^{+}(CH_3)_2\text{-}C_6H_{12}\text{-}N^{+}(CH_3)_2\text{-}C_6H_{13}](Br^{-})_2$ (denoted as C22-6-6) and $[C_{22}H_{45}{-}N^{+}(CH_3)_2{-}C_6H_{12}{-}N^{+}(CH_3)_2{-}CH_2{-}(C_6H_4){-}CH_2{-}N^{+}(CH_3)_2{-}C_6H_{12}{-}N^{+}(CH_3)_2{-}CH_2{-}(C_6H_4){-}CH_2{-}N^{+}(CH_3)_2{-}C_6H_{12}{-}N^{+}(CH_3)_2{-}C_{22}H_{45}](Br^{-})_2(Cl^{-})_4$ (denoted as C22N6) were used. Their preparation consisted of multiple steps. For both SDAs the first step was identical and composed of the reaction of 1-bromodocosane with six times molar excess of *N,N,N',N'*-tetramethyl-1,6-diaminohexane (Figure 15). The reactants were mixed in a 1:1 vol ratio of toluene and acetonitrile, using 25 ml of the mixture per 1 g of 1-bromodocosane. The reaction was carried out at 60 °C under reflux for 12 h. The solvents were subsequently evaporated and the product was washed with diethyl ether and dried at room temperature. The purity of the product was checked with ^{1}H NMR spectroscopy.

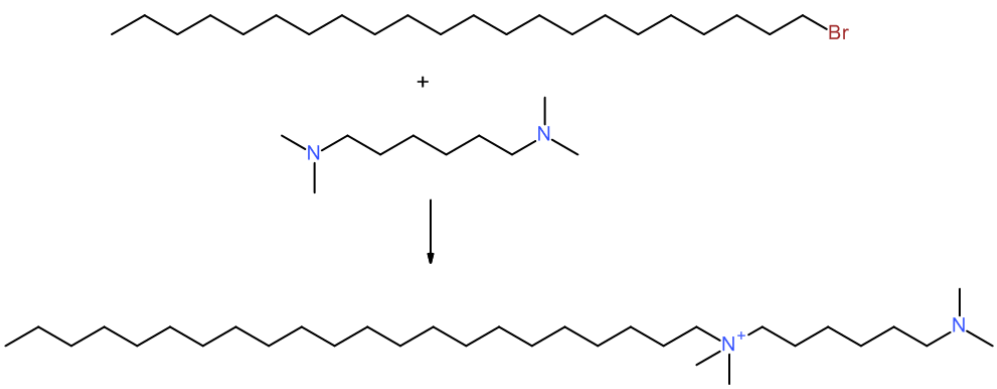

Figure 15: The first step of preparation of C22-6-6 and C22N6 SDA.

The second step in preparing the C22-6-6 was a reaction of the product obtained from the first step with three times molar excess of 1-bromhexane (Figure 16) in chloroform, using 8.5 ml of the mixture per 1 g of the precursor. The reaction was carried out at 80 °C under reflux for 24 h. Afterwards the solvent was evaporated, the product thoroughly washed with diethyl ether and then dried at room temperature. The purity of the final C22-6-6 product was checked with ^{1}H NMR spectroscopy.

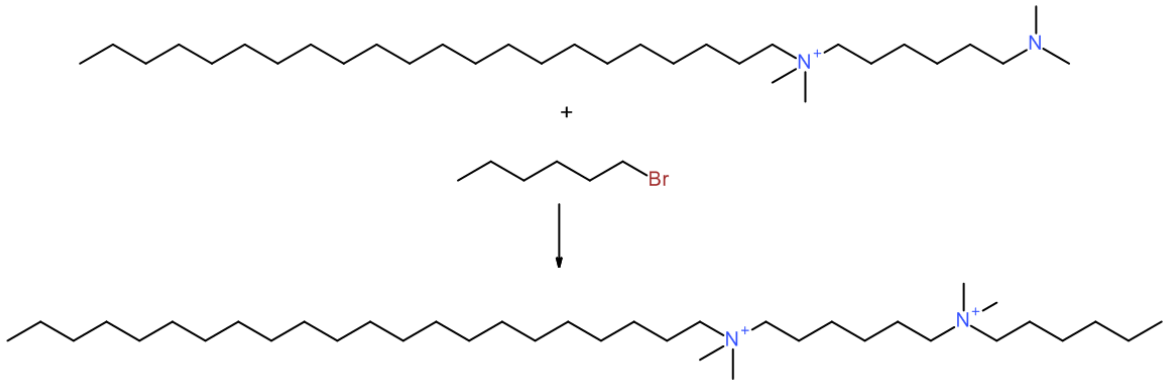

Figure 16: The second step of preparation of C22-6-6 SDA.

The second step in preparing the C22N6 was a reaction of the product obtained from the first step with ten times molar excess of 1,4-bis(chloromethyl)benzene in a 2:1 mixture of chloroform and acetonitrile, using 36 ml of the mixture per 1 g of the precursor (Figure 17). The reaction was carried out at 65 °C under reflux for 24 h. Afterwards the solvents were evaporated, the product thoroughly washed with diethyl ether and acetone and then dried at room temperature. The purity of the product was checked with ^{1}H NMR spectroscopy.

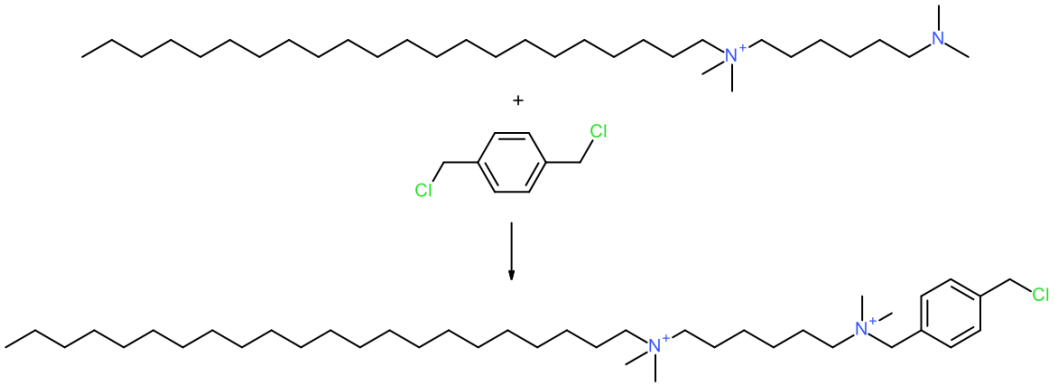

Figure 17: The second step of preparation of C22N6 SDA.

The last step was a reaction of *N,N,N',N'*-tetramethyl-1,6-diaminohexane with twice molar amount of the product obtained from the second step in 6.3 ml of chloroform per 1 g of the precursor (Figure 18). The reaction was carried out at 85 °C under reflux for 24 h. When finished, the chloroform was evaporated, the product was washed with diethyl ether and dried at room temperature. The purity of the final product was checked with ^{1}H NMR spectroscopy.

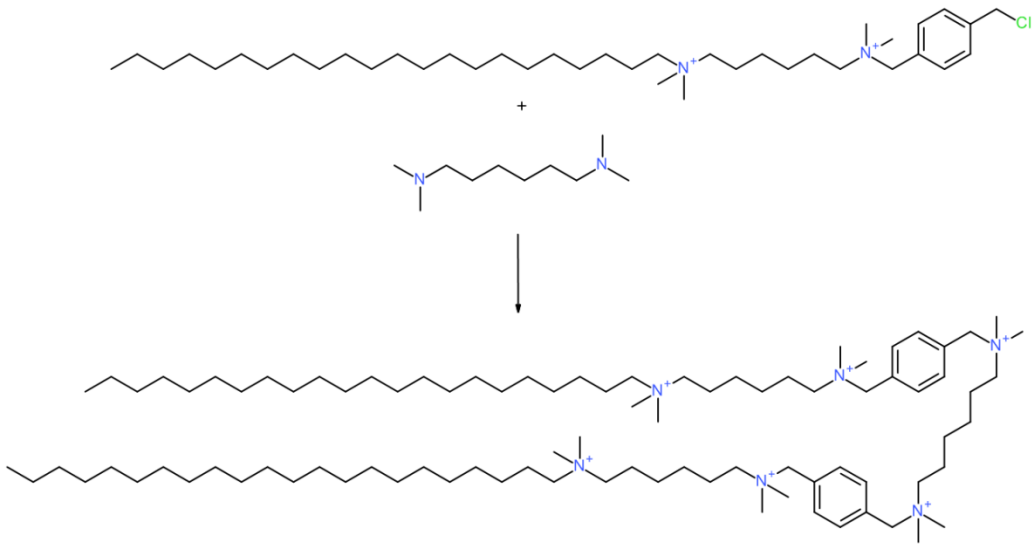

Figure 18: The third step of preparation of C22N6 SDA.

3.3. Synthesis of the zeolite samples

For clarity all prepared zeolite samples, their brief description and abbreviations used in the text are summarized in the Table 4

Table 4: List of prepared zeolite samples and their abbreviations.

Zeolite structure	**Composition**	**Form**	**Abbreviation**	**Note**
MTW	aluminosilicate	bulk	Bulk MTW	
MTW	aluminosilicate	desilicated	DeSi-TPA MTW	blocked micropores
MTW	aluminosilicate	desilicated	DeSi-TBA MTW	blocked micropores
MTW	aluminosilicate	desilicated	DeSi-Na MTW	blocked micropores
MTW	aluminosilicate	desilicated	DeSi-TPA MTW HCl washed	
MTW	aluminosilicate	desilicated	DeSi-TBA MTW HCl washed	
MTW	aluminosilicate	desilicated	DeSi-Na MTW HCl washed	
MTW	aluminosilicate	nanosponge	Nanosponge MTW	
MFI	aluminosilicate	bulk	H^+MFI	Commercial MFI
MFI	aluminosilicate	bulk	Li^+MFI	Commercial MFI, ion exchanged to Li^+ form
MFI	aluminosilicate	bulk	Na^+MFI	Commercial MFI, ion exchanged to

				Na^+ form
MFI	titanosilicate	bulk	TS-1	
MFI	aluminosilicate	bulk	MFI-15	Si/Al = 15
MFI	aluminosilicate	bulk	MFI-75	Si/Al = 75
MFI	aluminosilicate	bulk	MFI-140	Si/Al = 140
MFI	aluminosilicate	bulk	bMFI (Al)	
MFI	aluminosilicate	nanosponge	nsMFI (Al)	
MFI	gallosilicate	bulk	bMFI (Ga)	
MFI	gallosilicate	nanosponge	nsMFI (Ga)	
MTW	aluminosilicate	bulk	bMTW (Al)	
MTW	aluminosilicate	nanosponge	nsMTW (Al)	
MTW	gallosilicate	bulk	bMTW (Ga)	
MTW	gallosilicate	nanosponge	nsMTW (Ga)	
***BEA**	aluminosilicate	bulk	cBEA (Al)	
***BEA**	aluminosilicate	nanosponge	nsBEA (Al)	
***BEA**	gallosilicate	bulk		not successful
***BEA**	gallosilicate	nanosponge		not successful

3.3.1.Bulk zeolites

The synthesis of bulk aluminosilicate **MFI** zeolite was carried out using tetrapropylammonium bromide as SDA. Potassium hydroxide was dissolved in distilled water and then aluminium nitrate nonahydrate was added. When completely dissolved, TPABr was added to the mixture. Finally, tetraethoxysilane was added and the mixture was left stirring for 5 h. The final molar composition of the gel was 100 SiO_2 : 0.5 Al_2O_3 : 31 K_2O : 37.5 SDA : 24000 H_2O. The crystallization was carried out in a Teflon-lined steel autoclave at 175 °C for 2 days with rotation. The product was recovered by filtration, washed with distilled water and dried at 65 °C. The calcination was carried out in a flow of air at 550 °C for 6 h.

Bulk gallosilicate **MFI** was prepared using the same procedure as for bulk aluminosilicate **MFI**. Instead of aluminium nitrate, corresponding amount of gallium nitrate was used as a gallium source.

For the synthesis of bulk aluminosilicate **MTW** zeolite tetraethylammonium hydroxide was used as SDA. Sodium aluminate was mixed with distilled water and when completely dissolved, TEA−OH was added to the mixture. In a separate vessel colloidal silica (Ludox HS-40) was diluted to 30%

solution with distilled water. Both solutions were mixed together and stirred until completely homogenous gel. The final molar composition of the gel was 100 SiO_2 : 1 Al_2O_3 : 1.46 Na_2O : 25 SDA : 1330 H_2O. The gel was transferred into a Teflon-lined steel autoclave and heated up to 160 °C for 6 days under static conditions. The product was separated by filtration, washed with distilled water and dried at 65 °C. The sample was calcined in a flow of air at 550 °C for 6 h.

Bulk gallosilicate **MTW** was prepared using the same procedure as the bulk aluminosilicate **MTW**. Instead of sodium aluminate, gallium nitrate was used as gallium source and additional sodium hydroxide was added to compensate for the sodium ions in sodium aluminate. The final molar composition of the gel was 100 SiO_2 : 1 Ga_2O_3 : 1.46 Na_2O : 25 SDA : 1330 H_2O. The calcination was carried out in a flow of air at 250 °C for 6 h followed by 450 °C for 2 h.

All samples were further ion-exchanged into NH_4^+-form by stirring with 1M ammonium nitrate for 4 h (1 g per 100 ml of solution) and this procedure was repeated four times. Afterwards, the samples were heated at 480 °C for 6 h to remove the ammonia and obtain the samples in H^+-form.

3.3.2.Hierarchical zeolites

3.3.2.1. Bottom-up

Nanosponge aluminosilicate **MFI** zeolite was prepared using the C22-6-6 as SDA. The SDA was dissolved in distilled water and 55 % solution of sodium silicate was added. In a separate container aluminium sulphate was dissolved in an equal volume of water, both solutions were mixed together, shaken vigorously and left stirring for 2 h. Further, 12.2 % sulphuric acid was added dropwise to the mixture followed by aging at 60 °C for 20 h. The final molar composition of the gel was 100 SiO_2 : 0.5 Al_2O_3 : 28 Na_2O : 7.5 SDA : 16.6 H_2SO_4 : 6000 H_2O. The Teflon-lined steel autoclave with the synthesis mixture was placed into an oven and heated up to 150 °C for 6 days with rotation. The product was filtered, washed with distilled water and dried at 65 °C. The calcination was carried out under a flow of air at 580 °C for 6 h.

Nanosponge gallosilicate **MFI** was prepared using the C22-6-6 as SDA following the same procedure as for the nanosponge aluminosilicate **MFI**. Instead of aluminium sulphate, corresponding amount of gallium nitrate was used as gallium source.

Nanosponge aluminosilicate **MTW** zeolite was prepared using the C22N6 as SDA. Sodium aluminate was dissolved in water solution of sodium hydroxide. The mixture was heated up to 60 °C and then the SDA was added and stirred until completely dissolved. The mixture was transferred to a polypropylene bottle, tetraethoxysilane was added and the whole bottle was shaken intensively to homogenize the gel. Further, an aging was carried out at 60 °C for 20 h. The final molar composition

of the gel was 100 SiO_2 : 1 Al_2O_3 : 13 Na_2O : 3.333 SDA : 4500 H_2O. The crystallization was carried out in a Teflon-lined steel autoclave at 150 °C for 6 days with rotation. The product was recovered by filtration, washed with distilled water, dried at 65 °C and calcined in a flow of air at 580 °C for 8 h.

Nanosponge gallosilicate **MTW** was prepared using the C22N6 as SDA following the same procedure as the nanosponge aluminosilicate **MTW**. Instead of sodium aluminate, gallium nitrate was used as gallium source and additional sodium hydroxide was added to compensate for the sodium ions in sodium aluminate.

Nanosponge aluminosilicate ***BEA** zeolite was prepared using the C22N6 as SDA following the same procedure as with nanosponge **MTW**. Only the composition of the gel was altered to result in final molar composition 100 SiO_2 : 3.333 Al_2O_3 : 11 Na_2O : 3.333 SDA : 5500 H_2O. The resulting gel was transferred into a Teflon-lined steel autoclave and the crystallization carried out at 140 °C for 5 days with rotation. The product was filtered, washed with distilled water and dried at 65 °C. The calcination was carried out under a flow of air at 580 °C for 8 h.

Synthesis of nanosponge gallosilicate ***BEA** was carried out using the C22N6 as SDA following the same procedure and gel composition as for nanosponge ***BEA** with sodium aluminate replaced by gallium nitrate. Various amounts of sodium hydroxide were added to achieve different pH values of the gel (from 7 to 13). Also water content was reduced by 60 % and mixture of potassium and sodium hydroxide with 1:3 ratio. Molar ratios of the compounds used to prepare the gallosilicate nanosponge ***BEA** were 100 SiO_2 : 3.333–5.32 Ga_2O_3 : 11–7.3 Na_2O : 0–2.4 K2O : 3.333 SDA : 0–3.37 HF : 5500-2640 H_2O Unfortunately none of these mixtures resulted in nanosponge ***BEA** even after prolonging the synthesis time up to 16 days.

All samples were further ion-exchanged into NH_4^+-form by stirring with 1M ammonium nitrate for 4 h (1 g per 100 ml of solution) and this procedure was repeated four times. Afterwards, the samples were heated at 480 °C for 6 h to remove the ammonia and obtain the samples in H^+-form.

3.3.2.2. Top-down

Desilication of the aluminosilicate bulk **MTW** zeolite was carried out at 65 °C for 30 min using three types of solutions: 1) 0.05M solution of tetrapropylammonium hydroxide in 0.2M solution of sodium hydroxide (further denoted as DeSi-TPA); 2) 0.05M solution of tetrabutylammonium hydroxide in 0.2M solution of sodium hydroxide (denoted as DeSi-TBA); 3) 0.2M sodium hydroxide solution (denoted as DeSi-Na). Each solution was first heated up to 65 °C and then the bulk **MTW** zeolite was added in a ratio of 30 ml of the solution per 1 g of the zeolite. After 30 min the vessel

was cooled down, zeolite sample filtered off and washed with distilled water until neutral pH. The desilicated sample was dried at 65 °C and calcined in a flow of air at 550 °C for 5 h.

The same desilication procedure was repeated on the same bulk **MTW**. Due to the suspicion that after desilication the pores can be blocked by structural debris, each sample was split in half before the calcination. One half of each sample was further stirred in 1M hydrochloric acid at 60 °C for 4 h (with ratio 30 ml per 1 g). Subsequently the samples were filtered off, washed with distilled water until neutral pH and dried at 65 °C. All samples were calcined in a flow of air at 550 °C for 5 h.

All samples were further ion-exchanged into NH_4^+-form by stirring with 1M ammonium nitrate for 4 h (1 g per 100 ml of solution) and this procedure was repeated four times. Afterwards, the samples were heated at 480 °C for 6 h to remove the ammonia and obtain the samples in H^+-form.

3.3.3.Ion exchange

The commercial **MFI** zeolite (in ammonium form) with the molar ratio Si/Al = 75 was calcined at 500 °C for 6 h to obtain the protonated form. Following the calcination portions of the calcined sample were ion exchanged with lithium chloride and sodium chloride solutions to lithium and sodium form respectively. The zeolite was stirred with 0.3 M chloride solution at 90 °C for 1 h using 100 ml of the solution per gram of the sample. The procedure was repeated five times and then the samples were dried at 60°C.

3.4. Tetrahydropyranylation of alcohols

The catalytic tests of the hierarchical **MTW** samples in tetrahydropyranylation were performed in the liquid phase under atmospheric pressure at room temperature in a multi-experiment workstation StarFish with stirring of 450 rpm. Prior to the experiment, 50 mg of the catalyst were activated at 450 °C for 90 min with a rate of 10 °C/min. Then 0.25 g of mesitylene (internal standard), 15 ml of 3,4-dihydro-2H-pyran and the catalyst were placed in a two-necked vessel equipped with a condenser and a thermometer. Sample in time zero was taken and then 18 mmol of alcohol (3,5,5-trimethylhexan-1-ol, tert-butanol, 2-cyclohexylethanol, 1-hexanol, 1-decanol or 1-hexadecanol) were added into the vessel to start the reaction. Samples of the reaction mixture were taken in 5 min, 15 min, 30 min, 1h, 2h, 4h, 6h and 24h, centrifuged to remove the catalyst and analysed by gas chromatography.

Turnover frequency was calculated based on formula (7) where n stands for starting molar amount of alcohol, $X(t)$ is the conversion at time t, c_{Lewis} and $c_{Brønsted}$ are the concentrations of catalytic sites (Lewis and Brønsted) and m is the weight of the catalyst. The turnover frequencies of

the hierarchical **MTW** in tetrahydropyranylation were calculated while assuming that all types of active sites contribute equally.

$$TOF = \frac{n.X(t)}{(c_{Lewis}+c_{Brønsted}).m.t} \quad (7)$$

The catalytic tests for the study of the mechanism of tetrahydropyranylation were performed in the liquid phase under atmospheric pressure at room temperature, 40 °C and 60 °C in a multi-experiment workstation StarFish with stirring of 450 rpm. Prior to the experiment, 100 mg of the catalyst were activated at 450 °C for 90 min with a rate of 10 °C/min. Then 0.4 g of mesitylene (internal standard), 15 mmol of 3,4-dihydro-2H-pyran, 10 ml of *n*-hexane and the catalyst were placed in a two-necked vessel equipped with a condenser and a thermometer and heated to the desired temperature. When the temperature was achieved sample in time zero was taken and then 9 mmol of 1-propanol were added into the vessel to start the reaction. Samples of the reaction mixture were taken in 10 min, 20 min, 30 min, 40 min, 1h, 2h, 3h, 4h, 5h and 24h, centrifuged to remove the catalyst and analysed by gas chromatography.

The Madon-Boudart test was performed using three samples of commercial bulk **MFI** zeolite with Si/Al = 140, 75 and 15. The catalyst activation and the test reaction, tetrahydropyranylation, were carried out by the same procedure as described in previous paragraph.

3.5. Pechmann condensation of phenols

The catalytic tests of the hierarchical aluminosilicate and gallosilicate zeolite samples in Pechmann condensation were performed in the liquid phase under atmospheric pressure at 110 °C in a multi-experiment workstation StarFish with stirring of 450 rpm. Prior to the experiment, 200 mg of the catalyst were activated at 450 °C for 90 min with a rate of 10 °C/min. Then 0.5 g of *n*-dodecane (internal standard), 8.5 mmol of resorcinol, 10 ml of nitrobenzene and the catalyst were placed in a two-necked vessel equipped with a condenser and a thermometer and heated to the reaction temperature. When the temperature was achieved sample in time zero was taken and then 10 mmol of ethyl acetoacetate were added into the vessel to start the reaction. Samples of the reaction mixture were taken in 10 min, 20 min, 30 min, 40 min, 1h, 2h, 3h, 4h, 5h and 24h. Directly after each sample was taken it was diluted to three times its mass with nitrobenzene, centrifuged to remove the catalyst and analysed by gas chromatography.

Turnover frequency was calculated based on formula (7), with the assumption that both Brønsted and Lewis acid sites are capable of catalysing the reaction. [107, 108]

3.6. Instrumentation

The structure and crystallinity of the zeolites were determined by X-ray powder diffraction using a Bruker AXS D8 Advance diffractometer equipped with a graphite monochromator and a position sensitive detector LYNXEYE XE-T using Cu K_α radiation in Bragg–Brentano geometry.

Argon adsorption/desorption isotherms were measured on a Micromeritics 3Flex volumetric Surface Area Analyzer at 87 K to determine surface area, pore volume and pore size distribution. Before the sorption measurements, all samples were degassed in a Micromeritics Smart Vac Prep instrument under helium at 250 °C (heating rate 1 °C/min) for 8 h. The specific surface area was evaluated by BET method using adsorption data in the range of a relative pressure from p/p0 = 0.05 to p/p0 = 0.25. The t-plot method was applied to determine the volume of micropores (Vmic). The adsorbed amount at relative pressure p/p0= 0.98 reflects the total adsorption capacity (Vtot). The pore size distributions were calculated using the BJH model from the desorption branch of the isotherms.

The concentration and type of acid sites were determined by adsorption of pyridine as a probe molecule and observed by FTIR spectroscope Nicolet 6700 AEM equipped with DTGS detector, using the self-supported wafer technique. Prior to adsorption of the probe molecule, self-supported wafers of zeolite samples were activated *in-situ* by overnight evacuation at temperature 450 °C. Pyridine adsorption proceeded at 150 °C for 20 min at partial pressure 3 Torr, followed by 20-min evacuation at 150 °C. The concentrations of Brønsted and Lewis acid sites in aluminosilicate samples were calculated from integral intensities of individual bands characteristic of pyridine on Brønsted acid sites at 1545 cm^{-1} and band of pyridine on Lewis acid site at 1455 cm^{-1} and extinction coefficients of ε(B) = 1.67 ± 0.1 $cm.\mu mol^{-1}$ and ε(L) = 2.22 ± 0.1 $cm.\mu mol^{-1}$, respectively. [78] The extinction coefficient used for calculation of Lewis acid sites concentration in titanosilicate TS-1 is ε(Lewis, Ti) = 0.66 ± 0.04 $cm{\cdot}\mu mol^{-1}$. [109] The spectra were recorded with a resolution of 4 cm^{-1} by collection 128 scans for single spectrum.

Morphology of the samples was studied with scanning electron microscopy using the JEOL JSM-5500LV microscope. Moreover, imaging of the samples was carried out on a FEI Scios Dualbeam SEM, powered by a Schottky FEG electron source and a resolution of 1 nm, equipped with an EDAX Octane Plus EDS, secondary and backscattered electron detector. Operating voltages were 2 kV at 0.1 nA currents at a working distance of 6.7 mm to ensure a sensitive mapping of the particles. The unground samples were placed on an adhesive Leith carbon tab held by an Al-stub disc. To improve

conductivity the samples were brushed with Ag-paste and further Au-sputter coated (5 mA per 30 s). EDX analyses were carried as point analyses for 100 seconds.

The high-resolution transmission electron microscopy (HRTEM) was performed using Jeol JEM-2011 electron microscope operating at an accelerating voltage of 200 kV. The HRTEM images were recorded using a 9 Gatan 794 CCD camera. STEM-EDS spectral imaging mapping was performed using FEI Titan^{TM} G2 80–200 STEM with a Cs probe corrector and ChemiSTEM^{TM} technology (X-FEG^{TM} and SuperX^{TM} EDS with four windowless Si drift detectors), operated at 200 kV was used in this study. STEM images were recorded using high-resolution HAADF detector.

Elemental composition of the samples was determined by the ICP-OES method on the Thermo Scientific iCAP 7000. Prior to the measurement samples were mineralized in mixture of concentrated hydrochloric, nitric and hydrofluoric acid.

The purity of prepared organic SDAs was verified by measuring 1H NMR spectra on a Varian Mercury 300 MHz spectrometer. D4 methanol was used as the solvent.

For the analysis of the samples of the tetrahydropyranylation over hierarchical **MTW** gas chromatograph Agilent 6850 GC equipped with DB-WAX column (length 20 m, diameter 0.180 mm, and film thickness 0.3 μm) and flame ionization detector was used.

For the analysis of the samples of the tetrahydropyranylation mechanism study and Pechmann condensation gas chromatograph Agilent 7890B GC equipped with HP-5 column (length 30 m, diameter 0.320 mm, and film thickness 0.25 μm) and flame ionization detector was used.

4. Results and discussion

4.1. Hierarchical MTW: Bottom-up and top-down

MTW zeolite can be prepared in a broad range of Si/Al molar ratio (15 - ∞). With the one-dimensional 12-ring channel system MTW provides selectivities fitting between medium-pore size **MFI** (10-10-10-ring channels) and large-pore ***BEA** (12-12-12-ring channels). Nevertheless, studies focused on the preparation and catalysis over the hierarchical **MTW** are rare.

Aluminosilicate **MTW** samples were prepared in the bulk and nanosponge form with similar final Si/Al molar ratio 52 and 54, respectively. The bulk sample was further desilicated, resulting in the desilicated samples designated as DeSi-TPA, DeSi-TBA and DeSi-Na depending on the used solution. The powder x-ray diffraction pattern (Figure 19) of the bulk **MTW** sample is in an agreement with the theoretical diffraction pattern of the **MTW** zeolite as shown in the database. [1] The images from SEM further show that the crystal framework was not destroyed during the

desilication. Nonetheless we can notice a slight decrease of intensity of the diffraction peaks. The reason is likely formation of mesopores and resulting lower density of the crystals. The lower intensities and broader signals of the nanosponge sample are caused by the same effect, only the mesoporous volume is likely larger. The nanosponge is formed of agglomerated thin nanocrystals (as discussed below), which have less crystal domains where the diffraction can occur.

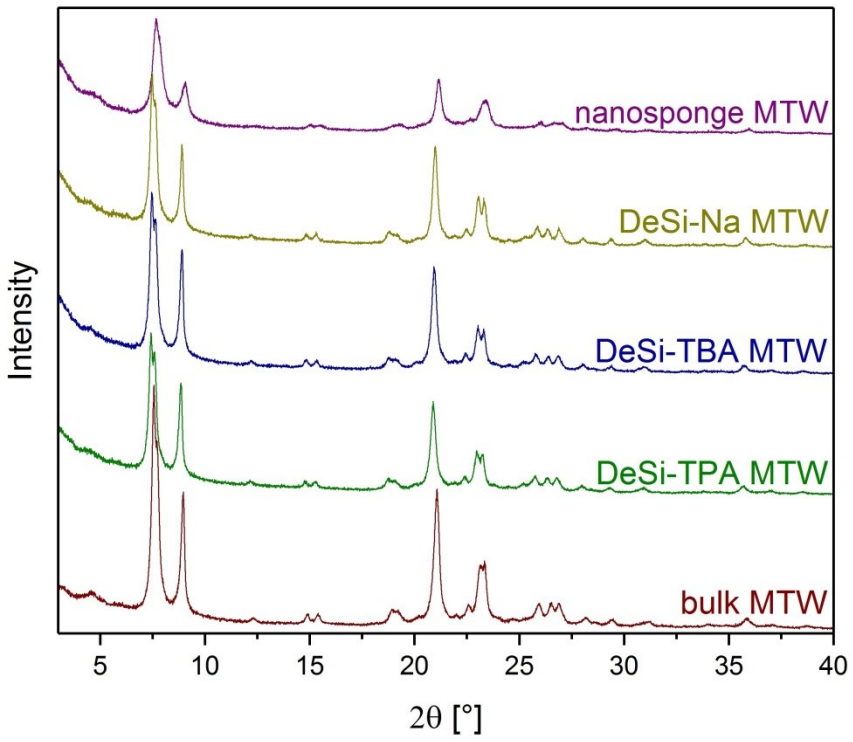

Figure 19: X-ray powder diffraction patterns of the bulk, desilicated and nanosponge **MTW** zeolite samples.

Direct observation of the morphology of the samples is enabled by the scanning electron microscopy (Figure 20 - Figure 24). The bulk **MTW** zeolite (Figure 20) forms crystals of size around 1-1.5 µm. Although the mesopores in the desilicated **MTW** crystals (Figure 21 - Figure 23) cannot be visible with the resolution, the presence of many smaller crystal fragments is a good sign of the successful desilication. In comparison with other samples the morphology of the nanosponge **MTW** (Figure 24) is different. The sample is not made of individual monocrystals but instead it consists of small nanocrystals aggregated into a larger assembly.

Also, the HR-TEM images show the difference between the bulk **MTW** (Figure 25), the desilicated sample (Figure 26) and the nanosponge (Figure 27). The images clearly confirm the creation of homogeneously distributed mesopores by the desilication while the crystal size and shape remained largely unaffected.

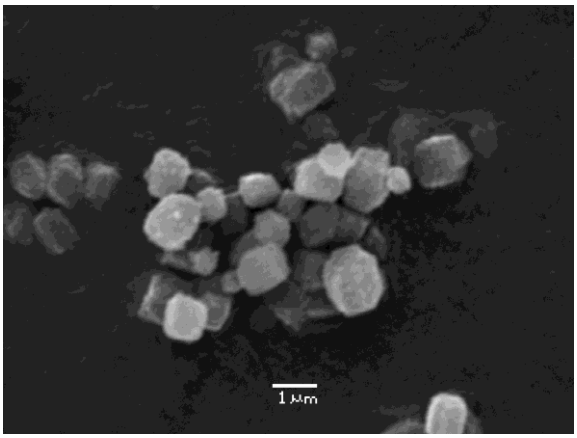

Figure 20: Bulk **MTW**

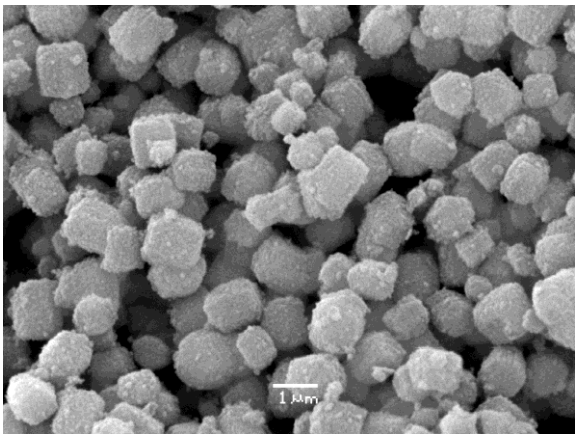

Figure 21: DeSi-TPA **MTW**

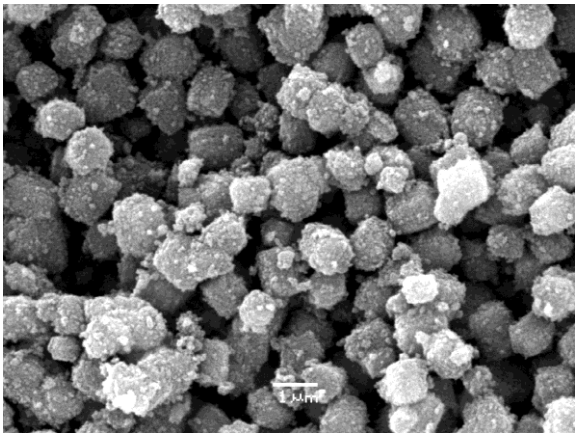

Figure 22: DeSi-TBA **MTW**

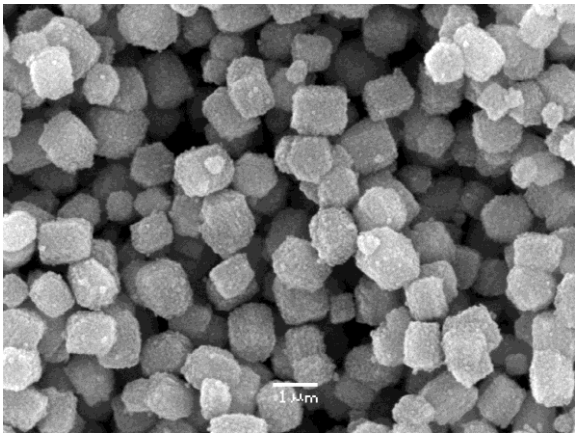

Figure 23: DeSi-Na **MTW**

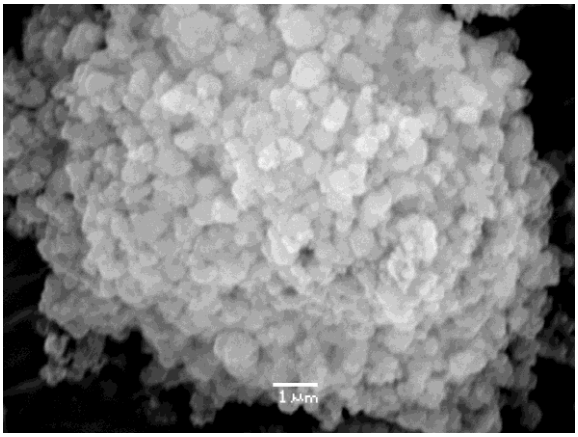

Figure 24: Nanosponge **MTW**

Figure 20 - Figure 24: Scanning electron microscopy images of the **MTW** zeolite samples.

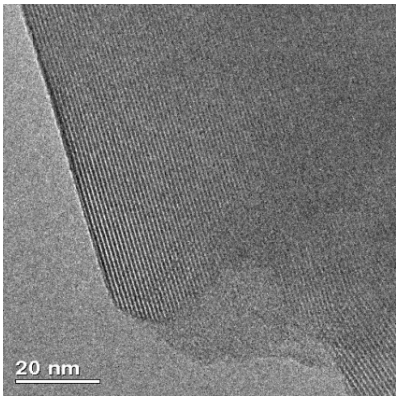

Figure 25: Bulk **MTW**

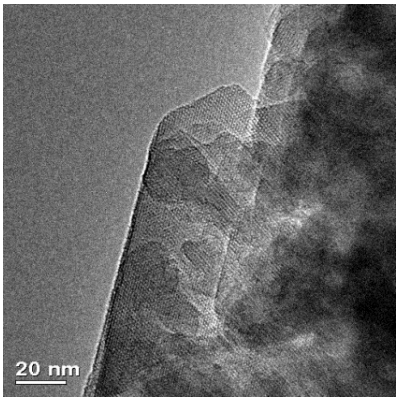

Figure 26: DeSi-TPA **MTW**

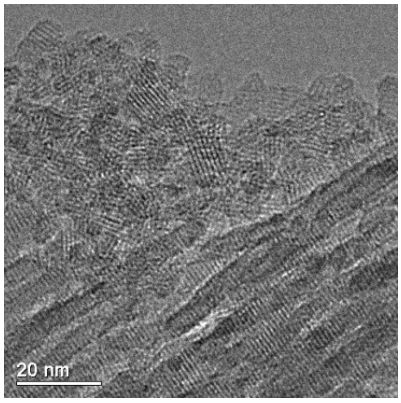

Figure 27: Nanosponge **MTW**

FiguresFigure 25 - Figure 27: Transmission electron microscopy images of the **MTW** zeolite samples.

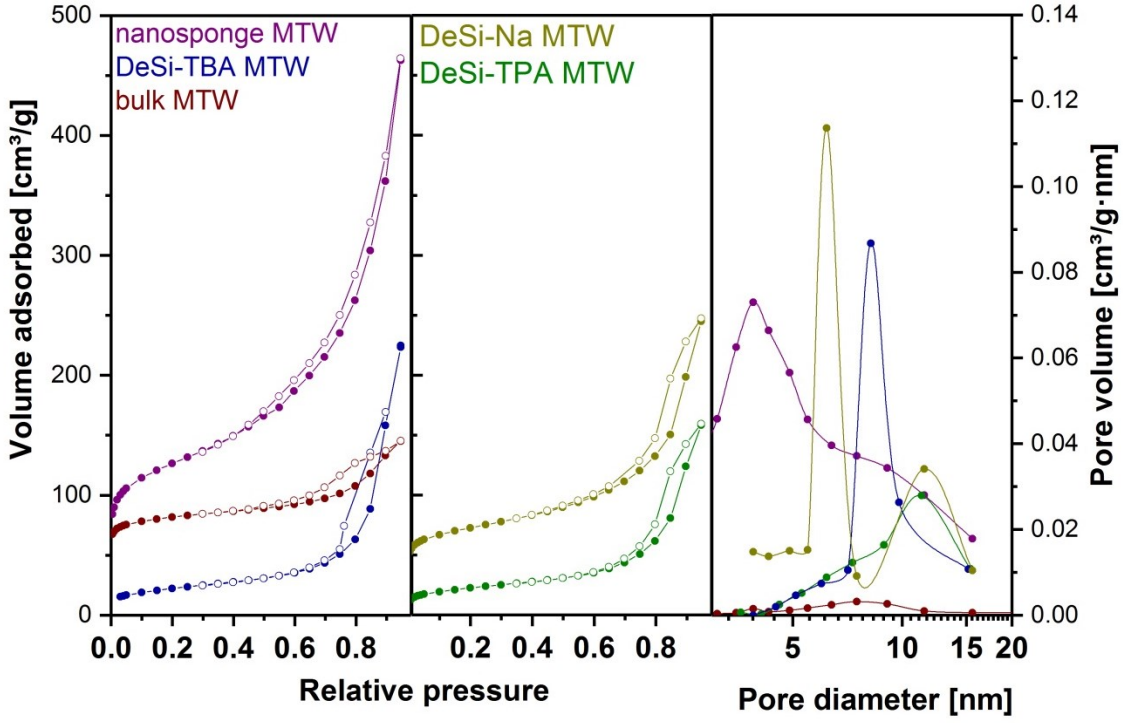

Figure 28: Argon adsorption isotherms and pore size distributions of the **MTW** zeolite samples.

Table 5: Textural properties of the **MTW** samples based on the argon adsorption measurement.

Sample	BET [m²/g]	S_{ext} [m²/g]	V_{tot} [cm³/g]	V_{mic} [cm³/g]
Bulk MTW	292	57	0.220	0.094
DeSi-TPA MTW	80	62	0.245	0.008
DeSi-TBA MTW	80	64	0.348	0.006
DeSi-Na MTW	236	125	0.382	0.057
Nanosponge MTW	454	287	0.716	0.070

Figure 28 shows the adsorption isotherms of prepared samples. The micropores are quickly filled with the gas molecules, which can be seen as the adsorbed volume growth in the low pressure region (relative pressure lower than 0.1). The adsorbed volume then stays almost constant for the bulk and desilicated samples. It increases at higher relative pressure due to capillary condensation in interparticle spaces and mesopores. Upon desorption the isotherms form a hysteresis loop. The reason of this phenomenon is different mechanism of desorption, where the pore opening plays a role as well. In the case of the nanosponge **MTW** the adsorbed volume keeps raising after the micropores are filled and then desorption branch follows very close the adsorption one. This means that the sample has very broad pore size distribution (as shown in pore size distribution diagram in Figure 28), starting from pores of only few nanometers wide up to 20 nm, thus creating an open and easily accessible porous system of total volume 0.716 cm^3/g and large external surface area 287 m^2/g (Table 5).

Somewhat surprising thing to be noticed is the significant decrease in the micropore volume in the DeSi-TPA and DeSi-TBA down to 0.006-0.008 cm^3/g compared to the bulk parent material with 0.094 cm^3/g. Since the x-ray powder diffraction patterns (Figure 19) have proven the preserved framework, we can conclude that the access to the micropores has to be blocked. As the sample was calcined prior the adsorption measurement, it cannot be blocked by the tetraalkylammonium ions or other organic residue but some inorganic matter instead.

In the FTIR spectra of the samples (Figure 29) we can observe the signal of the terminal silanol groups at 3744 cm^{-1}, which increases with the increase in the external surface area after the desilication. The signal is even more intensive for the nanosponge **MTW** due to its large external surface. The signals of acidic hydroxyl bridges can be seen around 3610 and 3575 cm^{-1}. The different wavenumbers likely correspond to groups with a different location in the framework. In the spectra of the bulk, nanosponge **MTW** and DeSi-Na the signal of hydroxyl bridges disappears after the adsorption of a probe molecule proving a good accessibility of acid centres for pyridine molecules. However, in the case of DeSi-TPA and DeSi-TBA the signal remains partially visible even after the pyridine adsorption, which means a part of the acid sites is not accessible to the pyridine. It supports the previous assumption of the blocked pore system.

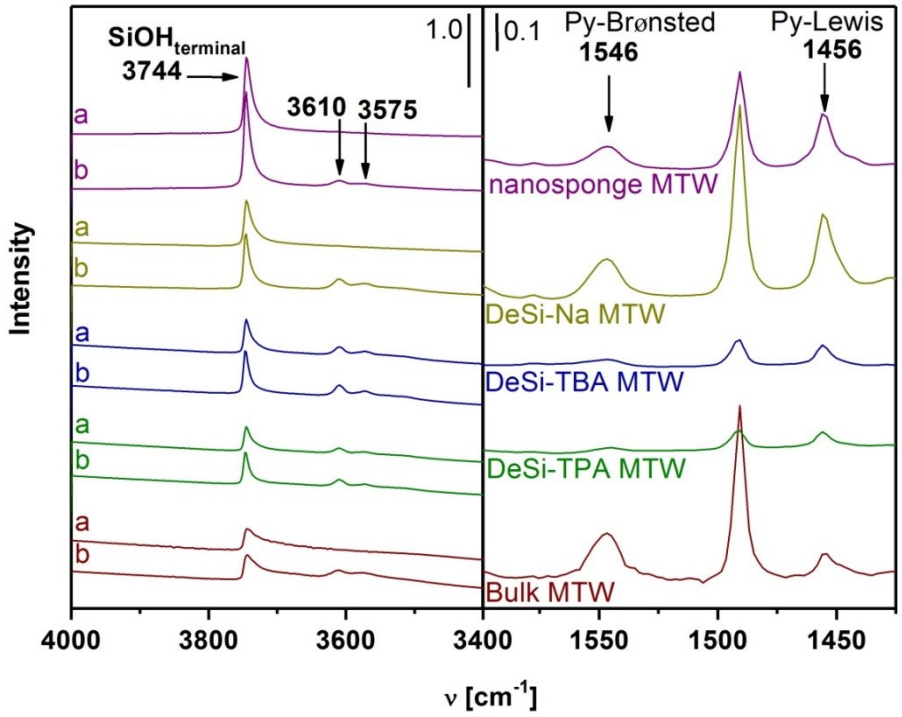

Figure 29: FTIR spectra of the **MTW** samples (b – before pyridine adsorption, a – after pyridine adsorption); region of OH vibrations (left) and region of pyridine ring vibrations (right).

Table 6: Acidic properties of the **MTW** samples based on the pyridine adsorption with FTIR measurement (c_L – concentration of Lewis acid sites, c_B – concentration of Brønsted acid sites) and Si/Al molar ratios based on the ICP-OES measurement.

Sample	Si/Al	c_L [mmol/g]	c_B [mmol/g]	$c_L + c_B$ [mmol/g]
Bulk MTW	52	0.027	0.111	0.138
DeSi-TPA MTW	45	0.017	0.011	0.028
DeSi-TBA MTW	45	0.022	0.013	0.035
DeSi-Na MTW	42	0.089	0.088	0.177
Nanosponge MTW	54	0.064	0.046	0.110

Vibrations of the pyridine ring can be observed in the spectra between 1600 and 1400 cm^{-1}. Peaks belonging to pyridine adsorbed to the Brønsted sites (1546 cm^{-1}) and to the Lewis sites (1456 cm^{-1}) can be clearly distinguished and quantified. The bulk zeolite contains mostly Brønsted sites (Table 6). After the desilication the total amount of acid sites in DeSi-TPA and DeSi-TBA decreased to 0.028 and 0.035 mmol/g, respectively, due to a portion of the sites being inaccessible for pyridine molecules. On the other hand, in the DeSi-Na only the concentration of Brønsted sites decreased to

0.088 mmol/g, whereas, the concentration of Lewis sites increased up to 0.089 mmol/g as a result of introduction of many defects into the structure.

It is clear that the channel blockage causes decrease of micropore volume and decrease of concentration of accessible acid sites. In order to overcome the issue, a second batch of samples was prepared by desilication of the parent bulk **MTW** under the same conditions. The desilicated samples were split in half and one part further washed with hydrochloric acid. The powder diffraction patterns (Figure 30) show again that the sample matches the simulated **MTW** pattern and the framework was not destroyed, neither by the desilication nor by the consequent washing.

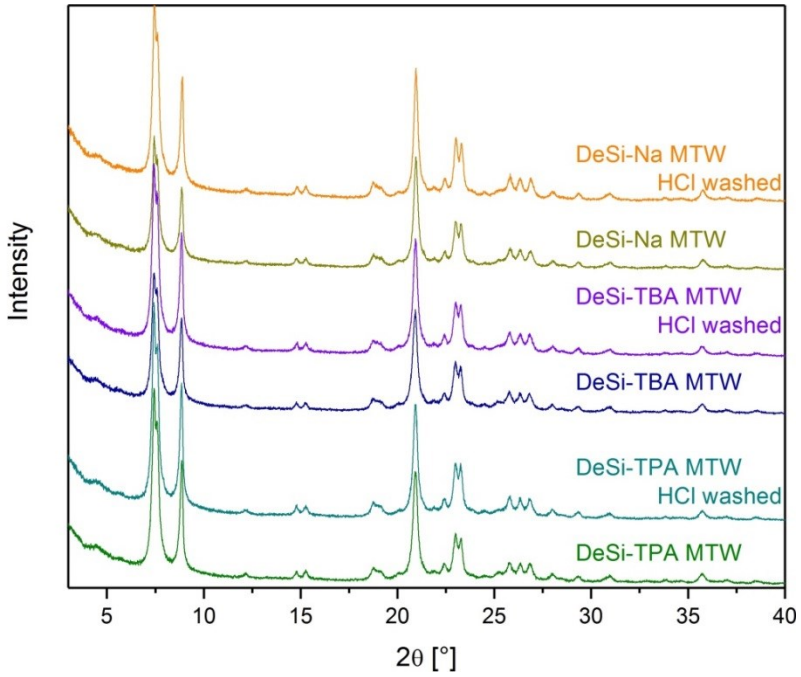

Figure 30: X-Ray powder diffraction patterns of the second batch of the desilicated **MTW** zeolite samples before and after washing with acid solution.

From the isotherms (Figure 31) we can clearly see the decrease in micropore volume of the samples desilicated using the tetraalkylammonium ions. The micropore volumes decreased from 0.094 cm^3/g to 0.008 and 0.006 cm^3/g (DeSi-TPA and DeSi TBA, respectively) in the first batch and to 0.020 and 0.013 cm^3/g in the second batch, whereas the micropore volumes of the DeSi-Na samples dropped only to 0.057 and 0.070 cm^3/g in the first and second batch, respectively. This, along with the XRD patterns, proves reproducibility of the desilication method. After the acid treatment the micropore volume is liberated (Table 7) in both DeSi-TBA and DeSi-TPA samples.

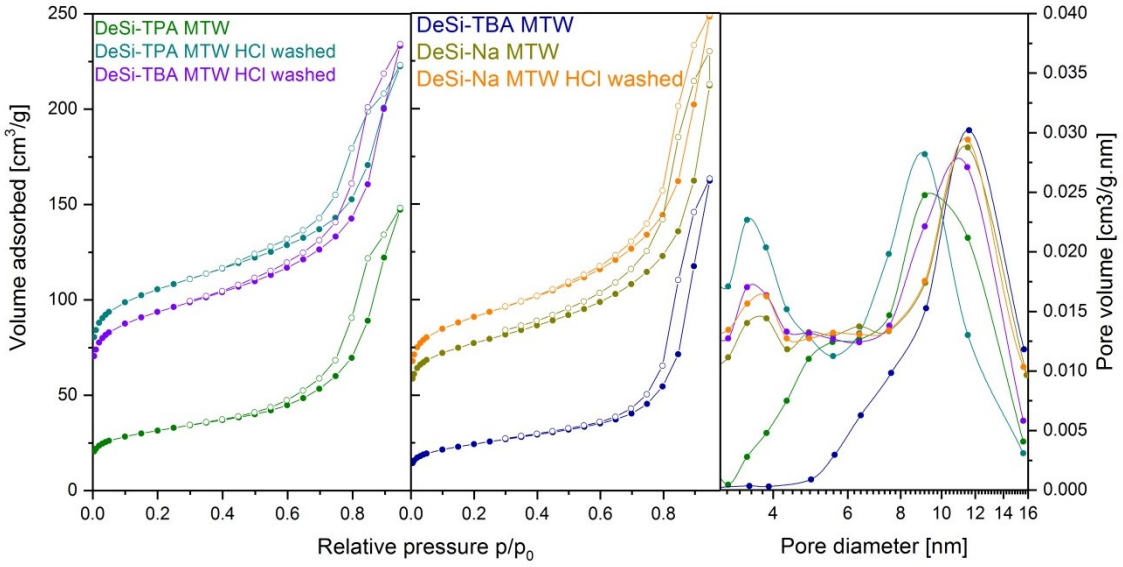

Figure 31: Argon adsorption isotherms and pore size distributions of the second batch of the desilicated **MTW** zeolite samples.

Table 7: Textural properties of the second batch of the desilicated **MTW** samples based on the argon adsorption measurement.

Sample	BET [m²/g]	S_{ext} [m²/g]	V_{tot} [cm³/g]	V_{mic} [cm³/g]
Bulk MTW	292	57	0.220	0.094
DeSi-TPA MTW	113	65	0.229	0.020
DeSi-TPA MTW HCl washed	380	126	0.345	0.108
DeSi-TBA MTW	87	57	0.253	0.013
DeSi-TBA MTW HCl washed	338	121	0.362	0.092
DeSi-Na MTW	278	113	0.329	0.070
DeSi-Na MTW HCl washed	327	131	0.384	0.083

For both samples desilicated in the presence of the tetraalkylammonium ions we can notice low concentration of acid sites (Table 8). They increase to more than two times its value after the acid washing. The signal of the bridging hydroxyl groups around 3610 cm^{-1} disappears after the adsorption of pyridine in the spectrum of washed DeSi-TBA and significantly decreased in the spectrum of washed DeSi-TPA (Figure 32) indicating their better accessibility. On the other hand, DeSi-Na sample, where the micropores were accessible after desilication, the concentration of acid sites significantly decreases after the washing. In this case, the good accessibility of the pores

enabled dealumination process, i.e. removing some of the aluminium atoms from the framework and thereby destroying portion of the acid sites. The dealumination also caused another increase of external surface area and total pore volume of the DeSi-Na sample (Table 7).

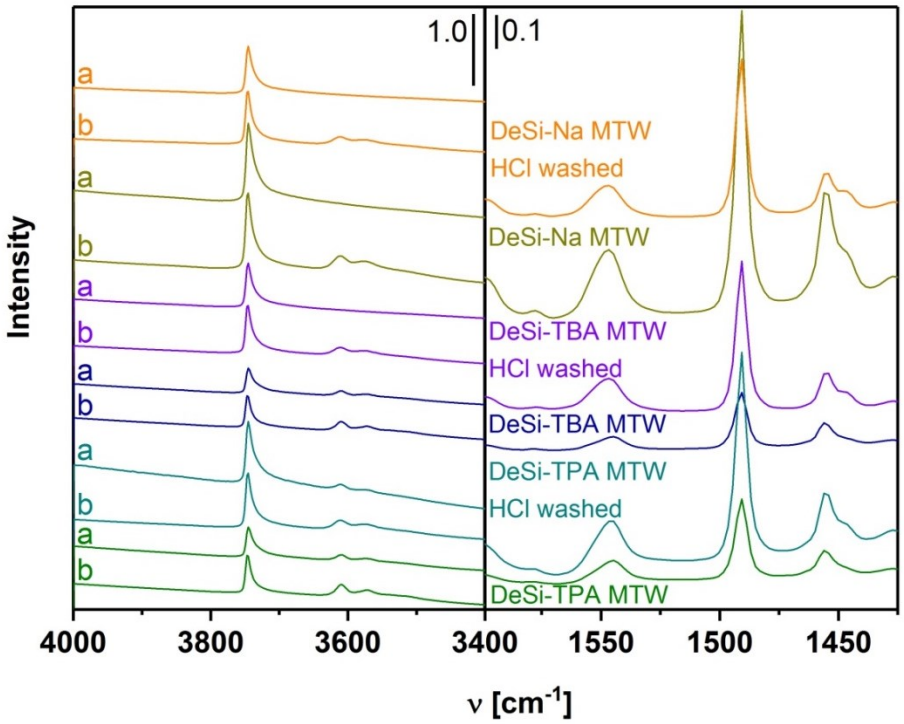

Figure 32: FTIR spectra of the second batch of the desilicated **MTW** samples (b – before pyridine adsorption, a – after pyridine adsorption).

Table 8: Acidic properties of the second batch of the desilicated **MTW** samples based on the pyridine adsorption with FTIR measurement (c_L – concentration of Lewis acid sites, c_B – concentration of Brønsted acid sites).

Sample	c_L [mmol/g]	c_B [mmol/g]	$c_L + c_B$ [mmol/g]
Bulk MTW	0.027	0.111	0.138
DeSi-TPA MTW	0.032	0.048	0.080
DeSi-TPA MTW HCl washed	0.073	0.125	0.198
DeSi-TBA MTW	0.028	0.029	0.057
DeSi-TBA MTW HCl washed	0.049	0.075	0.124
DeSi-Na MTW	0.147	0.165	0.312
DeSi-Na MTW HCl washed	0.055	0.076	0.131

Based on comparison of the elemental maps of bulk **MTW** (Figure 34) and DeSi-TPA after HCl washing (Figure 36) we can conclude that the aluminium distribution has not been significantly changed. Moreover, Figure 35 nicely demonstrates the liberated micro-mesopore system in contrast with the bulk **MTW** in Figure 33.

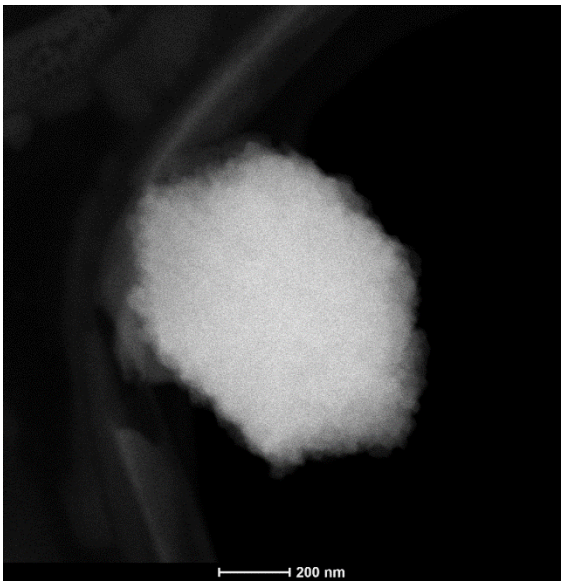

Figure 33: Bulk **MTW**

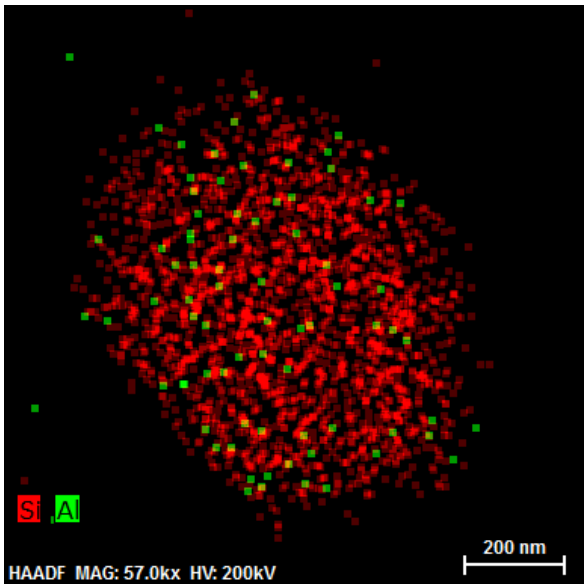

Figure 34: Bulk **MTW** elemental map

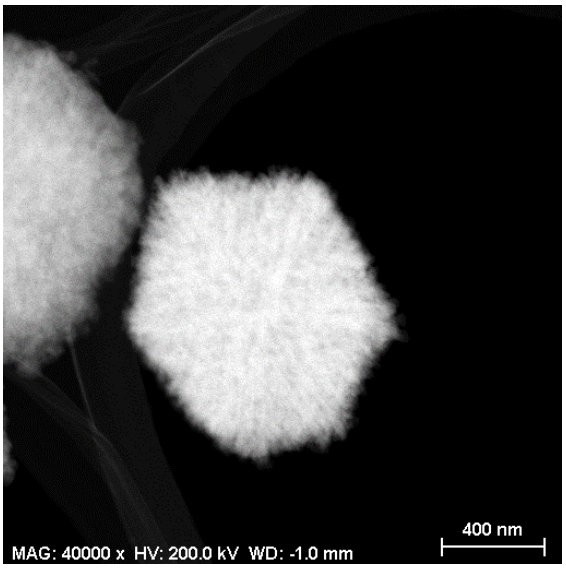

Figure 35: DeSi-TPA **MTW** HCl washed

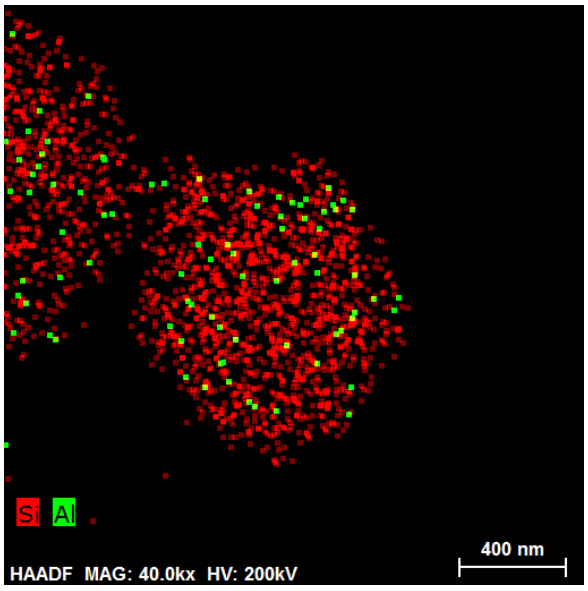

Figure 36: DeSi-TPA **MTW** HCl washed elemental map

FiguresFigure 33 -Figure 36: Transmission electron microscopy images and elemental maps of the **MTW** zeolite samples.

The activity of desilicated and nanosponge **MTW** materials was evaluated in the tetrahydropyranylation of alcohols. Linear primary alcohols (1-hexanol, 1-decanol, 1-hexadecanol) were used for the first set of catalytic tests. Due to their structural similarity the main difference in their activity was expected to be caused mainly by their chain length. The tetrahydropyranylation reaction can proceed over both Brønsted and Lewis acid sites therefore the total concentration of acid sites in respective materials as determined by pyridine adsorption and conversion of alcohols in 2 hours was used for the turn-over frequencies (TOF) calculations. It was assumed that any acid sites that are not accessible to pyridine molecules are not accessible to the reactants as well. In the catalytic tests of 1-hexanol, 1-decanol, and 1-hexadecanol, most of the catalysts reach the maximal conversions (plateau) after 6 h of the reaction time (Figure 37). In the case of nanosponge **MTW** zeolite, for 1-hexanol and 1-decanol the plateau was caused by the total consumption of the reactant. On the other hand, the decrease in the reaction rate over the other samples at the conversions lower than 50% can be explained by partial deactivation of their active sites. When the smallest linear alcohol 1-hexanol was used as the reactant, activities in terms of turn-over frequencies decreased in the following order: DeSi-TBA **MTW**, nanosponge **MTW** and DeSi-TPA **MTW** (Figure 38), whereas the TOF values of remaining samples were nearly negligible in comparison. As expected, the conversions over all samples as well as the TOF values gradually decreased with the increase of the chain-length of the alcohol. The more significant decrease in the activity of the desilicated samples with the increasing substrate molecule size indicates that their active sites are not as easily accessible in comparison with the nanosponge **MTW**.

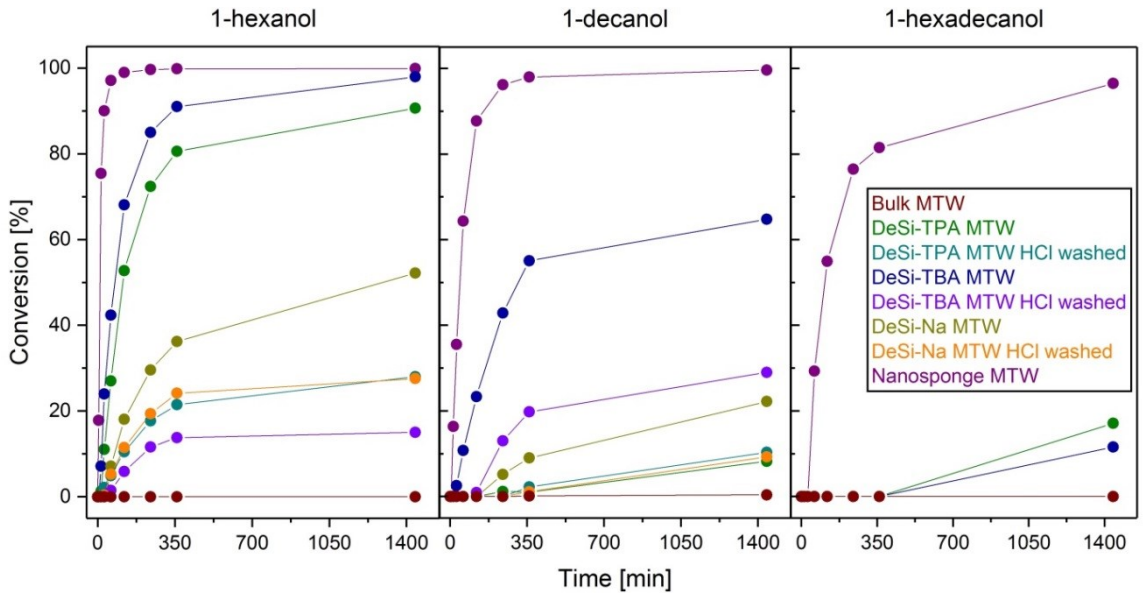

Figure 37: Conversions of linear alcohols over **MTW** zeolite samples.

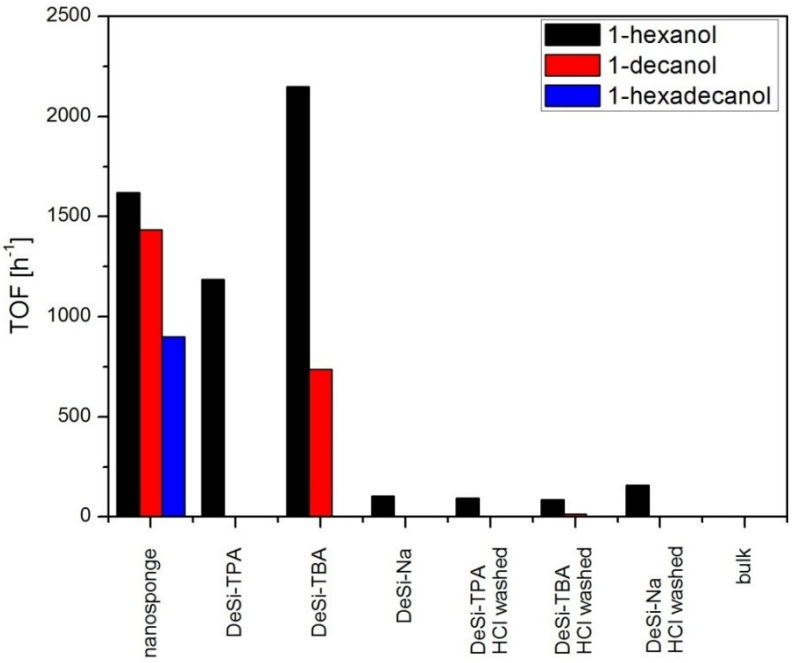

Figure 38: Turn over frequencies of **MTW** samples for linear alcohols in 2 hours.

For the second set of catalytic tests a group of branched alcohols (3,5,5-trimethylhexan-1-ol, 2-cyclohexylethanol and *t*-butanol) was used. In contrast to the reaction of linear alcohols, the DeSi-TPA **MTW** and DeSi-TBA **MTW** in the tetrahydropyranylation of branched alcohols provided conversions nearly comparable to the nanosponge **MTW** (Figure 39). The TOF values of these samples are again comparable to the nanosponge **MTW** (Figure 40), with the DeSi-TBA **MTW** even exceeding the nanosponge independently on the type of reagent.

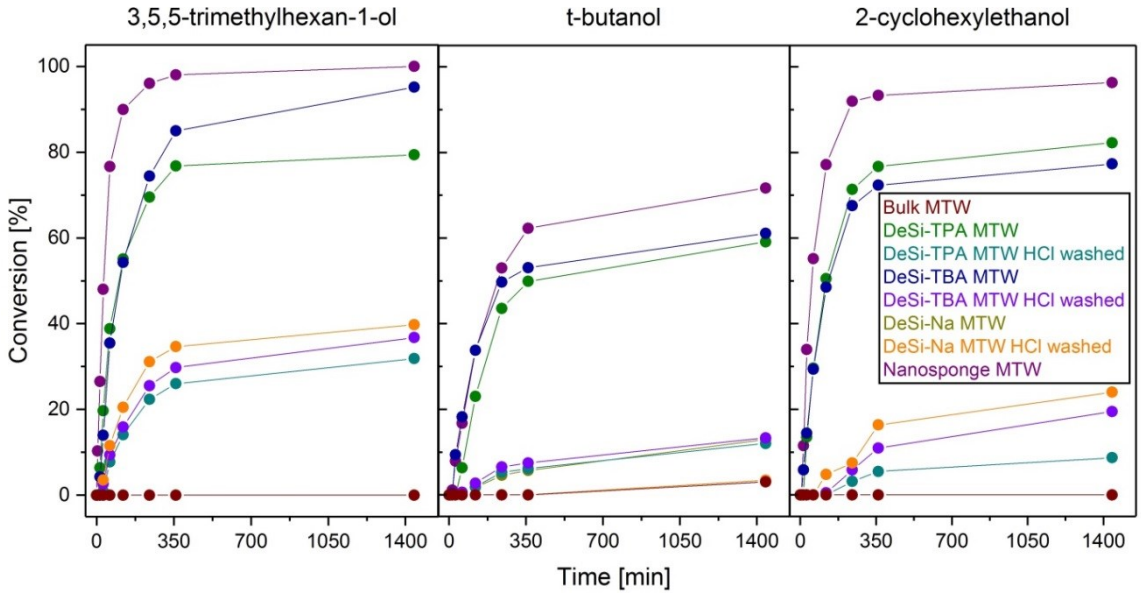

Figure 39: Conversions of branched alcohols over **MTW** samples.

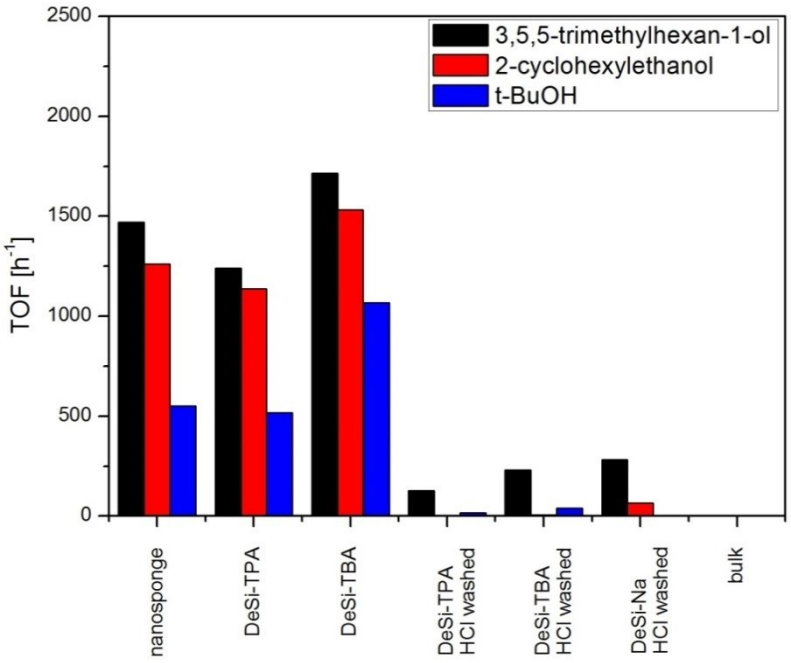

Figure 40: Turn over frequencies of **MTW** samples for branched alcohols in 2 hours.

The results of tetrahydropyranylation of 1-hexanol and all three branched alcohols show that despite the micropore blockage the DeSi-TPA **MTW** and DeSi-TBA **MTW** samples can achieve reasonable conversions. This indicates that the reaction is catalysed only by the acid sites located on their external surface. The overall activity of named samples was expected to grow after the liberation of pore system by the washing with HCl solution, however, after the treatment the activity dropped significantly. This unexpected observation can be explained by the diffusional constraints in pore system of **MTW**. The one-dimensional channels present in bulk parent **MTW** present a long diffusion path for the reactant and product molecules through the crystal and thus the reaction rate is negligible. Even the auxiliary mesopore system created by the desilication did not facilitate the molecular transport as proved by very low activity of all desilicated samples (washed with HCl). On the contrary, in nanosponge **MTW** the reaction mostly proceeded on the external surface of nanosized crystals. The smaller crystallites of the nanosponge also present shorter diffusion path for the product and reactant molecules.

4.2. Mechanism of tetrahydropyranylation

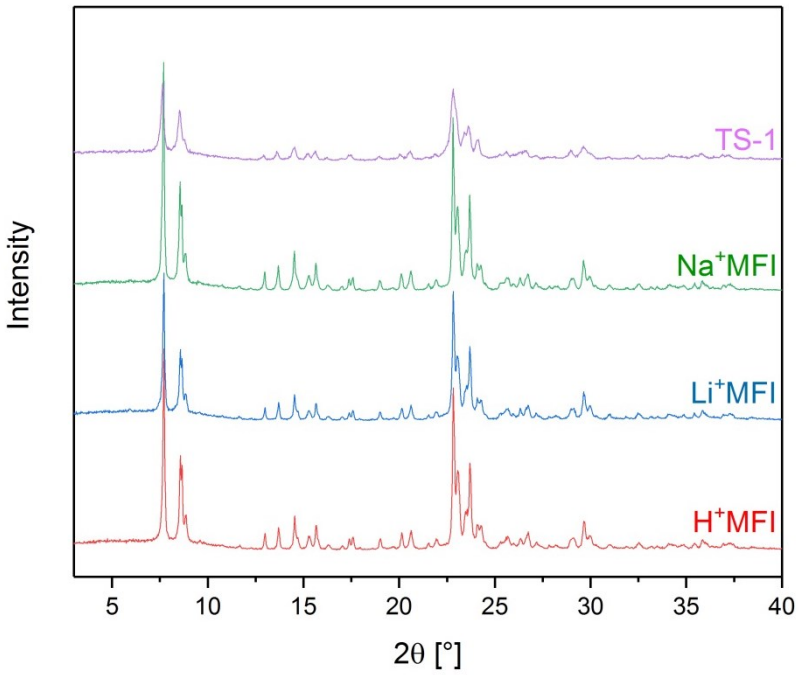

Figure 41: X-ray powder diffraction patterns of the **MFI** samples.

Although tetrahydropyranylation is a fairly common reaction, studies of its mechanism and suitability of the type of acidity are scarce. In this context, a detailed study aimed at identifying active sites and corresponding reaction mechanisms should help us to design better zeolite-based catalysts because zeolites can have both Brønsted and Lewis acid sites with tuneable concentrations. As tetrahydropyranylation is a representative of nucleophilic double bond attack reactions, the results are expected to be applicable to other catalytic reactions of similar type. Zeolite **MFI** was chosen for its wide use in research and industry and for its availability in many forms including aluminosilicate and titanosilicate.

The commercially available bulk **MFI** sample was calcined to its protonated form (denoted as H^+MFI) and ion exchanged to the Li^+ and Na^+ form (denoted as Li^+MFI and Na^+MFI, respectively). The aim was to poison portion of its Brønsted acid sites by the alkali cations and thus prepare a set of materials varying in acidity. The x-ray powder diffraction patterns (Figure 41) confirm that the crystallinity of the samples was not compromised during the ion-exchange. Given the lower intensities and broader diffraction peaks we can assume the morphology of the titanosilicate TS-1 is different than of the aluminosilicate samples, however, we can still clearly distinguish individual diffraction lines typical for the **MFI** structure. The data from argon adsorption (Figure 42 and Table 9) prove that textural properties of the **MFI** sample did not change after the ion exchange. The higher

external surface area of the TS-1 sample along with the shape of its isotherm, also imply difference in morphology between the TS-1 and aluminosilicate **MFI** samples.

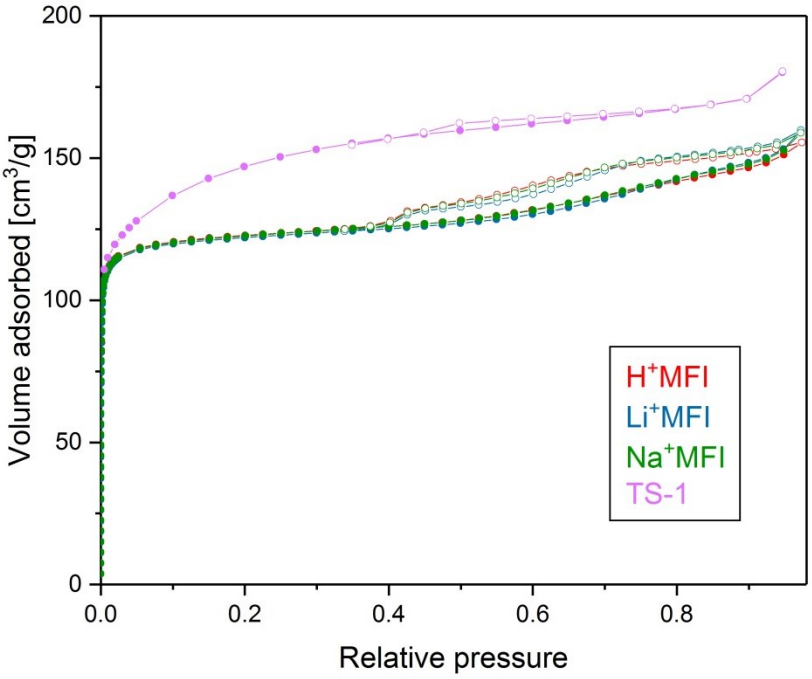

Figure 42: Argon adsorption isotherms of the **MFI** samples.

Table 9: Textural properties of the **MFI** samples based on the argon adsorption measurement.

Sample	BET [m²/g]	S_{ext} [m²/g]	V_{tot} [cm³/g]	V_{mic} [cm³/g]
H^+MFI	375	38	0.199	0.139
Li^+MFI	373	38	0.204	0.139
Na^+MFI	374	39	0.203	0.139
TS-1	510	316	0.279	0.096

The concentrations of Brønsted and Lewis acid sites in the **MFI** samples were obtained from FTIR spectra of adsorbed pyridine (Figure 43). The peak at 1545 cm^{-1} assigned to an interaction of pyridine with Brønsted sites is the most intensive in H^+MFI spectra, whereas the band at 1455 cm^{-1} which belongs to interaction of pyridine with Lewis-type sites is less intensive. On the contrary, in the spectra of Li^+MFI, Na^+MFI and TS-1 the band at 1545 cm^{-1} is barely noticable whereas the band of Lewis sites is relatively high and its maximum is shifted towards 1445 cm^{-1}. This band is likely caused by adsorption of the pyridine molecules to the the weakly Lewis acidic alkali ions inside of the

channels. For the sake of comparison, we assumed the extinction coefficients for alkali ion Lewis acid sites to be the same as for aluminium Lewis acid site. Upon closer examination we can also see a smaler band at 1455 cm^{-1} which indicates a presence of framework aluminium based Lewis acid sites. [110, 111] The shift of Lewis band to 1447 cm^{-1} in TS-1 is caused by weaker interaction of the titanium center with pyridine. Also its intensity is seemingly lower, however, it has to be taken into account that the extinction coeficients for pyridine adsorbed on Lewis acid sites in titanosilicates and aluminosilicates are different. [109]

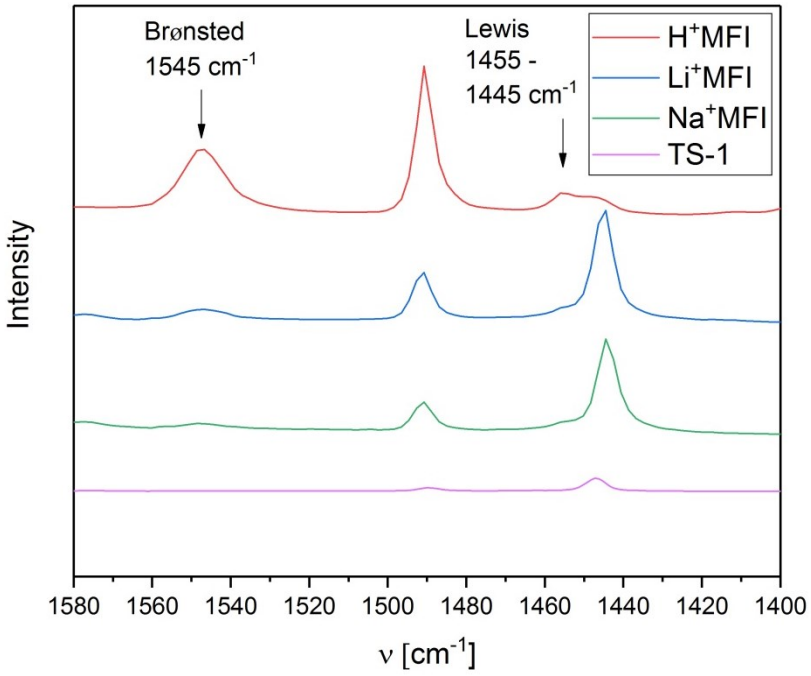

Figure 43: FTIR spectra the **MFI** samples after the adsorption of pyridine

Table 10: Acidic properties of the **MFI** samples based on the pyridine adsorption FTIR measurement ($c_{L(Al,\ Ti)}$ – concentration of Lewis acid sites corresponding to pyridine adsorption on aluminium and titanium Lewis acid sites - 1455 and 1447 cm^{-1} respectively; $c_{L(Li/Na)}$ – concentration of Lewis acid sites corresponding to pyridine bound to the Na^+ or Li^+ ions - 1445 cm^{-1}; c_B – concentration of Brønsted acid sites).

	H^+MFI	Li^+MFI	Na^+MFI	TS-1
c_B [mmol/g]	0.21	0.04	0.01	0
$c_{L(Al,\ Ti)}$ [mmol/g]	0.05	0.05	0.05	0.14
$c_{L(Li/Na)}$ [mmol/g]	-	0.13	0.11	-

Figure 44 shows the conversions of individual samples at 60 °C, 40 °C and room temperature. We can notice a slow increase in the conversion caused by consumption of 1-propanol even in the reaction mixture without any catalyst (denoted as "blank"), which indicates that the reaction can proceed without any catalyst into some extent. Nevertheless, addition of any of the studied catalysts always resulted in higher conversions. Among studied samples the H^+MFI clearly dominates, reaching 100 % conversion after only 30 minutes at 60 °C. The conversions of 1-propanol over individual samples after 5 hours decrease in the following order: H^+MFI (100%) > Na^+MFI (85%) > TS-1 (63%) > Li^+MFI (52%). At 40 °C (Figure 44) we can observe significant decrease in the conversions over mentioned samples except H^+MFI. The conversions after 5 hours dropped to 100, 21, 20 and 7 % following the same trend. The conversions given by all samples at room temperature with the exception of H^+MFI (Figure 44) almost match those of the blank experiment, which means the catalysts do not contribute to the reaction.

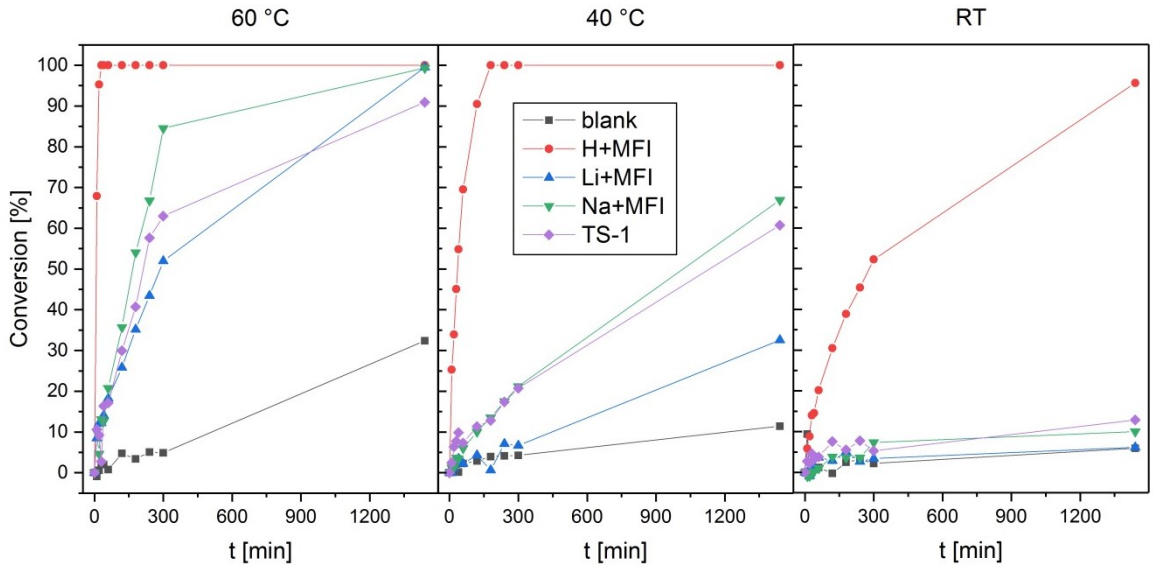

Figure 44: Conversions of 1-propanol over **MFI** samples at 60° C, 40° C and room temperature.

The results were compared with theoretical calculations provided by colleagues at the Department of Physical and Macromolecular Chemistry. All calculations were performed with DHP and methanol as model molecules for simplicity. In order to determine the effect of alcohol size on THP reaction energetics, two models using both 1-propanol and methanol molecules in the Li^+MFI were compared and showed that alcohol size, in this size range, plays a minor role. Different reaction rates for propanol and methanol would most likely result from other effects, such as differences in the diffusion rate in zeolite channels, rather than differences between the intrinsic reactivity.

Table 11 shows values of estimated activation barriers, E_a, for all **MFI** models considered. The Al-MFI (Brønsted) represents purely Brønsted acidic zeolite. The model called Al-MFI (Lewis) contains only framework aluminium based Lewis sites. Although the low activation barrier of the Brønsted acid sites corresponds well with the high conversions of 1-propanol over the mainly Brønsted acidic H^+MFI, the difference between activation barriers of H^+MFI and other (predominantly Lewis acidic) catalysts is larger than expected. Also there is an inconsistency between the calculated barriers and experimental data of the Na^+MFI and Li^+MFI. Inclusion of diffusion barriers, adsorption-desorption equilibria of the molecules moving through the channel system, can potentially resolve the inconsistency between experimental and calculated data.

Table 11: Energetic activation barriers for the tetrahydropyranylation of methanol as calculated for the distinct active sites in **MFI** framework.

System	No catalyst	Li^+MFI (Lewis)	Na^+MFI (Lewis)	TS-1 (Lewis)	Al-MFI (Lewis)	Al-MFI (Brønsted)
E_a [kcal/mol]	41.3	30.8	36.1	23.8	20.9	4.5

The relative importance of reaction rate and the mass transport rate in a porous catalyst are commonly evaluated by the Thiele modulus. Based on a value of Thiele modulus, catalytic reactions can be categorized either as reaction-controlled ($\varphi < 0.1$), diffusion-controlled ($\varphi > 5$), or transition controlled ($0.1 < \varphi < 5$). [112, 113] The estimated values of Thiele modulus (considering a first-order reaction in a straight cylindrical pore) are shown in Table 12 for all the **MFI** models considered in the study. Although our evaluation of Thiele modulus is only approximate, huge Thiele modulus calculated for THP in H^+MFI in the relevant temperature range (3.92×10^8, 1.96×10^8 and 5.35×10^7 at room temperature, 40°C and 60°C, respectively) confirms the previous claims that tetrahydropyranylation in H^+MFI is running under the diffusion-controlled conditions.

Table 12: Thiele modulus values for the calculated systems and temperatures.

System	RT	40°C	60°C
Li-MFI (Lewis)	9.18×10^1	9.56×10^1	5.20×10^1
Na-MFI (Lewis)	5.48×10^{-2}	8.14×10^{-2}	7.31×10^{-2}
TS-1 (Lewis)	1.05	1.35	1.25
Al-MFI (Lewis)	2.86×10^{-3}	4.89×10^{-3}	6.74×10^{-3}
Al-MFI (Brønsted)	3.92×10^8	1.96×10^8	5.35×10^7

The Madon-Boudart test was performed to confirm the theoretical assumptions on the diffusion. Three samples of commercial bulk **MFI** zeolite with Si/Al = 140, 75 and 15 (denoted as MFI-140, MFI-75 and MFI-15, respectively) were used. Expectedly, the concentrations of acid sites of individual samples (Table 13) increase with the aluminium content. Although the samples possess both Lewis and Brønsted acidity, the concentration of Brønsted acid sites is dominant in each sample.

Table 13: Acidic properties of the **MFI** samples based on the pyridine adsorption with FTIR measurement (c_L – concentration of Lewis acid sites, c_B – concentration of Brønsted acid sites).

Sample	c_L [mmol/g]	c_B [mmol/g]	$c_L + c_B$ [mmol/g]
MFI-15	0.139	0.266	0.405
MFI-75	0.050	0.210	0.260
MFI-140	0.024	0.046	0.070

Figure 45 shows the conversions of 1-propanol in tetrahydropyranylation over the **MFI** samples at 60 °C, 40 °C and room temperature. At raised temperature the MFI-15 and 75 clearly dominate, reaching 100% conversion within 1 hour at 60 °C and within 3 hours at 40 °C. The MFI-140 on the other hand gives only 50% conversion at 60 °C and 37% at 40 °C in respective times. At room temperature the conversions of samples after 24 h decrease in following order: MFI-75 (100%) > MFI-15 (84%) > MFI-140 (52%).

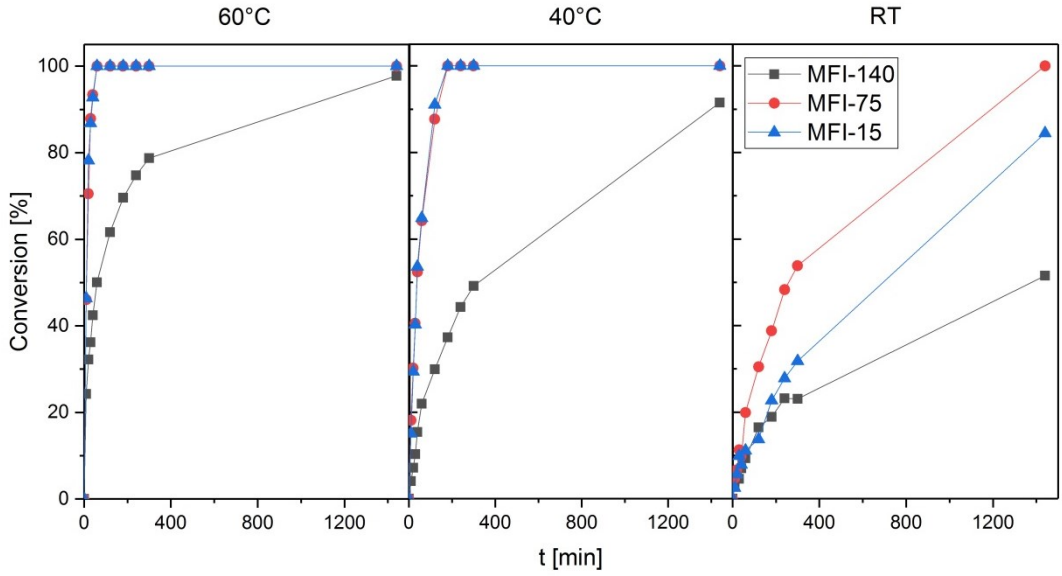

Figure 45: Conversions of 1-propanol over the MFI-140, 75 and 15.

The conversions were re-calculated to the reaction rates and normalised by the concentrations of acid sites in respective samples. The Figure 46 shows that for each temperature the reaction rates decrease in following order: MFI-140 > MFI-75 > MFI-15.

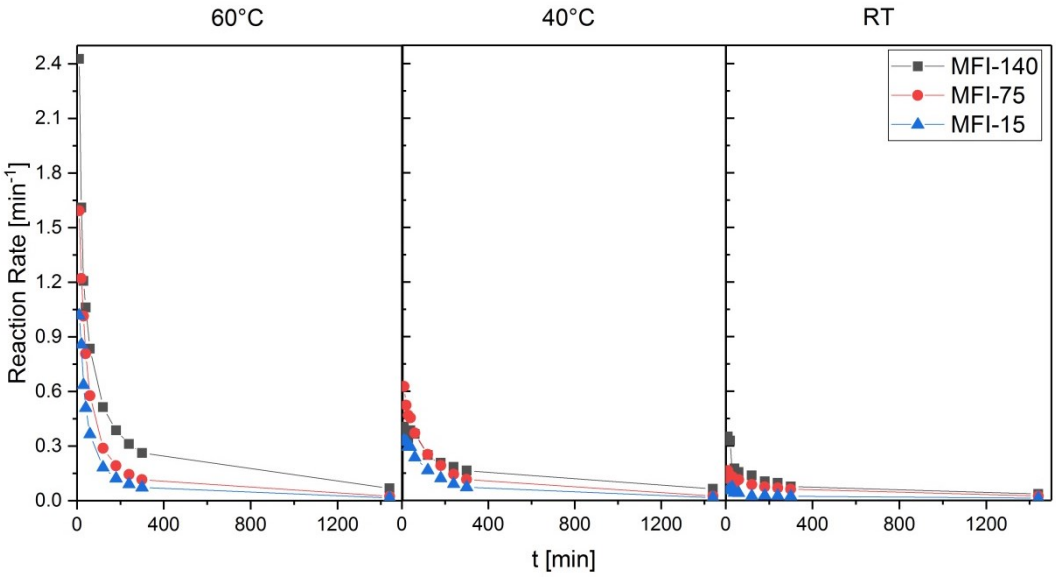

Figure 46: Reaction rates of the tetrahydropyranylation catalysed by the MFI-140, 75 and 15 normalised to the concentrations of active sites.

Figure 47 shows the clearly non-linear dependence of the initial reaction rates (at 10 minutes reaction time) plotted against the concentration of acid sites of the catalysts for each temperature which implies the diffusion contributes to the overall rate of the reaction. Due to that the obtained normalised reaction rates cannot be used for calculating accurate activation energies by the Arrhenius equation.

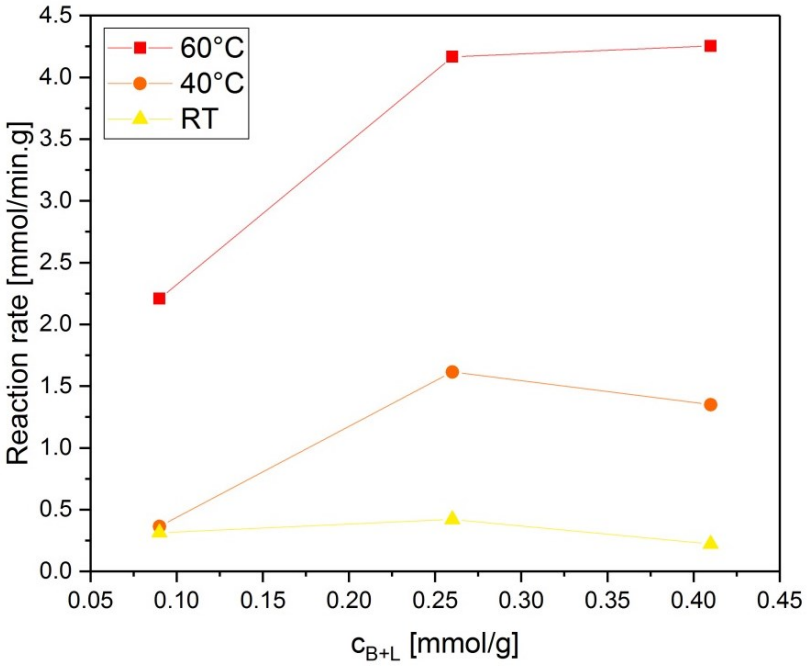

Figure 47: Dependence of the reaction rates (at 10 minutes reaction time) on the concentration of acid sites in the catalyst.

To summarize the results, samples containing high concentration of Brønsted acid sites show better performance than predominantly Lewis acidic samples. Based on the calculated Thiele modulus and the results of the Madon-Boudart test it is clear that the reaction rate is significantly influenced by diffusion of reactants and products through the channel system.

4.3. Impact of zeolite framework and type of acid sites on catalysis of Pechmann condensation

Aluminosilicate and gallosilicate forms of zeolites **MFI** (with three-dimensional 10-ring channels), **MTW** (with one-dimensional 12-ring channels) and ***BEA** (with three-dimensional 12-ring channels) in bulk and hierarchical nanosponge form were chosen to evaluate the impact of the framework topology, morphology and composition in the catalysis of Pechmann condensation of resorcinol.

The aim was to prepare each type of zeolite in the bulk and nanosponge form ideally with the same concentration of acid sites. This task has been fulfilled fairly well (as discussed further bellow), with the exception of gallosilicate ***BEA** zeolites which were too unstable for preparation by the direct hydrothermal method despite multiple synthesis attempts with varying synthesis gel compositions.

4.3.1. Characterization of prepared zeolites

*Aluminosilicate and gallosilicate **MFI***

Samples of **MFI** zeolite were prepared in the form of aluminosilicate (labelled with (Al) suffix) and gallosilicate (labelled with (Ga) suffix), both in the bulk (denoted as bMFI) and nanosponge form (denoted as nsMFI). The Si/T molar ratio (where T = Al or Ga) in the synthesis gel was 100. Crystallinity of the samples was determined by the x-ray diffraction. Figure 48 shows the powder diffraction patterns of all four samples, which are in agreement with simulated powder patterns in the database. [1] Broadening of the diffraction lines of the samples in the nanosponge form is a result of the diffraction on its thin crystallites.

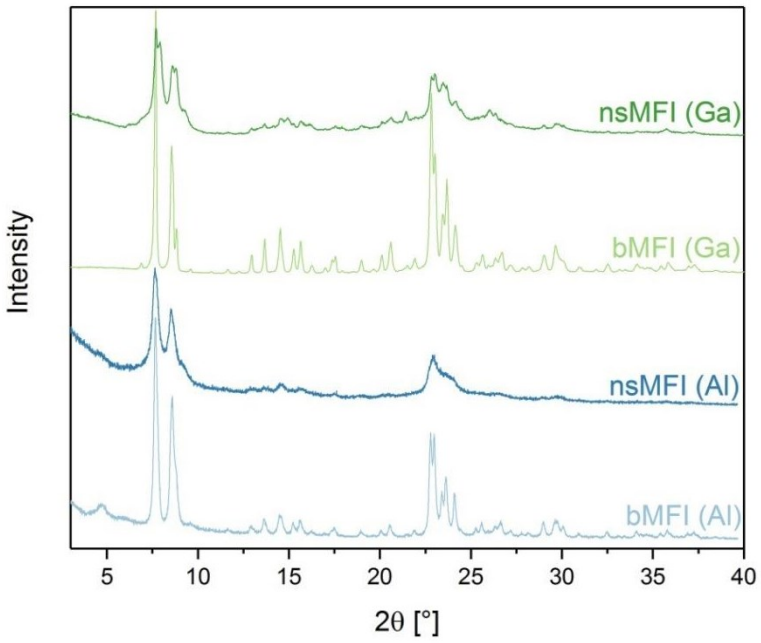

Figure 48: X-ray powder diffraction patterns of the **MFI** samples.

Textural properties of the samples were investigated by the adsorption of argon. Adsorption isotherms are displayed in the Figure 49. Each isotherm shows a significant increase in the adsorbed volume of argon bellow the relative pressure 0.05 which is a result of their microporous nature. With further increasing pressure the isotherms of the bulk samples stay mostly flat, whereas the isotherms of both nanosponge samples keep increasing up to the relative pressure 0.975. This increase indicates presence of mesopores as can be seen from the pore size distribution of the samples. Relatively thin hysteresis loop of the nanosponge samples suggests majority of the mesopores is directly accessible from the external surface. From the Table 14 we can clearly see the

difference between bulk and nanosponge samples. The external surface area of the bulk samples does not exceed 20 m^2/g, whereas both nanosponges have external surface area higher than 150 m^2/g. Similarly the total pore volumes of the nanosponge samples are more than two times higher than total pore volumes of their bulk counterparts.

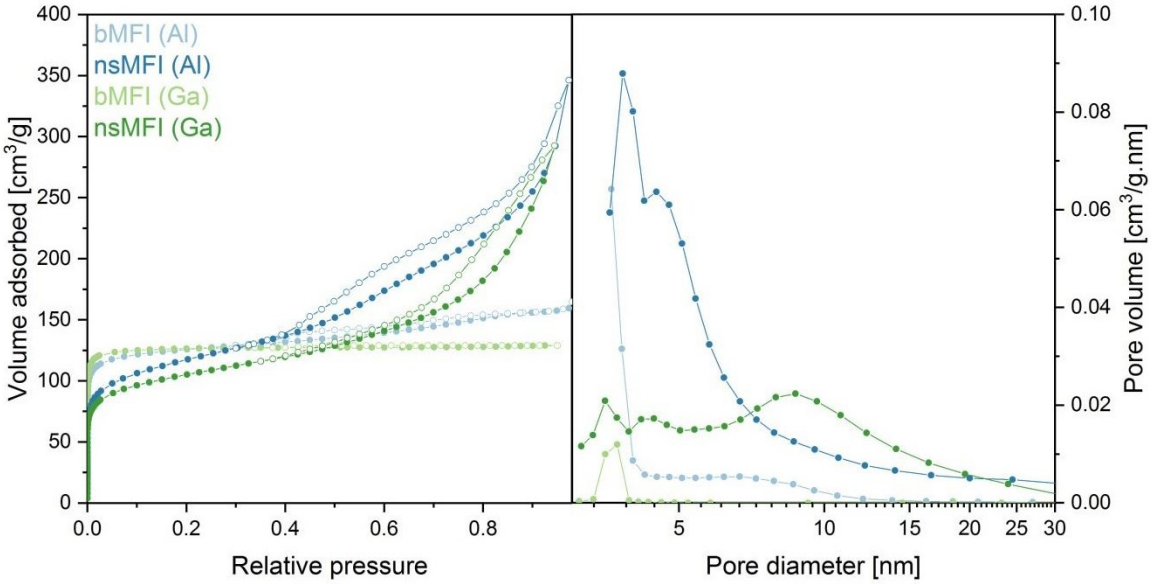

Figure 49: Argon adsorption isotherms and pore size distributions of the **MFI** samples.

Table 14: Textural properties of the **MFI** samples based on the argon adsorption measurement.

Sample	BET [m²/g]	S_{ext} [m²/g]	V_{tot} [cm³/g]	V_{mic} [cm³/g]
bMFI (Al)	270	6	0.112	0.108
nsMFI (Al)	364	202	0.443	0.098
bMFI (Ga)	385	18	0.165	0.160
nsMFI (Ga)	327	154	0.374	0.087

The FTIR spectroscopy measurement of the **MFI** samples after adsorption of pyridine was used to investigate the concentration of Brønsted and Lewis acid sites (Figure 50). Each spectrum contains a peak at 1545 cm^{-1} which corresponds to a pyridine adsorbed on Brønsted sites. Another peaks which lie at 1455 cm^{-1} and 1445 cm^{-1} belong to a pyridine adsorbed on Lewis acid sites of different strength. [92] The concentrations of acid sites of individual samples are listed in Table 155. The aluminosilicate bulk **MFI** contains nearly equal amount of Lewis and Brønsted sites (0.13 and 0.14 mmol/g, respectively). The overall concentration of acid sites in the nanosponge sample is lower than in the bulk one. It also contains more Brønsted sites (0.10 mmol/g) compared to the Lewis sites

(0.07 mmol/g). Total concentrations of acid sites in both gallosilicate MFI zeolites (0.09 and 0.08 mmol/g for the bulk and nanosponge sample, respectively) are comparable and noticeably lower than for their aluminosilicate counterparts (0.27 and 0.17 mmol/g for the bulk and nanosponge sample, respectively). This is a direct result of less favourable incorporation of gallium into the structure during the synthesis. Despite the synthesis mixture having the same molar composition (Si/T 100), the gallosilicate product contains less gallium and thereby lower amount of acid sites compared to the aluminosilicate. Also, it is noteworthy to point out that the peak of weak Lewis sites at 1445 cm^{-1} is dominant for both gallosilicate **MFI** samples, whereas in aluminosilicates the stronger Lewis sites (1455 cm^{-1}) are more common.

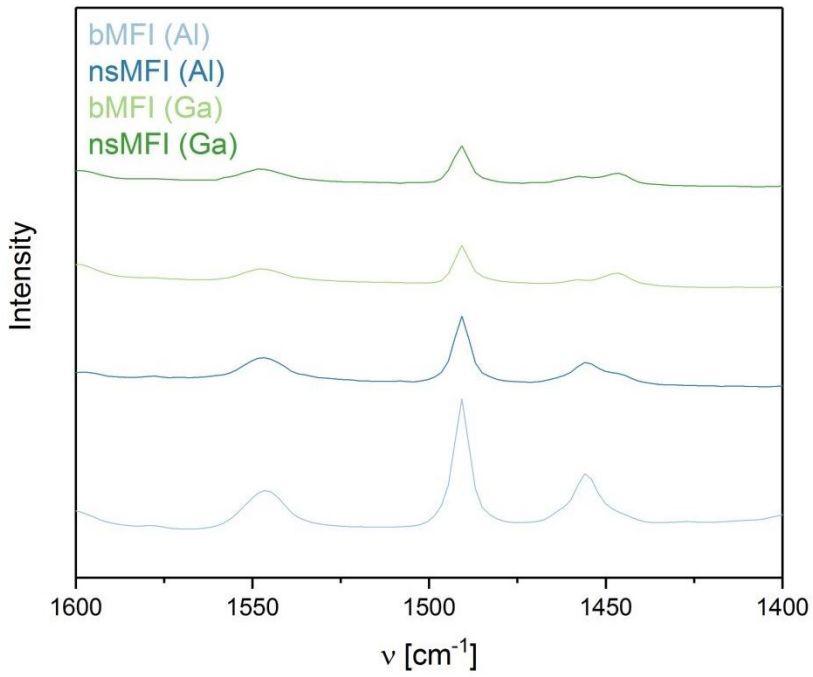

Figure 50: FTIR spectra the **MFI** samples after the adsorption of pyridine.

Table 15: Acidic properties of the **MFI** samples based on the pyridine adsorption with FTIR measurement (c_L – concentration of Lewis acid sites, c_B – concentration of Brønsted acid sites).

	bMFI (Al)	nsMFI (Al)	bMFI (Ga)	nsMFI (Ga)
c_B [mmol/g]	0.14	0.10	0.05	0.04
c_L [mmol/g]	0.13	0.07	0.04	0.04
$c_L + c_B$ [mmol/g]	0.27	0.17	0.09	0.08

*Aluminosilicate and gallosilicate **MTW***

MTW zeolite samples were prepared in the form of aluminosilicate and gallosilicate, both in the bulk and nanosponge form (denoted in the same manner as MFI) from the synthesis gel with Si/T = 50 (where T = Al, Ga). Their crystallinity was investigated by the x-ray diffraction. The diffraction patterns of the bulk aluminosilicate **MTW** in Figure 51 matches well with the simulated powder patterns in the database. [1] On the other hand the powder diffraction pattern of the bulk gallosilicate **MTW** contains several extra diffraction lines at 7.7° and 21.5°. Their presence indicates second minor phase in the sample, which was identifies as **MFI**. The **MFI** phase was formed during the calcination of the as-synthesized gallosilicate **MTW** due to its higher thermal stability compared to the **MTW**. Despite using low temperature and slow heating rate during the calcination, formation of the **MFI** could not be completely prevented. However, due to its narrower pores and relatively low quantity, its presence should not have significant effect on the reaction. Diffraction patterns of both nanosponge samples match the data in the database and again broadening of the diffraction lines is observable. The diffraction lines of the **MFI** competing phase in the gallosilicate nanosponge **MTW** are not visible. However, due to the broadening of the diffraction lines they may be hidden in the noise.

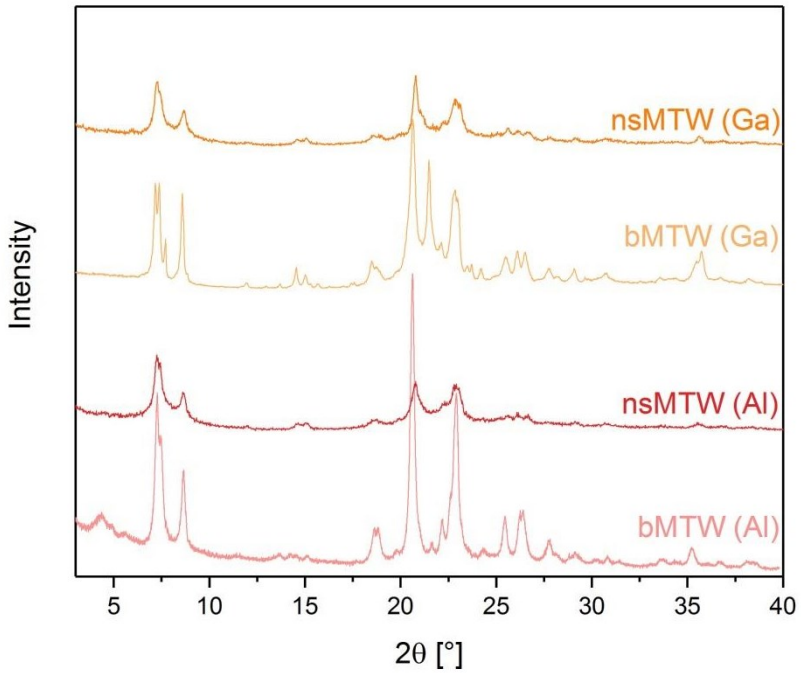

Figure 51: X-ray powder diffraction patterns of the **MTW** samples.

The adsorption isotherms of the **MTW** samples are shown in Figure 52. Up to the relative pressure 0.05 the argon is being adsorbed into the micropores. Similarly to the **MFI**, for the bulk samples the adsorbed amount stays nearly constant with increasing pressure, whereas for both

nanosponge samples keeps increasing after the relative pressure 0.05, which indicates presence of mesopores. The thin hysteresis loop of the nanosponge samples suggests most of the mesopores are directly accessible from the external surface. Although the differences in textural properties are not as striking as were for the **MFI** samples, same trends can be observed. Table 16 presents the external surface area of the both nanosponge samples reaching 161 and 266 m^2/g, whereas the external surface areas of the bulk samples are only 57 and 67 m^2/g. More striking is the difference in the total pore volumes, where both the nanosponge samples have 0.674 and 0.729 cm^3/g, while the total pore volume of the bulk samples is 0.22 and 0.17 cm^3/g.

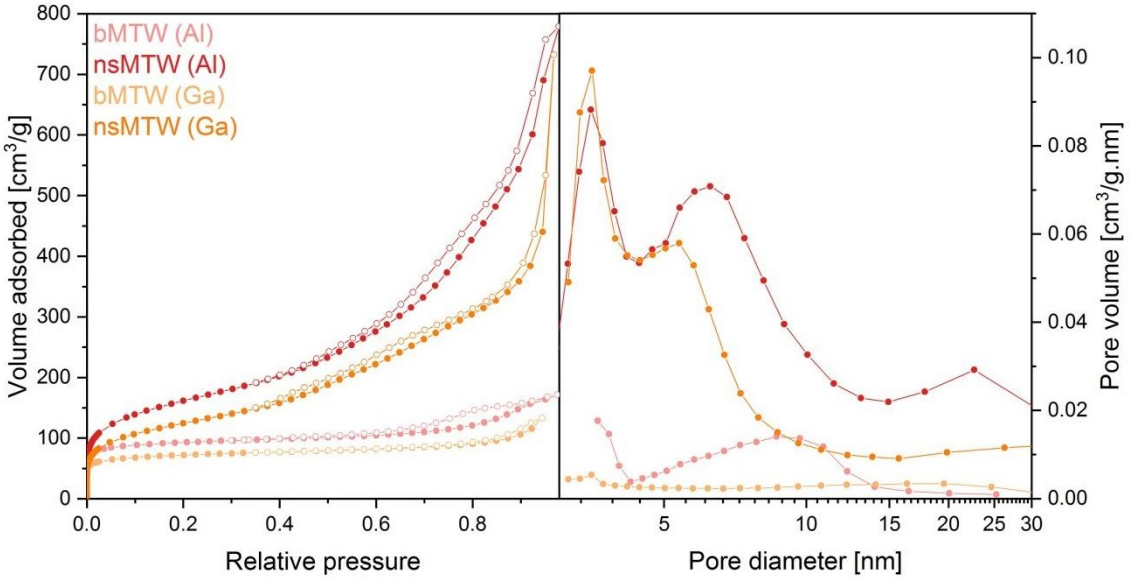

Figure 52: Argon adsorption isotherms and pore size distributions of the **MTW** samples.

Table 16: Textural properties of the **MTW** samples based on the argon adsorption measurement.

Sample	BET [m²/g]	Sext [m²/g]	Vtot [cm³/g]	Vmic [cm³/g]
bMTW (Al)	292	57	0.220	0.094
nsMTW (Al)	379	266	0.729	0.038
bMTW (Ga)	223	67	0.170	0.083
nsMTW (Ga)	396	161	0.674	0.099

The concentrations of acid sites in the **MTW** samples were investigated by adsorption of pyridine followed by FTIR spectroscopy. Figure 53 shows the spectra after adsorption of pyridine. The band at 1545 cm^{-1} corresponds to a pyridine adsorbed on Brønsted sites and the bands at 1455 cm^{-1} and 1445 cm^{-1} to a pyridine adsorbed on strong and weak Lewis acid sites, respectively. Table 17 contains the concentrations of acid sites of the samples. The aluminosilicate bulk **MTW** is predominantly

Brønsted acidic with 0.11 mmol/g compared to 0.03 mmol/g of Lewis acid sites. On the other hand the nanosponge form contains slightly more Lewis sites (0.06 mmol/g) than Brønsted sites (0.05 mmol/g). The concentrations of acid sites in gallosilicate nanosponge **MTW** are very similar (0.06 mmol/g of Brønsted sites and 0.04 mmol/g of Lewis sites). Due to the more difficult incorporation of gallium into the structure the gallosilicate bulk **MTW** contains lower amount of acid sites (0.04 mmol/g and 0.06 mmol/g of Brønsted and Lewis sites, respectively) than the aluminosilicate bulk **MTW**.

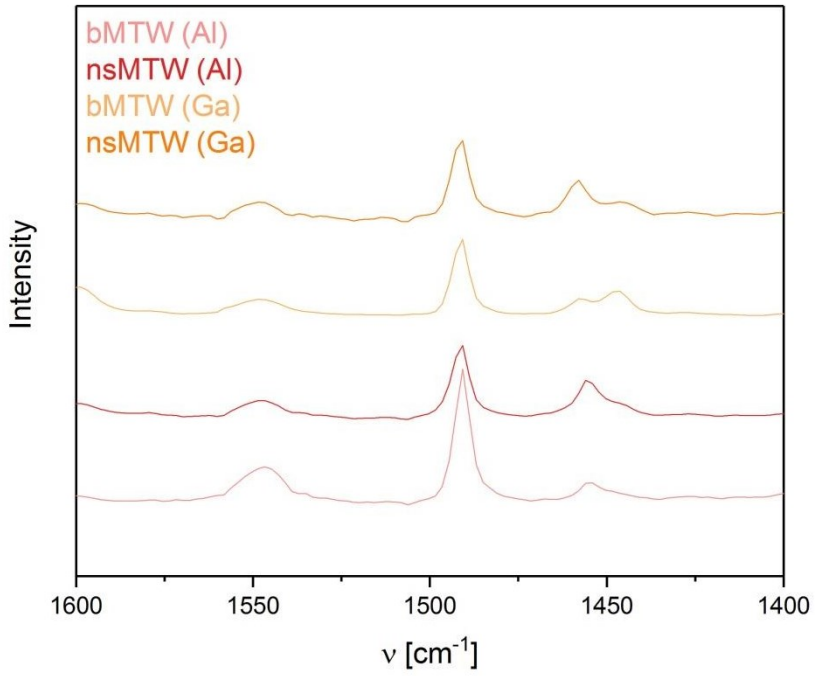

Figure 53: FTIR spectra the **MTW** samples after the adsorption of pyridine.

Table 17: Acidic properties of the **MTW** samples based on the pyridine adsorption with FTIR measurement (c_L – concentration of Lewis acid sites, c_B – concentration of Brønsted acid sites).

	bMTW (Al)	nsMTW (Al)	bMTW (Ga)	nsMTW (Ga)
c_B [mmol/g]	0.11	0.05	0.04	0.04
c_L [mmol/g]	0.03	0.06	0.06	0.06
$c_L + c_B$ [mmol/g]	0.14	0.11	0.10	0.10

*Aluminosilicate and gallosilicate ***BEA***

Commercial aluminosilicate ***BEA** (denoted as cBEA) with the Si/Al molar ratio 15 was used as the bulk sample. The aluminosilicate nanosponge ***BEA** (denoted as nsBEA) was prepared from the

synthesis gel with Si/Al molar ratio 15. The attempts to directly synthesize also the gallosilicate samples widely failed most probably due to their lower hydrothermal stability. Crystallinity of the samples was investigated by the x-ray diffraction. The diffraction patterns of the bulk and nanosponge ***BEA** in Figure 54 are in a good agreement with the simulated powder patterns in the database. [1] The broad diffraction lines at 7.6° and 22.4° in both patterns are a result of the disordered nature of the ***BEA** structure.

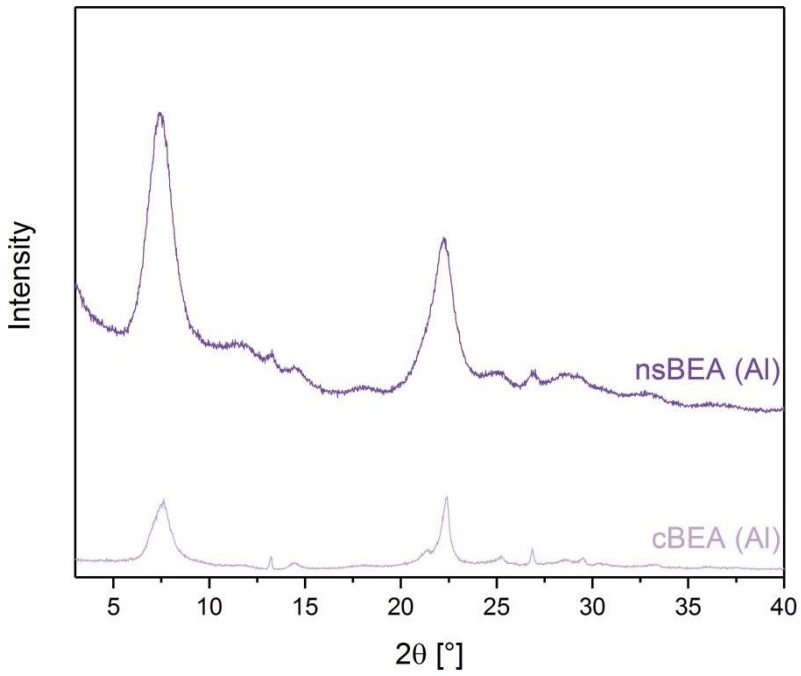

Figure 54: X-ray powder diffraction patterns of the ***BEA** samples.

Textural properties of the ***BEA** samples were investigated by the adsorption of argon. The adsorption isotherms are shown in the Figure 55. The micropores are quickly filled at the low relative pressure range and for the bulk ***BEA** sample the isotherm stays flat with increasing pressure. On the other hand the adsorbed amount on the nanosponge ***BEA** increases further. The hysteresis loop is relatively thin, indicating well accessible mesopores. The two samples can be easily discerned by the external surface area, which is 170 m^2/g for the bulk sample, while the nanosponge ***BEA** has an external surface area 626 m^2/g. Similarly the difference in total pore volumes is clear; 0.301 cm^3/g and 1.387 cm^3/g for the bulk and nanosponge samples, respectively.

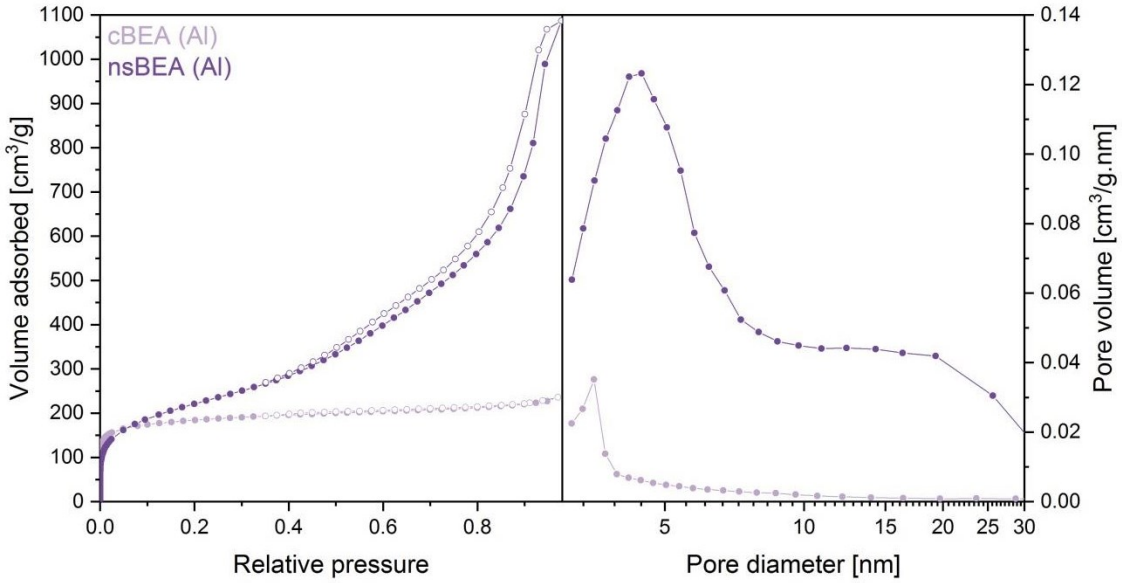

Figure 55: Argon adsorption isotherms and pore size distributions of the ***BEA** samples.

Table 18: Textural properties of the ***BEA** samples based on the argon adsorption measurement.

Sample	BET [m²/g]	Sext [m²/g]	Vtot [cm³/g]	Vmic [cm³/g]
cBEA	560	170	0.301	0.227
nsBEA	712	626	1.387	0.069

The concentrations of Brønsted and Lewis acid sites in the ***BEA** samples were determined by the pyridine adsorption followed by FTIR measurement. Both spectra in Figure 56 show a peak of pyridine adsorbed on Brønsted sites at 1545 cm^{-1} and a band of pyridine adsorbed on Lewis-type sites at 1455 and 1445 cm^{-1}. The majority of the acid sites (Table 19) in the bulk ***BEA** sample are Brønsted acidic, 0.30 mmol/g, whereas only 0.10 mmol/g are Lewis sites. On the other hand, in the nanosponge ***BEA** Lewis sites are dominant with 0.22 mmol/g and only 0.11 mmol/g of Brønsted sites.

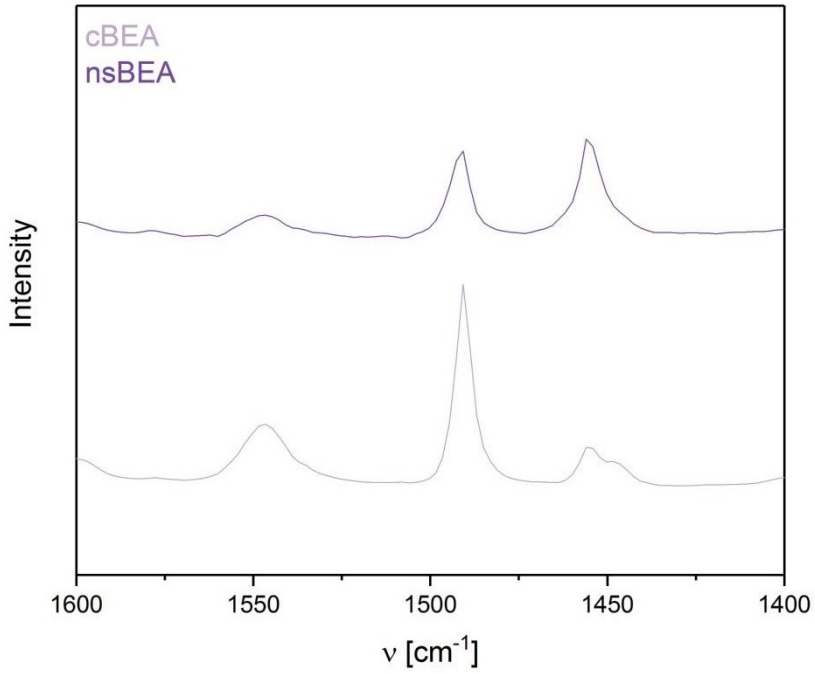

Figure 56: FTIR spectra of the ***BEA** samples after the adsorption of pyridine.

Table 19: Acidic properties of the ***BEA** samples based on the pyridine adsorption with FTIR measurement (c_L – concentration of Lewis acid sites, c_B – concentration of Brønsted acid sites).

	cBEA	nsBEA
c_B [mmol/g]	0.30	0.11
c_L [mmol/g]	0.10	0.22
$c_L + c_B$ [mmol/g]	0.40	0.33

*Acidity strength in aluminosilicate and gallosilicate nanosponge **MTW***

Adsorption of pyridine followed by its desorption at different temperatures was used to compare the strength of acid sites in aluminosilicate and gallosilicate samples. Samples of nanosponge **MTW** zeolite are used as a representative example. The Figure 57 shows the spectra after desorption of pyridine at 150, 250, 350 and 450 °C. The band at 1545 cm^{-1} (pyridine adsorbed on Brønsted sites) stays nearly unchanged till 350 °C and only at 450 °C decreases, which implies a strong bond between the site and the adsorbed pyridine molecule. On the other hand, the bands of the pyridine adsorbed on Lewis acid sites (bands at 1455 cm^{-1} and 1445 cm^{-1}) change with the increasing temperature. After increasing the temperature from 150 °C to 250°C the band at 1445 cm^{-1} disappears. This corresponds to desorption of the pyridine from weak Lewis acid sites. With the

further increasing temperature, the peak at 1455 cm^{-1} decreases slightly. Nevertheless, no significant difference between the gallosilicate and aluminosilicate samples can be observed. The strength of their acid sites in nanosponge form was concluded to be comparable.

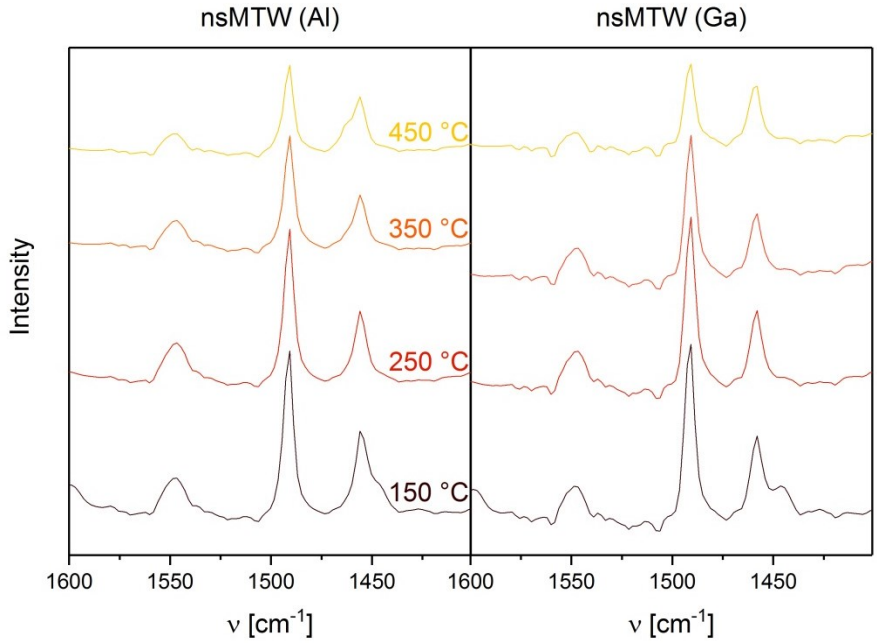

Figure 57: FTIR spectra of the aluminosilicate and gallosilicate nanosponge **MTW** after desorption at varying temperatures.

4.3.2. Pechmann condensation of resorcinol

Aluminosilicate and gallosilicate forms of **MFI**, **MTW** and ***BEA** zeolites were investigated in the Pechmann condensation of phenols. 1,3-Dihydroxybenzene, also called resorcinol, was used as a substrate. The reaction was performed in an excess of ethyl acetoacetate, the second reactant.

The Figure 58Figure 58 shows the conversions of the resorcinol over **MFI** samples up to 24 hours of the reaction time, as well as yields of observable products. Apparently only the aluminosilicate nanosponge form is active. We can see a slow increase in the conversion which reaches 15 % after 24 hours. Simultaneously, the corresponding growth of the yield of the product, hymecromone (7-hydroxy-4-metylcoumarine), can be seen as well. Formation of any side-products has not been detected during the experiment. The conversion over the bulk **MFI** samples is near zero. Their extremely low external surface area is likely the cause of their poor activity. The narrow 10-ring channels of the **MFI** structure, although interconnected in three dimensions, significantly hinder the diffusion of reactants and mainly products and therefore the reaction proceeds at observable rate only when the hierarchical catalyst is applied. Aluminosilicate nanosponge **MFI** has second highest

concentration of acid sites (0.17 mmol/g) after bulk aluminosilicate **MFI** and the largest external surface area (202 m^2/g) among **MFI** samples. Therefore, it is expected that the reaction here proceeds on acid sites located on the accessible external surface.

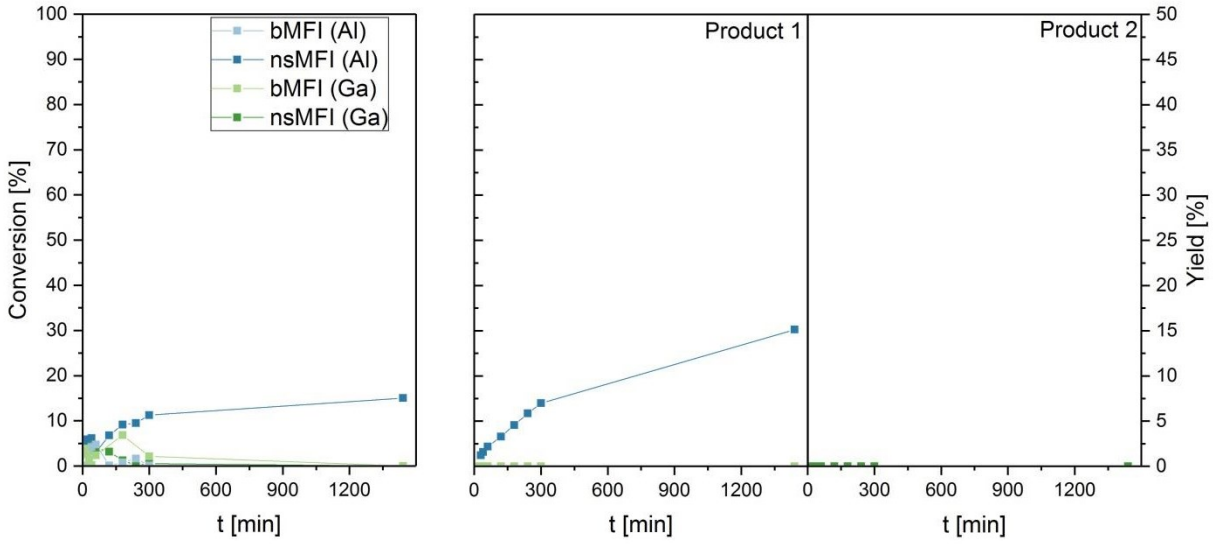

Figure 58: Conversions of resorcinol over **MFI** samples and yields of observable products.

The Figure 59 shows the conversions of the resorcinol over **MTW** samples up to 24 hours of the reaction time, as well as yields of products. The conversions over bulk samples after 24 hours reached 11 and 7 % over the aluminosilicate and gallosilicate, respectively. Yields of the target product (hymecromone) nearly match the conversions and no side-products were detected. The nanosponge forms give higher conversions; 40 % over aluminosiliate and 36 % over gallosilicate after 24 hours and yields of the target product 31% and 30 % for aluminosilicate and gallosilicate respectively. Both nanosponge materials have very similar textural properties as well as total concentration of acid sites (Table 16 and 17). Therefore their catalytic performance is consistence with their properties. Unlike the reactions over **MFI** samples, here we can detect formation of unknown second product after 5 hours of the reaction. The yield of the product reaches 5 % after 24 hours. The large external surface of the nanosponge facilitates the molecular transport, however, at the same time enables bulkier molecules to undergo subsequent reactions on its surface and thereby to form the undesired side-product. Due to large 12-ring channels in **MTW** the reaction can proceed on centres located within the crystals, however, as one-dimensional they represent too long diffusion pathway in bulk materials. In nanosponge where **MTW** is in a form of ultrathin crystal assemblies the molecular transport of reactants and products through each channel is significantly improved.

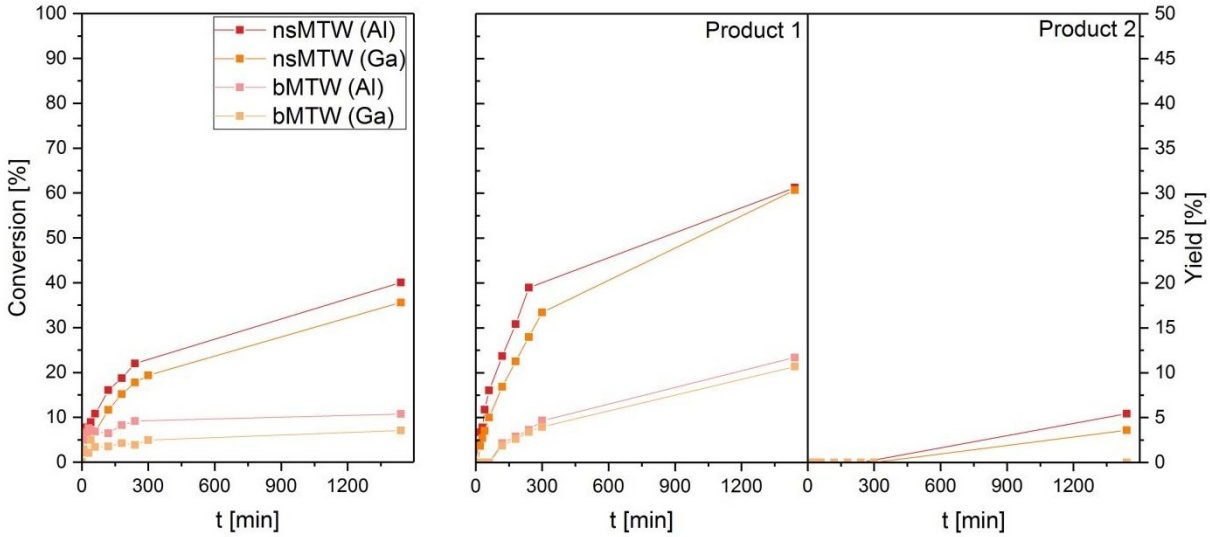

Figure 59: Conversions of resorcinol over **MTW** samples and yields of observable products.

The conversions of the resorcinol over ***BEA** samples up to 24 hours of the reaction time, as well as yields of observable products are depicted in Figure 60. The difference in conversion after 24 hours over both samples is rather small despite the vast differences in textural properties and acidity. More interestingly the bulk ***BEA** sample gives little higher conversion (72 %) than the nanosponge (69 %). This difference is even more pronounced when shorter reaction times are concerned. It implies that for ***BEA** structure the limitation by diffusion is not as prominent and ergo the additional mesoporosity does not augment the reaction rate significantly, because its interconnected 12-ring channels allow fast diffusion of reactants and products. Another observation distinct from reactions over the **MFI** and **MTW** samples is the decrease of the yield of the first product after 5 hours from 38 % to 28 % over the cBEA sample. Simultaneously the formation of second product can be observed. This indicates a presence of subsequent reaction where the first product, hymecromone, reacts to form an unknown secondary product.

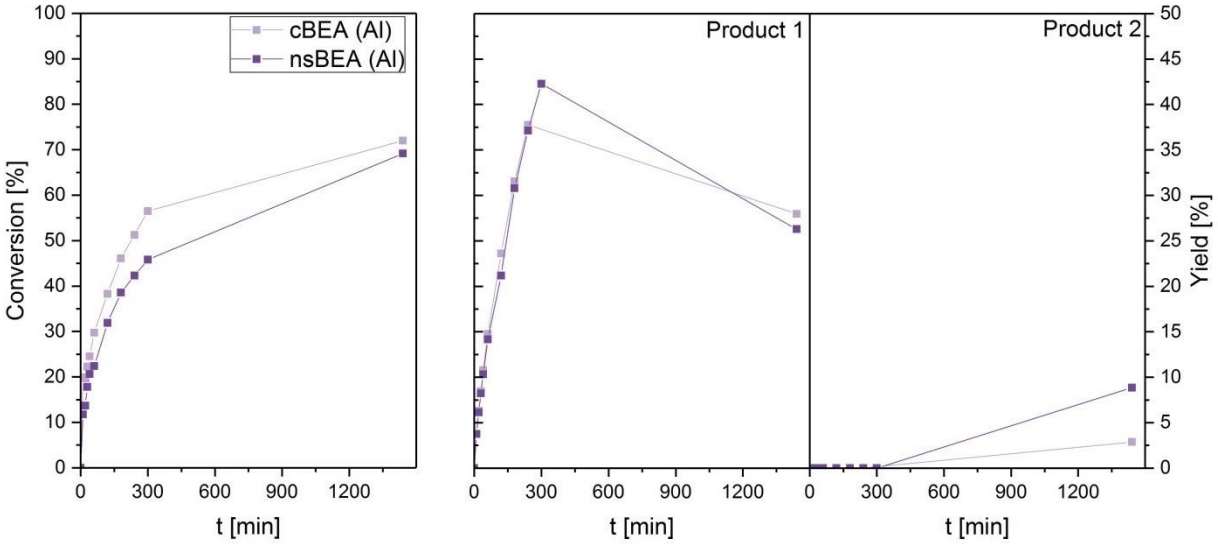

Figure 60: Conversions of resorcinol over ***BEA** samples and yields of observable products.

Conversions of resorcinol over each sample at 3 hours were used to calculate the turn over frequencies of individual samples (Figure 61). In all cases the turnover frequency of the nanosponge is higher than the turnover frequency of its bulk counterpart. The additional mesoporosity facilitates the diffusion of reactants and products, thereby increasing the turnover frequency. The difference is larger for **MFI** (10-10-10-ring channels) and **MTW** (12-ring channels) samples and nearly negligible for ***BEA** (12-12-12-ring channels) samples. It can be deduced that the enhancement of turn-over frequency by the additional mesoporosity becomes less significant with the increasing size and connectivity of the channel system. Due to the low conversions and low concentrations of acid sites in gallosilicate **MFI** samples, the results are inevitably affected by high relative error. From comparison of the turn over frequencies of the **MTW** zeolites it can be concluded that the activity of aluminosilicates is comparable to the gallosilicates.

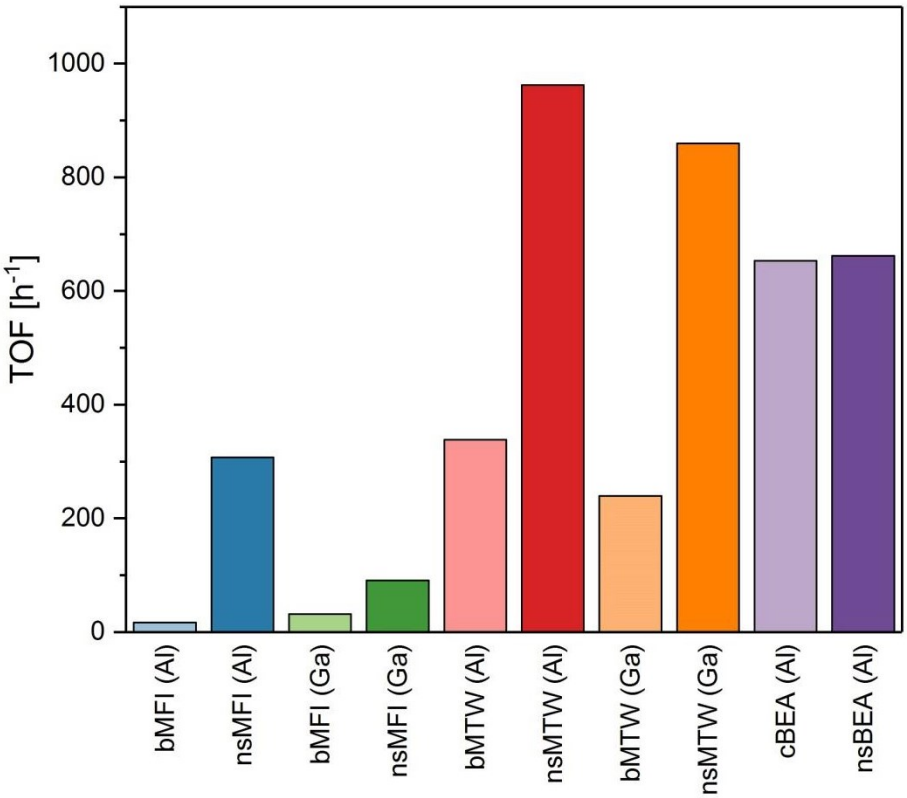

Figure 61: Turn over frequencies of the samples for Pechmann condensation of resorcinol in 3 hours.

5. Conclusions

The aim of the first part of the work was to compare hierarchical forms of zeolite **MTW** prepared by “top-down” and “bottom-up” approaches in the tetrahydropyranylation of alcohols. Zeolite **MTW** was prepared by the direct hydrothermal synthesis in the bulk form as well as in the hierarchical nanosponge form with Si/Al close to 50. The bulk sample was subsequently desilicated, to introduce mesoporosity into the crystals. Solutions of sodium hydroxide with addition of tetrapropylammonium hydroxide, tetrabutylammonium hydroxide or without any additive were used for that purpose. The desilication by pure sodium hydroxide solution resulted in increased external surface area of the sample, coming from the newly created mesopores. The desilication of **MTW** in the presence of tetraalkylammonium cations resulted in a different outcome compared to more often studied **MFI**. In the case of **MTW**, the tetraalkylammonium cations blocked the channel openings and consequently structural debris created during the desilication could not diffuse out of the crystal. This resulted in the micropore blockage and drop of BET surface area and pore volumes. The deviation is ascribed to the different dimensionality of channel system in **MTW** (12R) and **MFI** (10-10-10R). Blocked micropores were possible to release by subsequent acid treatment.

All samples were tested in tetrahydropyranylation of alcohols with varying chain length. Unexpectedly, in all catalytic tests, the desilicated materials with blocked pores exhibited significantly higher activity compared to their acid washed counterparts (with released pore system). The long diffusion path of the reactant/product molecules through the one-dimensional channels of **MTW**, although containing some mesopores, most likely causes the decrease of the reaction rate. Although the conversions of reactants over nanosponge **MTW** are the highest in all tested reactions, the desilicated materials with blocked pores show nearly comparable conversion and activity in the means of TOF values when branched alcohols are used as the substrate. The explanation is that when the micropores are inaccessible, the reaction proceeds over the active centres located on the external surface of the catalyst, where the reaction rate is not limited by diffusion through micropores.

The aim of the second part of the work was to investigate the effect of particular types of acid centres on the catalytic performance of the zeolite in tetrahydropyranylation. Commercial **MFI** zeolite was converted to its protonated form and subsequently partially ion exchanged with lithium or sodium cations to poison portion of its Brønsted acid sites. In this way samples with different concentrations of Brønsted and Lewis acid sites were prepared. With addition of purely Lewis acidic titanosilicate TS-1, all samples were tested in the tetrahydropyranylation of 1-propanol at room temperature, 40 °C and 60 °C.

The material with the largest concentration of Brønsted acid sites (H^+MFI) are the most active catalysts, giving 100 % conversion after only few hours at raised temperature (60 and 40 °C) and 96 % conversion after 24 hours at room temperature. Samples with predominant Lewis acidity (Li^+MFI, Na^+MFI, TS-1) provide lower conversions which strongly depend on the reaction temperature. The samples appeared virtually inactive at RT, whereas conversions between 99 and 91 % were observed at 60°C after 24 hours. The results of the Madon-Boudart test, which was performed using three samples of **MFI** zeolite with different Si/Al ratios, showed that the reaction rate limiting step is the diffusion of reactants and products through the micropores. The diffusion barrier does not allow calculation of the activation energies from the experimental data alone.

In conclusion, samples containing Brønsted acid sites are more suitable for catalysis of tetrahydropyranylation as it was confirmed also by the theoretical calculations. The application of hierarchical zeolite is advised to diminish the diffusion limitation and to enable reactions of bulkier molecules.

In the third part of the work, zeolites **MFI**, **MTW** and ***BEA** were prepared in the bulk and nanosponge form by the direct hydrothermal synthesis. **MFI** and **MTW** were prepared both as

aluminosilicates and gallosilicates. The lower stability of gallosilicate ***BEA** compromised the synthesis attempts and therefore only the aluminosilicate was further investigated. Crystallinity and textural properties of the **MFI** samples allow clearly discern the bulk and nanosponge form. Properties of aluminosilicate and gallosilicate samples in respective form are in a good agreement. Due to its lower hydrothermal stability the gallosilicate **MTW** is prone to formation of competing phases (**MFI**) during the crystallization and calcination. Yet again, all bulk and nanosponge samples show striking differences in their external surface areas and pore volumes. ***BEA** zeolites also show clear difference of the textural properties between the bulk and nanosponge form, although the surface area of the bulk form is already large compared to the **MTW** and **MFI** samples.

The catalysts were tested in Pechmann condensation of resorcinol. Both bulk **MFI** samples appeared inactive. Only the aluminosilicate nanosponge **MFI** reached 15 % conversion after 24 hours with corresponding yield of a single product, whereas no conversion or product formation was observed for its gallosilicate counterpart. Similar conversions (11 % and 7 %) and product yields were observed for both bulk **MTW** samples. The nanosponge **MTW** samples give higher conversions, 40 % and 36 % for the aluminosilicate and gallosilicate, respectively. The conversions of resorcinol over bulk and nanosponge ***BEA** are very similar, 72 % and 69 % respectively. Due to its wide 12-12-12-ring channel system the mass transport is faster and therefore the additional mesoporosity has no significant impact on the reaction rate.

In summary, with the increasing diameter and connectivity of the channels the conversion of reactants over individual samples increases accordingly. In the case of studied zeolites it follows the order **MFI** < **MTW** < ***BEA**. Correspondingly, the differences in activity (in terms of turn-over frequencies) between the bulk and hierarchical zeolites become less significant with increasing channel size and connectivity. On top of that, due to the lower constraints imposed by frameworks of increasing size of the channels, the selectivity decreases, which results in formation of secondary subsequent products. Judging from the results of **MTW** zeolite catalysts, the activity of aluminosilicates in the Pechmann condensation is comparable to the gallosilicates. Taking their generally higher hydrothermal stability into account, the aluminosilicates are more easily applicable as catalysts for the reaction.

6. Literature

[1] C. Baerlocher, L.B. McCusker, D.H. Olson, Atlas of Zeolite Framework Types, Elsevier, Amsterdam, 2007.
[2] J. Čejka, N. Žilková, Syntéza a Struktura zeolitů, Chem. Listy 94 (2000) 278-287.
[3] S.o.C.o.P.S. International Union of Pure and Applied Chemistry Physical Chemistry Division Commission on Colloid and Surface Chemistry, Recommendations for the characterization of porous solids (Technical Report), Pure Appl. Chem., 66 (1994) 1739–1758.

[4] C. Colella, M. Gennaro, R. Aiello, Use of Zeolitic Tuff in the Building Industry, Reviews in Mineralogy and Geochemistry, 45 (2001) 551-587.
[5] J. Perez-Ramirez, C.H. Christensen, K. Egeblad, C.H. Christensen, J.C. Groen, Hierarchical zeolites: enhanced utilisation of microporous crystals in catalysis by advances in materials design, Chemical Society Reviews, 37 (2008) 2530-2542.
[6] P. Eliášová, M. Opanasenko, P.S. Wheatley, M. Shamzhy, M. Mazur, P. Nachtigall, W.J. Roth, R.E. Morris, J. Čejka, The ADOR mechanism for the synthesis of new zeolites, Chemical Society Reviews, 44 (2015) 7177-7206.
[7] W.J. Roth, P. Nachtigall, R.E. Morris, J. Čejka, Two-Dimensional Zeolites: Current Status and Perspectives, Chemical Reviews, 114 (2014) 4807-4837.
[8] T. Maesen, Chapter 1 - The Zeolite Scene – An Overview, in: J. Čejka, H. van Bekkum, A. Corma, F. Schüth (Eds.) Studies in Surface Science and Catalysis, Elsevier, 2007, pp. 1-12.
[9] R.E. Morris, Modular materials from zeolite-like building blocks, J. Mater. Chem., 15 (2005) 931-938.
[10] K. Byrappa, M. Yoshimura, Hydrothermal Synthesis and Growth of Zeolites, in: K. Byrappa, M. Yoshimura (Eds.) Handbook of Hydrothermal Technology, William Andrew Publishing, Norwich, NY, 2001, pp. 315-414.
[11] C. Baerlocher, L.B. McCusker, in, Database of Zeolite Structures: http://www.iza-structure.org/databases/.
[12] E.M. Flanigen, Chapter 2 Zeolites and molecular sieves: An historical perspective, in: H. van Bekkum, E.M. Flanigen, P.A. Jacobs, J.C. Jansen (Eds.) Studies in Surface Science and Catalysis, Elsevier, 2001, pp. 11-35.
[13] L.B. McCusker, C. Baerlocher, Chapter 2 - Zeolite Structures, in: J. Čejka, H. van Bekkum, A. Corma, F. Schüth (Eds.) Studies in Surface Science and Catalysis, Elsevier, 2007, pp. 13-37.
[14] S. De, S. Dutta, B. Saha, Critical design of heterogeneous catalysts for biomass valorization: current thrust and emerging prospects, Catalysis Science & Technology, 6 (2016) 7364-7385.
[15] W. Loewenstein, The distribution of aluminum in the tetrahedra of silicates and aluminates, American Mineralogist, 39 (1954) 92-96.
[16] P. Wu, T. Tatsumi, A new generation of titanosilicate catalyst: preparation and application to liquid-phase epoxidation of alkenes, Catalysis Surveys from Asia, 8 (2004) 137-148.
[17] J. Přech, Catalytic performance of advanced titanosilicate selective oxidation catalysts – a review, Catalysis Reviews, 60 (2018) 71-131.
[18] A. Tuel, Y.B. Taarit, Synthesis of TS-1 from titanosilicate gels containing TPAOH/TEAOH and TPAOH/NH4OH mixtures, Microporous Materials, 1 (1993) 179-189.
[19] G. Bellussi, M.S. Rigutto, Chapter 19 Metal ions associated to molecular sieve frameworks as catalytic sites for selective oxidation reactions, in: H. van Bekkum, E.M. Flanigen, P.A. Jacobs, J.C. Jansen (Eds.) Studies in Surface Science and Catalysis, Elsevier, 2001, pp. 911-955.
[20] S. Gopal, K. Yoo, P.G. Smirniotis, Synthesis of Al-rich ZSM-12 using TEAOH as template, Microporous and Mesoporous Materials, 49 (2001) 149-156.
[21] M.K.R. E. J. Rosinski, Crystalline zeolite ZSM-12, US3832449A, 1974.
[22] W. Wu, W. Wu, O.V. Kikhtyanin, L. Li, A.V. Toktarev, A.B. Ayupov, J.F. Khabibulin, G.V. Echevsky, J. Huang, Methylation of naphthalene on MTW-type zeolites. Influence of template origin and substitution of Al by Ga, Applied Catalysis A: General, 375 (2010) 279-288.
[23] K. Iyoki, Y. Kamimura, K. Itabashi, A. Shimojima, T. Okubo, Synthesis of MTW-type Zeolites in the Absence of Organic Structure-directing Agent, Chemistry Letters, 39 (2010) 730-731.
[24] W. Zhang, P.G. Smirniotis, Effect of Zeolite Structure and Acidity on the Product Selectivity and Reaction Mechanism forn-Octane Hydroisomerization and Hydrocracking, Journal of Catalysis, 182 (1999) 400-416.
[25] C.W. Jones, S.I. Zones, M. E. Davis, m-Xylene reactions over zeolites with unidimensional pore systems, Applied Catalysis A: General, 181 (1999) 289-303.

[26] J.B. Higgins, R.B. LaPierre, J.L. Schlenker, A.C. Rohrman, J.D. Wood, G.T. Kerr, W.J. Rohrbaugh, The framework topology of zeolite beta, Zeolites, 8 (1988) 446-452.
[27] S. Smeets, X. Zou, Zeolite Structures, Chapter 2 in: R.E.M. Jiří Čejka, Petr Nachtigall (Ed.) Zeolites in Catalysis: Properties and Applications, The Royal Society of Chemistry, 2017, pp. 37-72.
[28] T. Conradsson, M.S. Dadachov, X.D. Zou, Synthesis and structure of (Me3N)6[Ge32O64]·(H2O)4.5, a thermally stable novel zeotype with 3D interconnected 12-ring channels, Microporous and Mesoporous Materials, 41 (2000) 183-191.
[29] A. Martínez, M.A. Arribas, S. Moussa, Application of Zeolites in the Production of Light Olefins and BTX Petrochemical Intermediates, in: R.E.M. Jiří Čejka, Petr Nachtigall (Ed.) Zeolites in Catalysis: Properties and Applications, The Royal Society of Chemistry, 2017, pp. 351-408.
[30] E.M.F. R. W. Grose, Novel zeolite compositions and processes for preparing and using same, US4257885A, Belgium, 1977.
[31] M. Taramasso, G. Perego, B. Notari, Preparation of porous crystalline synthetic material comprised of silicon and titanium oxides, US4410501A, SnamProgetti SpA, United States, 1983.
[32] K. Byrappa, M. Yoshimura, Hydrothermal Technology—Principles and Applications, in: K. Byrappa, M. Yoshimura (Eds.) Handbook of Hydrothermal Technology, William Andrew Publishing, Norwich, NY, 2001, pp. 1-52.
[33] J. Yu, Synthesis of Zeolites, in: J. Čejka, H. van Bekkum, A. Corma, F. Schüth (Eds.) Studies in Surface Science and Catalysis, Elsevier, 2007, pp. 39-103.
[34] W. Meise, S. FE, Kinetic Studies on Formation of Zeolite-A, Advances in Chemistry Series, (1973) 169-178.
[35] A. Corma, F. Rey, J. Rius, M.J. Sabater, S. Valencia, Supramolecular self-assembled molecules as organic directing agent for synthesis of zeolites, Nature, 431 (2004) 287-290.
[36] J. Dwyer, Evaluation and Tailoring of Acid-Base Properties of Zeolites, in: F.L. E.G. Derouane, C. Naccache, F. Ramôa Ribeiro (Ed.) Zeolite Microporous Solids: Synthesis, Structure and Reactivity, Springer, 1992, pp. 303-319.
[37] B.M. Lok, T.R. Cannan, C.A. Messina, The role of organic molecules in molecular sieve synthesis, Zeolites, 3 (1983) 282-291.
[38] C.S. Gittleman, S.S. Lee, A.T. Bell, C.J. Radke, Zeolite synthesis from tetraalkylammonium silicate gels, Microporous Materials, 3 (1995) 511-530.
[39] M.V. Shamzhy, O.V. Shvets, M.V. Opanasenko, P.S. Yaremov, L.G. Sarkisyan, P. Chlubná, A. Zukal, V.R. Marthala, M. Hartmann, J. Čejka, Synthesis of isomorphously substituted extra-large pore UTL zeolites, J. Mater. Chem., 22 (2012) 15793-15803.
[40] W. Schwieger, A.G. Machoke, B. Reiprich, T. Weissenberger, T. Selvam, M. Hartmann, Chapter 4 Hierarchical Zeolites, in: Zeolites in Catalysis: Properties and Applications, The Royal Society of Chemistry, 2017, pp. 103-145.
[41] S. Mintova, J. Čejka, Chapter 9 - Micro/Mesoporous Composites, in: J. Čejka, H. van Bekkum, A. Corma, F. Schüth (Eds.) Studies in Surface Science and Catalysis, Elsevier, 2007, pp. 301-VI.
[42] X. Wei, P.G. Smirniotis, Synthesis and characterization of mesoporous ZSM-12 by using carbon particles, Microporous and Mesoporous Materials, 89 (2006) 170-178.
[43] C. Jo, K. Cho, J. Kim, R. Ryoo, MFI zeolite nanosponges possessing uniform mesopores generated by bulk crystal seeding in the hierarchical surfactant-directed synthesis, Chemical Communications, 50 (2014) 4175-4177.
[44] W.J. Roth, B. Gil, W. Makowski, B. Marszalek, P. Eliášová, Layer like porous materials with hierarchical structure, Chemical Society Reviews, 45 (2016) 3400-3438.
[45] R. Srivastava, M. Choi, R. Ryoo, Mesoporous materials with zeolite framework: remarkable effect of the hierarchical structure for retardation of catalyst deactivation, Chemical Communications, 43 (2006) 4489-4491.
[46] J. Kim, M. Choi, R. Ryoo, Effect of mesoporosity against the deactivation of MFI zeolite catalyst during the methanol-to-hydrocarbon conversion process, Journal of Catalysis, 269 (2010) 219-228.

[47] W. Kim, J.-C. Kim, J. Kim, Y. Seo, R. Ryoo, External Surface Catalytic Sites of Surfactant-Tailored Nanomorphic Zeolites for Benzene Isopropylation to Cumene, ACS Catalysis, 3 (2013) 192-195.
[48] M. Choi, H.S. Cho, R. Srivastava, C. Venkatesan, D.-H. Choi, R. Ryoo, Amphiphilic organosilane-directed synthesis of crystalline zeolite with tunable mesoporosity, Nature Materials, 5 (2006) 718-723.
[49] D. Xu, Y. Ma, Z. Jing, L. Han, B. Singh, J. Feng, X. Shen, F. Cao, P. Oleynikov, H. Sun, O. Terasaki, S. Che, π–π interaction of aromatic groups in amphiphilic molecules directing for single-crystalline mesostructured zeolite nanosheets, Nature Communications, 5 (2014) 4262.
[50] M. Kubů, M. Opanasenko, M. Shamzy, Modification of textural and acidic properties of -SVR zeolite by desilication, Catalysis Today, 227 (2014) 26-32.
[51] M. Kubů, M. Opanasenko, D. Vitvarová, Desilication of SSZ-33 zeolite – Post-synthesis modification of textural and acidic properties, Catalysis Today, 243 (2015) 46-52.
[52] V.J. Frilette, M.K. Rubin, SORPTION AND CATALYTIC PROPERTIES OF NATURAL MORDENITE, Journal of Catalysis, 4 (1965) 310-&.
[53] H.K. Beyer, I.M. Belenykaja, F. Hange, M. Tielen, P.J. Grobet, P.A. Jacobs, PREPARATION OF HIGH-SILICA FAUJASITES BY TREATMENT WITH SILICON TETRACHLORIDE, Journal of the Chemical Society-Faraday Transactions I, 81 (1985) 2889-2901.
[54] J.C. Groen, J.A. Moulijn, J. Pérez-Ramírez, Decoupling mesoporosity formation and acidity modification in ZSM-5 zeolites by sequential desilication–dealumination, Microporous and Mesoporous Materials, 87 (2005) 153-161.
[55] D. Verboekend, J. Perez-Ramirez, Desilication Mechanism Revisited: Highly Mesoporous All-Silica Zeolites Enabled Through Pore-Directing Agents, Chemistry-a European Journal, 17 (2011) 1137-1147.
[56] R.P. Townsend, E.N. Coker, Chapter 11 Ion exchange in zeolites, in: H. van Bekkum, E.M. Flanigen, P.A. Jacobs, J.C. Jansen (Eds.) Studies in Surface Science and Catalysis, Elsevier, 2001, pp. 467-524.
[57] M. Shamzhy, M. Opanasenko, P. Concepción, A. Martínez, New trends in tailoring active sites in zeolite-based catalysts, Chemical Society Reviews, 48 (2019) 1095-1149.
[58] H. Koller, C.-Y. Chen, S.I. Zones, Selectivities in Post-Synthetic Modification of Borosilicate Zeolites, Topics in Catalysis, 58 (2015) 451-479.
[59] V. Kasneryk, M. Opanasenko, M. Shamzhy, Z. Musilová, Y.S. Avadhut, M. Hartmann, J. Čejka, Consecutive interlayer disassembly–reassembly during alumination of UOV zeolites: insight into the mechanism, Journal of Materials Chemistry A, 5 (2017) 22576-22587.
[60] M. Shamzhy, F.S.d.O. Ramos, Tuning of acidic and catalytic properties of IWR zeolite by post-synthesis incorporation of three-valent elements, Catalysis Today, 243 (2015) 76-84.
[61] M.V. Shamzhy, P. Eliášová, D. Vitvarová, M.V. Opanasenko, D.S. Firth, R.E. Morris, Post-Synthesis Stabilization of Germanosilicate Zeolites ITH, IWW, and UTL by Substitution of Ge for Al, Chemistry – A European Journal, 22 (2016) 17377-17386.
[62] R. Fricke, H. Kosslick, G. Lischke, M. Richter, Incorporation of Gallium into Zeolites: Syntheses, Properties and Catalytic Application, Chemical Reviews, 100 (2000) 2303-2406.
[63] R.M. Barrer, B.M. Munday, Cation exchange reactions of zeolite na-P, Journal of the Chemical Society A: Inorganic, Physical, Theoretical, (1971) 2909-2914.
[64] P. Fletcher, R.P. Townsend, Ion-exchange of amminated palladium and platinum in synthetic sodium zeolites, Zeolites, 3 (1983) 129-133.
[65] A. Corma, Transformation of hydrocarbons on zeolite catalysts, Catalysis Letters, 22 (1993) 33-52.
[66] A. Akah, M. Al-Ghrami, Maximizing propylene production via FCC technology, Applied Petrochemical Research, 5 (2015) 377-392.
[67] E. Roduner, Understanding catalysis, Chemical Society Reviews, 43 (2014) 8226-8239.

[68] J. Weitkamp, M. Hunger, Chapter 22 - Acid and Base Catalysis on Zeolites, in: J. Čejka, H. van Bekkum, A. Corma, F. Schüth (Eds.) Studies in Surface Science and Catalysis, Elsevier, 2007, pp. 787-835.
[69] B. Smit, T.L.M. Maesen, Towards a molecular understanding of shape selectivity, Nature, 451 (2008) 671-678.
[70] S.M. Csicsery, Shape-selective catalysis in zeolites, Zeolites, 4 (1984) 202-213.
[71] P.M.M. Blauwhoff, J.W. Gosselink, E.P. Kieffer, S.T. Sie, W.H.J. Stork, Zeolites as Catalysts in Industrial Processes, in: J. Weitkamp, L. Puppe (Eds.) Catalysis and Zeolites: Fundamentals and Applications, Springer Berlin Heidelberg, Berlin, Heidelberg, 1999, pp. 437-538.
[72] G. Bartoli, R. Giovannini, A. Giuliani, E. Marcantoni, M. Massaccesi, P. Melchiorre, M. Paoletti, L. Sambri, Solvent-Free Carbon–Oxygen Bond Formation Catalysed by CeCl3·7 H2O/NaI: Tetrahydropyranylation of Hydroxy Groups, European Journal of Organic Chemistry, 2006 (2006) 1476-1482.
[73] T.W. Greene, P.G.M. Wuts, Protection for the Hydroxyl Group, Including 1,2- and 1,3-Diols, Chapter 2 in: Protective Groups in Organic Synthesis, John Wiley & Sons, Inc., 2002, pp. 17-245.
[74] B. Tamami, K. Parvanak Borujeny, Chemoselective tetrahydropyranylation of alcohols and phenols using polystyrene supported aluminium chloride as a catalyst, Tetrahedron Letters, 45 (2004) 715-718.
[75] G.P. Romanelli, G. Baronetti, H.J. Thomas, J.C. Autino, Efficient method for tetrahydropyranylation/depyranylation of phenols and alcohols using a solid acid catalyst with Wells–Dawson structure, Tetrahedron Letters, 43 (2002) 7589-7591.
[76] M. Kotke, P.R. Schreiner, Generally applicable organocatalytic tetrahydropyranylation of hydroxy functionalities with very low catalyst loading, Synthesis, (2007) 779-790.
[77] A. Hegedüs, I. Vígh, Z. Hell, Zeolite-Catalyzed Environmentally Friendly Tetrahydropyranylation of Alcohols and Phenols, Synth. Commun., 34 (2004) 4145-4152.
[78] H.S. Shin, M. Opanasenko, C.P. Cabello, R. Ryoo, J. Čejka, Surfactant-directed mesoporous zeolites with enhanced catalytic activity in tetrahydropyranylation of alcohols: Effect of framework type and morphology, Applied Catalysis A: General, 537 (2017) 24-32.
[79] J.R. Johnson, The Perkin Reaction and Related Reactions, Organic Reactions, 1 (2011) 210-265.
[80] R.L. Shriner, The Reformatsky Reaction, Organic Reactions, 1 (2011) 1-37.
[81] I. Yavari, R. Hekmat-Shoar, A. Zonouzi, A new and efficient route to 4-carboxymethylcoumarins mediated by vinyltriphenylphosphonium salt, Tetrahedron Letters, 39 (1998) 2391-2392.
[82] S. Tyndall, K.F. Wong, M.A. VanAlstine-Parris, Insight into the Mechanism of the Pechmann Condensation Reaction Using NMR, The Journal of Organic Chemistry, 80 (2015) 8951-8953.
[83] J. Daru, A. Stirling, Mechanism of the Pechmann Reaction: A Theoretical Study, The Journal of Organic Chemistry, 76 (2011) 8749-8755.
[84] L.L. Woods, J. Sapp, A NEW 1-STEP SYNTHESIS OF SUBSTITUTED COUMARINS, J. Org. Chem., 27 (1962) 3703-3705.
[85] J.R.F. Alfred Russell, 2,6-Dihydroxyacetophenone, Organic Syntheses Collective, 3 (1955) 281.
[86] M. Opanasenko, M. Shamzhy, J. Čejka, Solid Acid Catalysts for Coumarin Synthesis by the Pechmann Reaction: MOFs versus Zeolites, ChemCatChem, 5 (2013) 1024-1031.
[87] J.-C. Kim, R. Ryoo, M.V. Opanasenko, M.V. Shamzhy, J. Čejka, Mesoporous MFI Zeolite Nanosponge as a High-Performance Catalyst in the Pechmann Condensation Reaction, ACS Catalysis, 5 (2015) 2596-2604.
[88] R.J. Madon, M. Boudart, EXPERIMENTAL CRITERION FOR THE ABSENCE OF ARTIFACTS IN THE MEASUREMENT OF RATES OF HETEROGENEOUS CATALYTIC REACTIONS, Industrial & Engineering Chemistry Fundamentals, 21 (1982) 438-447.
[89] R.E. Morris, P.K. Allan, Chapter 6 Structure Determination, in: Zeolites in Catalysis: Properties and Applications, The Royal Society of Chemistry, 2017, pp. 194-239.
[90] K. Abbasian, M.H. Abdollahi, Electromagnetically induced transparency-based gas detector design using Michelson interferometer, International Nano Letters, 3 (2013) 34-41.

[91] A. Jentys, J.A. Lercher, Chapter 8 Techniques of zeolite characterization, in: H. van Bekkum, E.M. Flanigen, P.A. Jacobs, J.C. Jansen (Eds.) Studies in Surface Science and Catalysis, Elsevier, 2001, pp. 345-386.
[92] J.A. Lercher, A. Jentys, Chapter 13 - Infrared and Raman Spectroscopy for Characterizing Zeolites, in: J. Čejka, H. van Bekkum, A. Corma, F. Schüth (Eds.) Studies in Surface Science and Catalysis, Elsevier, 2007, pp. 435-476.
[93] A. Jentys, K. Kleestorfer, H. Vinek, Concentration of surface hydroxyl groups on MCM-41, Microporous and Mesoporous Materials, 27 (1999) 321-328.
[94] E.M. Flanigen, H. Khatami, H.A. Szymanski, INFRARED STRUCTURAL STUDIES OF ZEOLITE FRAMEWORKS, Advances in Chemistry Series, (1971) 201-229.
[95] C.A. Emeis, Determination of Integrated Molar Extinction Coefficients for Infrared Absorption Bands of Pyridine Adsorbed on Solid Acid Catalysts, Journal of Catalysis, 141 (1993) 347-354.
[96] J.W. Ward, The nature of active sites on zeolites: I. The decationated Y zeolite, Journal of Catalysis, 9 (1967) 225-236.
[97] C. Morterra, G. Magnacca, V. Bolis, On the critical use of molar absorption coefficients for adsorbed species: the methanol/silica system, Catalysis Today, 70 (2001) 43-58.
[98] M. Thommes, Chapter 15 - Textural Characterization of Zeolites and Ordered Mesoporous Materials by Physical Adsorption, in: J. Čejka, H. van Bekkum, A. Corma, F. Schüth (Eds.) Studies in Surface Science and Catalysis, Elsevier, 2007, pp. 495-523.
[99] W. Zhou, Chapter 8 Electron Microscopy of Zeolites, in: Zeolites in Catalysis: Properties and Applications, The Royal Society of Chemistry, 2017, pp. 277-309.
[100] J.M. Thomas, O. Terasaki, P.L. Gai, W. Zhou, J. Gonzalez-Calbet, Structural Elucidation of Microporous and Mesoporous Catalysts and Molecular Sieves by High-Resolution Electron Microscopy, Accounts of Chemical Research, 34 (2001) 583-594.
[101] D. Shindo, T. Oikawa, Basic Principles of Analytical Electron Microscopy, in: Analytical Electron Microscopy for Materials Science, Springer Japan, Tokyo, 2002, pp. 1-11.
[102] J.I. Goldstein, D.E. Newbury, P. Echlin, D.C. Joy, C.E. Lyman, E. Lifshin, L. Sawyer, J.R. Michael, Electron Beam–Specimen Interactions, in: Scanning Electron Microscopy and X-ray Microanalysis: Third Edition, Springer US, Boston, MA, 2003, pp. 61-98.
[103] W. Zamechek, R.G. Pankhurst, in: Proceedings of the International ICP Winter Conference, San Juan, Puerto Rico, 1980, pp. 121.
[104] J.M. Williams, NMR spectroscopy, 2nd edition H. Gunther published by John Wiley & Sons, Chichester, Rapid Communications in Mass Spectrometry, 9 (1995) 1330-1330.
[105] N.A. Katsanos, R. Thede, F. Roubani-Kalantzopoulou, Diffusion, adsorption and catalytic studies by gas chromatography, Journal of Chromatography A, 795 (1998) 133-184.
[106] F.W. Jones, Estimation of Flame-Ionization Detector Relative Response Factors for Oligomers of Alkyl and Aryl Ether Polyethoxylates using the Effective Carbon Number Concept, Journal of Chromatographic Science, 36 (1998) 223-226.
[107] A. Khalafi-Nezhad, S. Mowlazadeh Haghighi, F. Panahi, Nano-TiO2 on Dodecyl-Sulfated Silica: As an Efficient Heterogeneous Lewis Acid–Surfactant-Combined Catalyst (HLASC) for Reaction in Aqueous Media, ACS Sustainable Chemistry & Engineering, 1 (2013) 1015-1023.
[108] H.M. Altass, A.S. Khder, Preparation, characterization of highly active recyclable zirconium and tin tungstate catalysts and their application in Pechmann condensation reaction, Reaction Kinetics Mechanisms and Catalysis, 125 (2018) 227-243.
[109] M. Teubnerová, Study of acid-base properties of zeolites with tetravalent cations by vibrational spectroscopy, Diploma thesis, Department of Analytical Chemistry, University of Chemistry and Technology, Prague, 2018, pp. 1-70.
[110] E.P. Parry, An infrared study of pyridine adsorbed on acidic solids. Characterization of surface acidity, Journal of Catalysis, 2 (1963) 371-379.
[111] G. Busca, Acidity and basicity of zeolites: A fundamental approach, Microporous and Mesoporous Materials, 254 (2017) 3-16.

[112] E.W. Thiele, Relation between Catalytic Activity and Size of Particle, Industrial & Engineering Chemistry, 31 (1939) 916-920.
[113] Q. Lu, C.-J. Chen, W. Luc, J.G. Chen, A. Bhan, F. Jiao, Ordered Mesoporous Metal Carbides with Enhanced Anisole Hydrodeoxygenation Selectivity, ACS Catalysis, 6 (2016) 3506-3514.